# A Molecular Dynamics Study of Interactions between Amyloid-β Peptides and Model Lipid Membranes

**Charles Hardy Davis**

A dissertation submitted to the faculty of the University of North Carolina at Chapel Hill in partial fulfillment of requirements for the degree of Doctor of Philosophy in the Department of Biochemistry and Biophysics.

Chapel Hill
2010

Approved By:

Advisor: Max Berkowitz, Ph.D.

Reader: Barry Lentz, Ph.D.

Reader: Nikolay Dokholyan, Ph.D.

Reader: Garegin Papoian, Ph.D.

Reader: Andrew Lee, Ph.D.

**Abstract**

Charles H. Davis: A Molecular Dynamics Study of Interactions between Amyloid-β Peptides and Model Lipid Membranes
(Under the direction of Max L. Berkowitz)

The Amyloid-β (Aβ) peptide is one of the main aggregate species in Alzheimer's disease. It is believed that the aggregation of Aβ is crucial to neurotoxicity, which is a hallmark of the disease. While it is clear that Aβ plays a significant role in the deterioration of neurons during the progression of this disease, both the toxic nature of Aβ and the initiation of Aβ aggregation are not well understood.

It has been observed that cell membranes, in particular anionic lipids, play a key role in accelerating Aβ aggregation *in vivo*. Interactions with anionic lipids promote secondary structure changes and a much higher rate of protein aggregation. However, it is unclear how interactions with cell membranes influence the earliest stages of aggregation, which are unavailable to the current resolution of experimental techniques. In this thesis, we present extensive molecular dynamics simulations performed to investigate the direct interaction between Aβ and anionic lipids in order to explain the origin of the substantial influence of cell membranes on Aβ aggregation.

From these molecular dynamics simulations, we have observed that anionic cell membranes likely promote aggregation through transiently increasing the local Aβ concentration by favorable protein-lipid interactions on the membrane surface. Further, we have determined that membranes do not directly influence Aβ structure on a monomer level, but the secondary structure change observed in experiments is likely due

to protein-protein interactions which are promoted on the membrane surface. Finally, we have determined that anionic lipids act as a catalyst for Aβ dimerization while uncharged lipids likely limit aggregation to only the dimer level. Through these molecular dynamics simulations, we have been able to obtain extensive data on Aβ-membrane interactions at a molecular level. Data such as this will be necessary towards developing a cure to halt Alzheimer's disease progression at its earliest stages.

**Acknowledgements**

I would like to start by thanking my advisor, Dr. Max Berkowitz, for his guidance over the last five years. Dr. Berkowitz has been an outstanding advisor and has always provided me with exactly the right amount of freedom to be successful. He gave me the opportunities to try new things and attempt difficult protocols, but always made sure I was focused on the goals of the work I was doing. He helped guide me through numerous obstacles and fellowship applications over the course of my study and I am gracious for his patience during these times. Dr. Berkowitz has been an ideal advisor during my time in graduate school and I know that I enjoyed a truly unique opportunity to study under a world-class researcher.

Further, I would like to thank the members of my committee, Dr. Barry Lentz, Dr. Nikolay Dokholyan, Dr. Garyk Papoian and Dr. Andrew Lee, for their guidance during this thesis work. I would like to thank Dr. Dokholyan and Dr. Papoian for helping me become a more confident researcher through my experiences either in a rotation or through various journal clubs. I would like to thank Dr. Lee for adding his much-needed structural experience to my committee. In particular, I am greatly indebted to Dr. Barry Lentz. Barry has been wonderful to me over the years and I appreciate all of the help he has provided to me along the way. I know that I would not be half the scientist I am now without the experiences I had in his classes, in particular our biophysics seminar class.

Next, I am greatly appreciative of the members of the Berkowitz lab, both past and present. I have really enjoyed the time I spent in lab with both Dr. Zhancheng Zhang

and Changsun Eun. They were always a spectacular resource for discussing science and also for making lab enjoyable each day. Both Zhancheng and Changsun are good friends and great scientists, and I wish them the best in their future endeavors. I would also like to acknowledge Dr. Lanyuan Lu and Dr. Shreyas Bhide for helping me as I was getting started in lab. While I did not get to share the lab with them, former Berkowitz lab members Dr. David Bostick and Dr. In-Chul Yeh were instrumental to different aspects of this thesis work. I would also like to note the undergraduate and rotation students, Jackson Chief Elk and Christine Hajdin, who helped me with this work. I would like to thank the UNC Research Computing group for providing all of the computer time over the years and helping me out when trouble arose. Finally, I would like to thank the National Institute of Health and the National Institute of Aging for providing funding of my last year of research through a Ruth L. Kirschstein National Research Service Award.

I would also like to thank members of both the Department of Biochemistry and the Molecular and Cellular Biophysics Program. Without these two groups, I would not have had the wonderful opportunities I was able to experience in graduate school at UNC. The administrative staffs of these programs, especially Lisa Phillippie and Lynn Ray, have been instrumental for my progression towards my Ph.D. Also, the other graduate students in these programs, which are too numerous to list, have been like family over the years and have made all of this work so much more enjoyable.

Finally, I would like to thank my family, especially my mother, Gilda Hollar, and my father, Chuck Davis. My parents helped to instill in me a great love of science that still caries on to today. My mother has provided me with an illustrious sense of confidence and love and has trained me to be an independent, progressive thinker. My

father has been very supportive through this entire process and has always been willing to stop everything and come help when needed. I also must thank my wonderful girlfriend, Erin Heenan. Without Erin by my side, I am positive I would have gone crazy at some point during these five years. Erin has been willing to listen to me prattle about the most absurd or ridiculous topics, such as molecular dynamics, and is still willing to listen. She has been perfect over these years and made graduate school a truly exciting and joyous experience.

## Table of Contents

## List of Tables

Page

## List of Figures

Page

## Abbreviations

| | |
|---|---|
| α | Alpha |
| Aβ | Amyloid-Beta |
| Aβ40 | 40 residue Amyloid-Beta peptide |
| Aβ42 | 42 residue Amyloid-Beta peptide |
| Aβ(1-40) | 40 residue Amyloid-Beta peptide |
| Aβ(1-42) | 42 residue Amyloid-Beta peptide |
| Aβ1-28 | Amyloid-Beta peptide containing only the first 28 residues |
| Aβ(17-42) | Amyloid-Beta peptide containing only the terminal 26 residues |
| Ala | Alanine |
| APP | Amyloid Precursor Protein |
| APP-C99 | Amyloid Precursor Protein Fragment C99 |
| ApoE | Apolipoprotein E |
| Asp | Aspartic Acid |
| Å | Angstrom |
| β | Beta |
| CD | Circular Dichroism |
| ΔA | Change in Helmholtz Free Energy |
| ΔG | Change in Gibbs Free Energy |
| COM | Center of Mass |
| DPPC | Dipalmitoylphophatidylcholine |
| DOPS | Dioleoylphosphatidylserine |

| | |
|---|---|
| DSSP | Direct Secondary Structure Prediction |
| fs | Femtosecond(s) |
| γ | Gamma |
| Glu | Glutamic Acid |
| Gly | Glycine |
| GM1 | Monosialotetrahexosylganglioside |
| His | Histidine |
| k (or $k_b$) | Boltzmann Constant |
| K | Kelvin |
| kcal | Kilocalorie(s) |
| kJ | Kilojoule(s) |
| LINCS | Linear Constraint Solver |
| Lys | Lysine |
| μM | Micromolar |
| MD | Molecular Dynamics |
| mol | Mole(s) |
| nm | Nanometer(s) |
| NMR | Nuclear Magnetic Resonance |
| NPT | Constant Pressure Simulation |
| ns | Nanosecond(s) |
| NVT | Constant Volume Simulation |
| P-LINCS | Parallel-Linear Constrant Solver |
| PC | Phophatidylcholine |

| | |
|---|---|
| PDB | Protein Databank |
| Phe | Phenylalanine |
| POPC | Palmitoyloleoylphosphatidylcholine |
| POPG | Palmitoyloleoylphosphatidylglycerol |
| PS | Phophatidylserine |
| ps | Picoseond(s) |
| REMD | Replica Exchange Molecular Dynamics |
| SPC/E | Simple Point Charge/Extended |
| SPME | Smooth Particle Mesh Ewald |
| T | Temperature |
| Val | Valine |
| W(z) | Potential of Mean Force along Reaction Coordinate *z* |
| WHAM | Weighted Histogram Analysis Method |
| 2D | Two-Dimensional |
| 3D | Three-Dimensional |

# Chapter 1:

# Introduction: The Role of the Amyloid-β Protein and Cell Membranes in Alzheimer's Disease

## Alzheimer's Disease and the Current State of Medicine

Over the past decades, a deeper understanding of the causes of disease and the development of a vast range of pharmaceuticals and targeted therapeutics have greatly improved the quality of life in the United States and throughout the developed world. These medical advancements have resulted in longer, fuller lives for a vast range of people. In the US, between 1967 and 2007, these improvements in medical care have resulted in an extension of almost 8 years to the average life expectancy, from 70.6 to 77.9 (1). Our more advanced knowledge of the causes and genetic cues for disease has also provided a higher quality for the later years of life. By improving diet and targeting risk factors such as high cholesterol, sedentary lifestyles or environmental toxins, people are able to determine potential health issues early and remain healthy, even until old age. The impact of these advances can be clearly seen in the data related to death from heart disease and cancer. While heart disease and cancer do remain the first and second causes of death, respectively, in the US (1), their prevalence is decreasing. Between 1999 and 2007, the percentage of deaths due to heart disease has decreased from 30.3% to 25.4% (1) and the total number of deaths due to heart disease per year decreased as well. For

cancer, over this same time period, the percentage of deaths in the US remained at approximately 23% (1), which is impressive considering that the large drop in deaths due to heart disease did not lead to more deaths due to cancer. Thus, over just 8 years, the prevalence of heart disease and cancer in US mortality rates is decreasing, in part due to our greater knowledge of the etiology and biology of disease.

However, these numbers mask problems that are arising with regards to health in the US. According to the US Census, in 1990, the elderly (65 years old or older) population of the US was 31.2 million, which was 12.6% of the population. In 2008, the US Census Bureau estimated that the elderly make up 12.8% of the population. While that does not seem like a large increase percentage-wise, 12.8% of the US population in 2008 would correspond to approximately 39 million elderly people, an increase of almost 8 million in less then 20 years. It is even more startling to realize that this does not yet account for the large majority of the "baby boomer" population, which will lead to a massive rise in the elderly population over the next 10 to 15 years. While, on the surface, this appears to be a great triumph of modern medicine, there are significant reasons for concern. Aside from the expansive increase in medical costs that will result due to the swelling of the elderly population, this population increase will result in a greater prevalence of diseases and disorders that specifically arise in the latest stages of life. In particular, the most common and most notorious of these disorders is Alzheimer's disease, which is characterized by slow deterioration of neural function and motor skills, loss of both short and long term memory, and eventual death. Mortality statistics demonstrate the increased pervasiveness of Alzheimer's disease in the US. Between

1999 and 2007, Alzheimer's disease moved from the 8th to the 6th most common cause of death in the US (1) with the percentage of deaths per year due to Alzheimer's disease increasing from 1.9% to 3.1%. Again, the percentages are deceiving as they mask that the number of deaths to due to Alzheimer's disease has increased from 44,536 in 1999 to 74,944 in 2007 (1), an increase of 168%. It is even more startling to realize that, of the five causes of death that are more prevalent then Alzheimer's disease, only the number of accidental deaths has significantly increased over this time (1). While it appears that current medicine is doing a fantastic job preventing the most common causes of death in the US and extending both life expectancy and quality of life, the treatment and prevention of death due to Alzheimer's disease appears to be lagging. With the current aging of the population and the upcoming boom in the elderly population due to the "baby boomer" generation, the prevalence of Alzheimer's disease will only increase, meaning that a significant public health response to this crisis and direct scientific progress towards a better understanding of this disease is necessary.

**The Biochemistry of Alzheimer's Disease**

While the public health aspects of Alzheimer's disease are rather startling and foreboding, the current state of scientific progress in understanding Alzheimer's disease and developing an appropriate treatment is not nearly as bleak. While Alzheimer's disease was first characterized over 100 years ago (2), work over the past 20 to 30 years (3, 4) has greatly increased our knowledge of the direct microscopic causes of this disease. Alzheimer's disease is a member of a class of disorders known as aggregation

diseases (5). In these diseases, many of which are neurodegenerative, proteins that are commonly endogenous to cells misfold and begin to aggregate (5-9). The aggregation of these proteins leads to the disruption of important cellular functions, such as signal transduction or trafficking within the cell (5, 10). Other aggregation disorders of some notoriety include Parkinson's disease, Bovine Spongiform Encephalopathy (Mad Cow disease) and Creutzfeldt-Jakob disease (8, 10). For these disorders, the initiation and progression of the disease is described by the amyloid hypothesis (4, 5, 10). In the amyloid hypothesis, either a protein with a physiologically stable fold will unfold, exposing residues that are primed for aggregation, or an intrinsically disordered protein with no stable fold will undergo structural fluctuations that expose specific residues. Similar misfolded proteins will interact and aggregate, leading to the formation of small oligomers. These small oligomeric aggregates will further coalesce to form ordered fibrils and eventually plaques. It was originally believed that the build-up of these fibrils and plaques would disrupt neuronal processes and metabolism, and lead to neuron degeneration and death (4, 5, 10). However, as more research is being performed on Alzheimer's disease, this paradigm of fibril or plaque toxicity for neurons is being revolutionized (4, 5, 10).

**The Role of the Amyloid-β Peptide in Alzheimer's Disease**

Before describing the roles of oligomers, fibrils and plaques in Alzheimer's disease, it is necessary to introduce further details of this disease. The major aggregate species in Alzheimer's disease is known as the Amyloid β (Aβ) peptide. Aβ is produced

as the proteolytic cleavage (Figure 1.1) of the Amyloid Precursor Protein (APP) (3, 11, 12). APP is a large (695-770 residues), transmembrane protein that is primarily expressed in neurons (3, 11-14). While the exact role of APP in the cell is unknown, it is believed to play a role in synapse formation and neural plasticity (13, 14). During the processing of APP by the cell, a series of secretases cleave the APP protein (Figure 1.1). First, APP is cleaved near its C-terminus by either an α-secretase or β-secretase enzyme (11, 15, 16). Subsequently, the truncated APP produced by this cleavage event is again cut by a γ-secretase, producing two final fragments released from APP (11, 15, 16). The α-secretase cuts further from the C-terminus of APP than β-secretase, producing a smaller fragment after γ-secretase processing (Figure 1.1a). This fragment, known as p3, is considered non-toxic and a result of normal APP processing in the neuron. However, cleavage of APP by β-secretase between residues 671 and 672 produces a truncated APP referred to as APP-C99 (11, 15, 16). APP-C99 is then cleaved by γ-secretase to produce the Aβ peptide (Figure 1.1b), which is between 38-43 residues long (17). The most common forms of Aβ produced by γ-secretase cleavage are the 40 and 42 amino acid fragments, known as Aβ40 or Aβ42 (6, 15, 18-20). Further, the location of APP processing within the cell may play a role in the preference of Aβ40 versus Aβ42 production (21). Thus, after γ-secretase cleavage, the Aβ peptide is free to be either released in solution or remain bound to the membrane surface. In current attempts towards treatment of Alzheimer's disease, APP and the secretases which act on APP have become a popular target (22). Recent work has implied that APP, due to a conserved GXXG motif, dimerizes (23) before secretase cleavage and that this dimerization of APP produces Aβ dimers that act as a seed for future Aβ aggregation, which increases the

importance of APP as a target for therapeutic treatment. Further, due to the relationship between the localization of secretases in neurons and the existence of cholesterol-enriched lipid rafts (24), there is interest in determining if there is a causal link between cholesterol levels in membranes, Aβ production, and Alzheimer's disease (25). While not the focus of this thesis, the role of APP in the earliest stages and progression of Alzheimer's disease is a popular subject in current biological research (22).

After release from APP, the Aβ peptide is able to initiate the amyloid aggregation cascade. There is no known biological function of Aβ within the cell. The Aβ peptide has a mostly random coil structure in solution (26, 27); however, it is able to adopt transient β-sheet or α-helical elements during normal structure fluctuations (26-29). The peptide consists of two general domains, a charged and hydrophilic N-terminus and a predominately hydrophobic C-terminus. The C-terminus of Aβ represents what was a transmembrane region of APP before secretase cleavage, while the N-terminus represents an external, solvent-accessible region of APP (3, 11, 12). Further, the production of multiple lengths of Aβ during secretase processing is of interest to the pathology of Alzheimer's disease (10, 30-32). While Aβ40 is the most common form of Aβ produced in neurons, Aβ42 is considered to be the more neurotoxic species (10, 30-32). The extent of Alzheimer's disease progression for early-onset situations tracks remarkably well with the amount of Aβ42 produced (33). Further, Aβ42 is considerably more fibrillogenic then Aβ40 (10, 30-32). It is unknown exactly why Aβ42 appears to be more toxic, but the additional isoleucine and alanine residues at the C-terminus of Aβ42 provides an even more hydrophobic nature to the peptide, which would promote aggregation in solution

and might explain the more fibrillogenic nature of Aβ42. Nevertheless, the microscopic and macroscopic differences between Aβ40 and Aβ42 within the pathology of Alzheimer's disease is a subject of intense on-going research and their differences have still not be completely clarified (10, 30). For the purposes of the work described in this thesis, we have used Aβ42 for all simulations.

The lack of stable structure for the Aβ peptides allows for exposed hydrophobic residues that promote peptide-peptide interactions in solution, which encourages aggregation and initiates the formation of higher order oligomers. It was initially believed that the production of fibrils and, subsequently, plaques was the ideal endpoint for the purposes of neural degeneration (4, 5, 10). Further, it has been observed that many different amyloidogenic peptides form a cross-β structure in fibrils, producing fibrils that are remarkably similar even with protein or peptide building blocks that share very little primary sequence similarity (34). Due to a shared structure and similar overall toxicity to neurons, fibrils and amyloid plaques were initially considered toxic to cells. While it has been shown that isolated fibrils can be somewhat toxic to cells in vivo (35, 36), recent evidence has shifted the dogma of neurotoxicity away from fibrils and towards smaller oligomers as the toxic elements in neurons (4, 5, 9, 37). Thus, in these previous studies demonstrating fibril toxicity, it is not clear if the fibrils themselves are toxic or if they play a role as a reservoir of Aβ aggregates that can be released after disruption of fibrils (35, 36). As technology has advanced, it has become possible for researchers to isolate small oligomers of Aβ. When these oligomers are added to cells, the cells demonstrate classic signs of neurotoxicity and even apoptosis (10, 38-40). It is

believed that these small Aβ oligomers are able to induce cell signaling mechanisms that start the initial stages of the cell death mechanisms within neurons and lead to neuronal dysfunction (10).

It is important to note that Aβ is not the only toxic species in Alzheimer's disease. The tau protein (10, 41) in neurons is also considered to be essential to toxicity in Alzheimer's disease. Upon activation, the tau protein is regulated by phosphorylation (10, 42), which leads to tau aggregation into neurofibrillar tangles and neuron death. It is not clear if tau is directly responsible for neuron toxicity or if tau merely plays a role in advancing a toxic signal, but the existence of tau in the cell is important for Aβ toxicity (10, 41). In particular, Aβ-related behavioral changes are dependent on tau while other aspects of Aβ induced toxicity, such as neurite dystrophy, are independent of tau (10). Recent studies (10, 43, 44) have focused on the relationship between Aβ and tau in Alzheimer's disease, but the direct link is still not clear. Further, the relationship between exogenious Aβ and intracellular tau is yet to be determined (10). Thus, there exists an important relationship between Aβ and tau that plays a key role in neuron toxicity, which would not be completely possible through Aβ aggregation alone.

**Cell Membranes as a Catalytic Agent for Peptide Aggregation**

With the newly heightened emphasis on the importance of Aβ oligomers in Alzheimer's disease, the earliest stages of Aβ aggregation have become an important topic of biophysical investigation. Certain aspects of Aβ aggregation are well

understood, such as fibril growth and branching (45). However, the earliest stages of Aβ oligomerization, such as dimer or trimer formation, are still vague. In particular, one important aspect of this process that is unclear is the role of monomer structure within the larger oligomer. As mentioned earlier, Aβ is predominantely unstructured as a monomer in solution (26, 27). However, when incorporated into an Aβ fibril, the monomeric unit has a very regular structure (46-49) with a β-sheet in the C-terminal section of the peptide (Figure 1.2). This structure is repeated with high fidelity throughout a given fibril (Figure 1.2). There is some controversy with regards to internal fibril structure as the monomeric or dimeric Aβ unit between two fibrils can differ (46-49). The large-scale structure of the fibril, such as width and number of protofibrils encompassed by the fibril (50, 51), can also vary. However, within a given fibril, the monomeric Aβ units are very regular (Figure 1.2). At some time during the aggregation process, Aβ must undergo a structural change from unstructured monomer to structured fibril. Early results (52-56) tend to indicate that small oligomers do not have the exceedingly stable structure of fibrils, but these results are not fully conclusive. Further, there is some belief that Aβ peptides can undergo different aggregation pathways (30, 55). These pathways involve varying amounts of structure formation for monomers within oligomers (30, 53), resulting in different oligomer structures that may be more neurotoxic (55) than others. This wide range of heterogeneous oligomeric structures using fundamentally homogeneous monomeric units implies that physical processes within the cell and unique conditions within a neuron are an integral aspect of Aβ aggregation. For most systems, high-resolution experimental methods would be able to clarify these questions. Methods such as nuclear magnetic resonance (NMR) spectroscopy or x-ray crystallography would

be able to identify precise structures of oligomers. However, the Aβ peptide begins to aggregate at such low concentration (57-59) that small oligomeric units are not stable at concentrations necessary to perform these experiments at an adequate resolution. Thus, a better understanding of structure within small oligomeric Aβ aggregates is necessary for extending our knowledge of Aβ and its role in neurotoxicity within neurons.

Another feature of the early stages of Aβ aggregation that is considered a growing area of research involves the concentration threshold for Aβ aggregation. In experiments performed *in vitro*, Aβ begins to aggregate in solution at a concentration of approximately 10 μM (4, 60, 61). For experiments performed *in vivo*, Aβ aggregation occurs at orders of magnitude lower concentration, approximately sub-μM (4, 58, 59). While many physical conditions within the cell, such as pH (62), salt concentration (63) and oxidation state (64) of specific residues within Aβ do play a role in the apparent difference in aggregation within a cell versus *in vitro*, it appears that the role of cell membranes in Aβ aggregation is substantial (4, 5, 30, 65). Cell membranes are able to significantly alter peptide aggregation through a variety of means (Figure 1.3) (4, 5, 65). Charged lipids headgroups are able to directly interact with charged residues within the peptide, altering peptide structure (5, 65, 66). By isolating the peptide to a two dimensional surface such as a lipid membrane, new minimum free energy structures (5, 65, 66) might be favored, leading to either unfolding or folding of the peptide (Figure 1.3a). Further, localizing multiple peptides to the surface will increase the local concentration of the peptide (Figure 1.3b) (5, 65, 66). By increasing the local concentration, the probability of peptides coming into contact and inducing aggregation

will be heightened, which will, in turn, increase the aggregation rate. Finally, a more subtle effect involves the change in pH near the surface of anionic lipid bilayers (57, 67, 68). Anionic lipid headgroups attract $H^+$ ions from solution, increasing the local $H^+$ concentration and decreasing the local pH (Figure 1.3c). While this appears to be a subtle effect, the results can be significant. A recent experiment (57) using palmitoyloleoylphosphatidylglycerol vesicles mixed with Aβ peptides demonstrated that Aβ localized to the surface of the vesicles and 3 histidines in Aβ became protonated upon binding. At physiological pH, Aβ has a -3 total charge. Thus, upon binding to an anionic bilayer, the net charge on Aβ drastically changes. These physical effects due to Aβ interactions with cell membranes considerably promote Aβ aggregation and help to explain the discrepancy in the concentration threshold for aggregation between *in vitro* and *in vivo* experiments.

**Direct Biological Effects of Aβ Interactions with Cell Membranes**

The interaction between Aβ and cell membranes also has biological implications for Aβ toxicity in Alzheimer's disease. As mentioned in a previous section, the Aβ peptide is derived from a transmembrane portion of APP. Thus, the hydrophobic C-terminus of Aβ is ideal for interaction with and insertion into a cell membrane. Even when Aβ is cleaved, there is still some doubt as to if Aβ is immediately released or if the C-terminus is able to anchor the peptide in the bilayer. Recent computational experiments (69) have indicated that the physiological Aβ peptide inserted as a monomer into the bilayer is not stable but will exit the bilayer and lay parallel to the bilayer surface.

Further, this strong interaction with the bilayer emphasizes one of the potential toxic mechanisms of Aβ. Experimental research has demonstrated that the interaction between Aβ and cell membranes leads to oxidation of the acyl chains of both phospholipids and cholesterol within the membrane (4, 64, 70). This oxidation event leads to the generation of free radicals that can be toxic to the cell. Further, oxidation has been shown to be dependent on metal concentrations within the cell, with $Cu^{2+}$ increasing Aβ toxicity while $Zn^{2+}$ appears to attenuate toxicity (10, 71). Conversely, it has also been shown that lipids are able to increase the oxidation of Aβ itself (4, 10, 72). By interacting with lipid oxidation products and metals in the cell, residues on Aβ, such as Tyr10 and Met35, become oxidized. These oxidized residues are then highly likely to form chemical cross-links with other Aβ peptides. Thus, oxidation near the cell membrane is able to form chemically stable Aβ dimers that act as a seed for further aggregation (10). Finally, a recent work (73) has shown that Aβ interactions with cell membranes stimulates further production of Aβ from APP. All of these factors exemplify the direct toxic nature of Aβ through interactions with cell membranes.

Another interesting biological aspect of this system is the potential of pore formation by Aβ. Early work with Aβ has shown that addition of Aβ to cells will create an ion current across the cell membrane (74). Further research into this system has shown that this interaction between Aβ and cell membranes disrupts $Ca^{+2}$ homeostasis across the membrane (74, 75). Some experimental work has hinted that the role of Aβ in this system is to thin the membrane (76, 77) to such an extent that ions are able to flow through the cell membrane non-specifically. It appears, though, that this effect is due to

the use of trace amounts of hexafluoro-isopropanol (78) and that the conductance across the membrane is due to the specific action of Aβ. Further, some of the most exciting work on this system involves a recent study using atomic force microscopy (79). In these experiments using a multitude of different amyloidogenic peptides, including Aβ, the atomic force microscopy results clearly show the formation of specific transmembrane pores. Using these results, the Nussinov group has used molecular dynamics simulations to model Aβ pore formation (74, 80). These simulations show that Aβ pores are not stable units (74, 80) similar to gated-ion channels or pores formed by antimicrobial peptides, but are fluctuating structures that constantly break apart and reform (Figure 1.4). These pores are formed out of β-hairpin units that interact through hydrogen bonding (Figure 1.4) (74, 80), unlike the stable ion channels that are predominantly α-helical in nature. Further, the β-hairpin monomers form small oligomeric units (74, 80) within the cell membrane, which appear to be stable. These oligomeric units then transiently interact to form unstable pores that allow ions to flow across the membrane, disrupting ion homeostasis and leading to neuron death. Thus, the direct biological consequences of Aβ-membrane interactions can be deadly to neurons in Alzheimer's disease.

Similar to the direct, toxic interactions that occur when Aβ binds to the membrane surface, membranes also play a crucial secondary role in Aβ neurotoxicity through strongly promoting Aβ aggregation (5, 65, 66). Regardless of the size of the toxic aggregate, membranes act as a templating agent for drastically increasing aggregation of Aβ for both *in vitro* and *in vivo* systems (5, 58, 81-84). Either through a concentration

effect, wherein the favorable interactions between Aβ and the membrane surface will locally increase Aβ concentration, or through direct peptide-lipid interactions, which could promote a secondary structure change that primes Aβ monomers for oligomerization (Figure 1.3), the membrane plays a key role in catalyzing aggregation (5, 65, 66) at concentrations much lower than in solution. In some of the earliest experiments (57, 82) investigating the Aβ-membrane system, the addition of lipid vesicles to Aβ peptides in solution induces aggregation at sub-μM concentration, similar to the concentration threshold for Aβ aggregation *in vivo*. Further, through use of circular dichroism (6), it was observed that adding these lipid vesicles to Aβ in solution induced a secondary structure change from random coil to β-sheet (Figure 1.5) (57, 82). These early experiments appear to confirm the theory that a membrane alone can account for a substantial extent of the difference between *in vitro* and *in vivo* aggregation. Experimental work using atomic force microscopy (83, 85) and electron microscopy (83, 86) has been able to visualize Aβ aggregation into both amorphous aggregates and protofibrils or fibrils on the surface of lipid membranes. These experiments, along with other work demonstrating a direct interaction between Aβ and cell membranes (4, 5, 66, 87), implicate Aβ-lipid interactions as an important causative factor in accelerating Aβ aggregation near neurons.

**Interaction Between Anionic Lipid Headgroups and Aβ Peptides**

One interesting property of this Aβ-lipid system that appears to play a crucial role in modulating the extent of the Aβ interaction with membranes is the nature of the lipid

headgroup. In some of the earliest experiments with this system, it was observed that anionic lipid headgroups effect Aβ aggregation and structure to a much greater extent then zwitterionic lipid headgroups (4, 5, 57, 65, 81, 82, 88). Anionic lipid headgroups are able to enhance the aggregation rate of Aβ in *in vitro* systems and induce significant structure change to β-sheet dominated aggregates (5, 57, 81, 82, 88, 89). Also, depending on the peptide-to-lipid ratio, interactions with anionic headgroups are able to induce α-helical structure (90) in Aβ that can undergo a conversion with the canonical β-sheet structure observed in Aβ protofibrils and fibrils. Similar to previously mentioned experiments, CD (57, 81, 82), isothermal calorimetry (57), flouresence (87, 88), neutron and x-ray diffraction (59, 91) and electron microscopy (88) have all been used to observe this strong interaction with anionic lipid headgroups (Figure 1.5). Further, $^{31}$P NMR (81) results have shown a direct interaction between Aβ and anionic lipids by demonstrating that Aβ binding causes shifts in the NMR spectra for anionic lipids. However, for model zwitterionic lipids, the interaction with the lipids appears to be more transient (4, 57, 81, 92, 93) and the secondary structure change observed with anionic lipids is much more restricted. The interactions between zwitterionic lipids and Aβ can be enhanced if the zwitterionic lipids are in a liquid-crystalline or gel state (4, 94, 95), but these interactions are still somewhat weak in comparison to the anionic lipid-induced aggregation. These results are consistent for lipid mixtures as well, as the influence on Aβ aggregation increases as the percentage of anionic lipids within the mixture increases (81, 87).

The differentiation between anionic and zwitterionic lipids and the extent of their roles in Aβ aggregation also has a significant biological implication. The major

zwitterionic lipid headgroup used in experiments is phosphatidylcholine (4, 57, 81, 87, 93-95). Further, phosphatidylcholine lipids are the most common lipids found in neurons (96), which enhances the importance of studies performed with these lipids. For anionic lipids, both phosphatidylglycerol (57, 59, 81, 82, 87) and phosphatidylserine (91, 97, 98) lipids have been commonly used in experiments. Some of the earliest experiments studying the role of lipid headgroup charge on Aβ aggregation used phosphatidylglycerol lipids (57, 82). While these anionic lipids are not found to nearly the same extent as zwitterionic lipids in neurons and other cells throughout the body, they play a crucial role in cell signaling mechanisms and with recruiting proteins to the cell membrane (99). Of direct importance to the etiology of Alzheimer's disease is the role of phosphatidylserine in cell death mechanisms. Cells that are either inducing or undergoing apoptosis commonly move phosphatidylserine lipids to the extracellular leaflet of the cell membrane as a signal to extracellular proteins (100, 101). It has been shown that the neuron death which accompanies Alzheimer's disease appears to begin with weakened or damaged cells (98). Also, it was determined that extracellular exposure of phosphatidylserine (98) was a distinctive characteristic of neurons that were particularly sensitive to Aβ. Thus, it is possible that direct interactions of Aβ with phosphatidylserine lipids are a mechanism for targeting either Aβ monomers or aggregates to weakened cells. These differences in the location and preponderance of zwitterionic versus anionic lipids in neurons likely play a significant role in the targeting of Aβ to specific neurons and in the toxicity of Aβ towards these neurons.

Several caveats exist with respect to the above conclusions concerning the importance of Aβ interactions with anionic lipids. The first caveat is that it is essential to understand how the *in vitro* system is prepared in arriving at these conclusions. The above conclusions assume that Aβ is mixed with a preformed lipid component in solution. However, it is possible to self-assemble the lipids with Aβ (4, 81). In these systems, it is possible for Aβ to intercalate into the lipid mixture and strong interactions are observed for both anionic and zwitterionic lipids. Also, some doubt has been shed on the above results with regards to the role of salt in this process (4). Excess salt is able to screen the electrostatic interactions between Aβ and anionic lipids. In particular, the anionic lipid headgroups will strongly attract cations from solution, which will weaken the electric field locally produced by these headgroups. Also, Aβ is a charged protein at physiological pH, which implies that salt will also associate with various residues on the protein. Salt will then screen any electrostatic interaction between lipids and proteins at large distances. This will require Aβ to have to diffuse closer to the bilayer surface for any interaction to occur, thus decreasing the probability for strong peptide-lipid interactions to be initiated. On a macroscopic scale, this should manifest as a slower Aβ aggregation rate in higher salt environments with less secondary structure change, which has been observed in experiment (4, 57, 93). In light of these controversies, there are still important questions remaining regarding the role of anionic lipids in promoting Aβ aggregation. Since Aβ does originate from a transmembrane protein, is Aβ already close enough to the bilayer surface to abrogate any effects of salt? Do other proteins play a role in bringing Aβ to the bilayer surface? Is it possible that Aβ binds to transmembrane proteins that help recruit Aβ to anionic lipids? These questions are still an active area of

research in Aβ toxicity and it does appear that interactions between Aβ and anionic lipids are vital to the favorable aggregation of Aβ on neurons.

**Other Specific Lipid-Peptide Interactions Key to Aβ Aggregation**

Along with the role anionic lipid headgroups play in Aβ aggregation, other lipids have shown a specificity towards promoting Aβ aggregation in neurons (4, 102). One of the most biologically relevant of these aggregation-promoting species is cholesterol. Cholesterol is a major constituent of cell membranes and acts to rigidify nearby lipids (102-105). Further, the ternary interaction between cholesterol, unsaturated phospholipids and saturated phospholipids leads to the formation of lipid rafts (102-105). These lipid rafts are highly structured domains in the cell membrane and are commonly surrounded by an excess of unstructured lipids. While controversy does exist with regards to the size and role of lipid rafts in biological systems, it appears that lipid rafts play a crucial role in cell signaling and in localizing transmembrane proteins to specific regions of the cell membrane (102-105). Due to the difference in thickness that exists between the ordered lipid raft and the disordered surrounding lipids, it has been shown that the edge of lipid rafts is a location of significant enzymatic activity on the cell surface (102, 106, 107). Of direct importance to Alzheimer's disease, APP appears to preferentially accumulate in lipid rafts (106, 107) and the secretases, which cleave APP and produce Aβ, are believed to be active at the interface between the raft and non-raft regions of the cell membrane. Finally, one of the largest known risk factors for Alzheimer's disease is high cholesterol (102). A genetic predisposition (102) towards

Alzheimer's disease has been found in populations with a specific alloform of ApoE, known as ApoE4. ApoE is a cellular lipoprotein involved in cholesterol transport (108); yet, the role of ApoE, and the ApoE4 variant, in Alzheimer's disease is unknown. However, this anecdotal genetic and biological evidence does hint at an important role of cholesterol in the progression of Alzheimer's disease.

In addition to the importance of lipid rafts to APP processing, it has been observed, similar to anionic lipids, that lipid rafts directly influence Aβ aggregation (4, 83, 102, 109-113). *In vitro*, mixing of lipid rafts with Aβ leads to direct binding of Aβ to the raft and increased Aβ aggregation (83, 109-113). Further, using neurons isolated from rat brain (114) and from human neuroblastoma cells (115), Aβ aggregates were identified at significant concentrations bound to the lipid rafts when the rafts were isolated from neurons. Thus, direct Aβ-raft interactions are believed to play a substantial role in Aβ aggregation. In considering previous results with phosphatidylcholine lipids, this is not as surprising. In studies with phosphatidylcholine, it was found that rigidifying the bilayer (4, 94, 95) improved the extent of lipid-protein interactions. As lipid rafts commonly contain sphingomyelin lipids with zwitterionic character (102), the rigid rafts would have a similar structure to liquid crystalline phosphatidylcholine lipids. However, the rigidification of the cell membrane within a lipid raft is not likely to be the only role of lipid rafts in enhancing Aβ aggregation.

Lipid rafts also play a role in sequestering specific lipids within the ordered domain of the raft. In particular, lipid rafts appear to preferentially sequester

gangliosides (4, 105). Gangliosides are glycosphingolipids that contain large sugar residues as a headgroup (4). These large sugar groups are able to extend from the cell membrane and interact with proteins at the periphery of the cell. Neurons are highly enriched in gangliosides, especially the ganglioside GM1 (4). It has been observed that Aβ peptides strongly interact with GM1 (4, 116-119). In particular, the hydrophobic region of Aβ undergoes substantial interactions with these lipids (4, 119). Experiments performed with Aβ40 and the truncated Aβ1-28 show that residues 29-40 of Aβ are necessary (119) for interactions with gangliosides. Further, Aβ binding to the membrane surface increases almost directly with the amount of gangliosides in the membrane (120). These results imply a direct interaction between the ganglioside and Aβ, which promote aggregation. It is still not clear exactly what role gangliosides play in Aβ aggregation. While Aβ bound directly to a ganglioside cluster can act as a seed for aggregation (4), it is not clear if the direct interaction between sugar residues and Aβ induces a structural change. Another possibility is that the large headgroups of GM1 help to bring Aβ from solution near the bilayer surface. Once near the bilayer surface, Aβ will be able to interact with the lipid raft and undergo conformational changes or aggregate due to the local concentration increase of peptide. In either scenario, gangliosides are significant for any pathological effects of lipid rafts on Aβ aggregation near neurons.

**Experimental Restrictions to Exploring Aβ-Lipid Interactions**

While experiments have been able to classify the extent of interactions that can occur between Aβ and a range of different membrane constituents, the nature of the Aβ

peptide creates a significant problem in understanding these systems at a molecular level. While many of the experiments mentioned in previous sections are able to clearly show an interaction between Aβ and cell membranes, the aggregation state of the peptide is either unknown or at an advanced state, such as a protofibril or fibril. For experiments, such as CD, which only provide generic values such as global secondary structure (57, 81, 82), it is unknown what aggregation state the peptide has obtained. This is a crucial point that must be significantly explored as it is difficult to make definitive conclusions regarding Aβ-membrane interactions without knowledge of the aggregation state when the measurement is made. This is especially true for interactions between Aβ and anionic lipids. The aggregation rate is enhanced (5, 57, 81, 82, 88, 89) to such an extent that aggregation begins at very low concentration of protein. In order to force the system to aggregate at a slow enough rate to observe discrete steps in aggregation, such as Aβ dimerization, the protein concentration would need to be at levels below concentrations that are able to be reputably observed by experimental techniques. While some new methods show promise at alleviating this issue in solution, such as mass spectrometry (53), these methods have not yet been adapted for use in studying Aβ-membrane interactions.

Due to these difficulties in resolving protein-lipid interactions from the protein-protein interactions inherent to the aggregation of Aβ, the earliest stages of Aβ aggregation on cell membranes is still not fully explored. As Aβ derives from a transmembrane protein (3, 11, 12), studies of monomer or dimer interactions with cell membranes are crucial to understanding the catalytic role of membranes in this process.

In particular, further investigations into the influence of anionic lipids on small Aβ aggregates, or even Aβ monomers, is necessary. As there are multiple means (4, 5, 65) for a membrane to influence aggregation, understanding the role of each of these processes on aggregation will be important for developing treatments to halt this progression. It is still unclear if direct interactions between the Aβ peptide and anionic lipids are able to lead to a secondary structure change (Figure 1.3a). It is possible that the secondary structure change observed in CD (57, 81, 82) is due to the membrane forcing an Aβ monomer to adopt a β-sheet conformation. However, it is also possible that the β-structure formed on the membrane is not due to direct protein-lipid interactions but is due to protein-protein interactions that are facilitated by the membrane during aggregation (Figure 1.3b). In such a case, the role of the membrane would be to attract Aβ monomers to the surface, thus binding peptides to a limited area and transiently increasing concentration (5, 65). Even if interactions between anionic lipids and Aβ promote a secondary structure change, this concentration effect would still exist and would help to explain the increase in aggregation rate on anionic lipids. Finally, the anionic lipids induce a local pH change (57, 67, 68) that would shift bound Aβ from a net negative charge to a neutral charge (Figure 1.3c). It has been observed that, in solution, the aggregation rate of Aβ peaks at a pH of approximately 5 (62), which is similar to the proposed pH on the surface of anionic bilayers (67, 68). This pH change could significantly effect the protein-protein interactions enhanced by membrane binding and possibly alter the structure of Aβ dimers and other small oligomers. The influence of this pH change implies the importance of further studying the difference between Aβ aggregation near an anionic versus a zwitterionic bilayer and understanding exactly why

anionic lipids promote aggregation while zwitterionic lipids have little influence on this process. All of these templating effects of membranes on Aβ monomers or small aggregates are crucial to the enhancement of aggregation at the membrane surface; however, current experimental techniques are not able to extract the contribution of each of these effects to the total enhancement. To an even greater extent, the description of these factors does not even touch on the role of Aβ insertion into the membrane and the role of Aβ pore formation (74) in neurotoxicity of this system. A better understanding of these factors is necessary in order to develop therapeutic approaches to prevent the earliest stages of aggregation before toxic oligomers can be formed.

One approach that has shown promise for investigating Aβ-membrane interactions is computer simulations, in particular molecular dynamics (MD) simulations (27-29, 69, 74, 121-139). In these MD simulations, model systems are used to extrapolate the roles of specific factors in promoting Aβ aggregation. Such simulations have been used to great success for studying Aβ dynamics and aggregation in solution (27-29, 121-135). These simulations have employed Aβ fragments (123, 124, 126-128, 130, 132, 135), full length Aβ monomers (27-29, 121, 135), small Aβ oligomers (122, 125-127, 131-133, 135) and Aβ fibrils (129, 134, 135). These simulations have been performed using explicit (27, 29, 123, 124, 127-131, 133) water molecules in solution and using implicit solvent (28, 121, 122, 125, 126, 132, 134, 135) techniques, which employ dielectric mediums in the place of explicit water molecules as a method for extending the time scale available to the simulation. These simulations have used either all-atom (27-29, 121-124, 127-130, 133-135) representations of Aβ, in which all heavy

atoms are explicitly defined, or coarse-grain (126, 131, 132) techniques, in which atoms are grouped together and represented by a reduced model, which also increases the length of potential simulations. Finally, some simulations with Aβ use advanced MD techniques (28, 121-125, 132, 135), such as replica exchange, to extend the available simulation times and to help the simulated proteins overcome free energy barriers that would be impossible to traverse in normal simulations. Some of these simulations have effectively supported (27-29, 121, 123, 124, 126, 132, 135) a random-coil structure of Aβ but have also shown that significant structural fluctuations within the Aβ monomer are important for oligomerization. Other simulations have investigated the stability (122, 125, 126, 131-133) of Aβ oligomers in order to help predict potential oligomer structures in experiment. MD simulations have been used to describe the process by which Aβ monomers are added to the growing end of Aβ fibrils, known as the "dock-lock mechanism" for fibril growth (134). However, as can be expected, all of these simulations have significant limitations. As common to all MD simulations, the largest limitation is that it is difficult for the system to be ergodic in the time limits of modern simulations (140). Because of the inherent limits to the speeds of modern supercomputers, even the most advanced simulations are limited to a microsecond timescale. Techniques such as coarse-graining or replica exchange are able to extend these simulations to higher timescales, but they still do not fully reach the timescales of biological processes in the millisecond to second timescales. Thus, most simulations are not able to explore the full configurational space of a peptide in a reasonable time (140). Also, there always exists the question of the quality of the approximations being made to the system. The largest issue here is with the choice of the force fields used to describe

all interactions in the system. Also, another important limitation is the much smaller size of the system used in simulations, which may not be a fair representation for biological length scales. While these limitations are critical to the interpretation of results obtained from MD simulations, the directed use of MD simulations to answer questions appropriate to the available timescales of simulations is still a reasonable approach to studying biological systems.

While MD simulations have been used to great success for investigating Aβ aggregation in solution, the extension of these same techniques to studying Aβ-lipid interactions on the membrane surface has been limited. To date, only a few simulation studies (69, 74, 80, 136-139, 141) have been performed on an Aβ-model membrane system. Of these studies, the majority (69, 136, 137, 141) have involved investigating the stability of a preinserted Aβ monomer into a membrane. As Aβ is predicted to have an α-helical structure when inserted in a membrane (69, 136, 137, 141), these works have investigated if the Aβ monomer is stable while inserted in the bilayer and what residues on the peptide play a role in this process. These studies have also investigated specialized aspects of this system; such as the angle the peptide takes with respect to the bilayer normal when inserted (69, 136, 137, 141). These studies have shown that the protein is marginally stable as a monomer (69, 136, 137, 141), but is able to move out of the transmembrane region of the bilayer and favorably interact (69) with the interfacial region of the membrane, which induces some disordering of the peptide structure. Further, large-scale coarse-grain simulations (142) have been performed with a large system of generic amyloidogenic peptides that could be primed for aggregation in

different environments. This work investigated (142) how membranes or vesicles would effect peptide aggregation, but the use of generic peptides and coarse-grain atoms meant that atomic level specificity was lost in the system and the connection to Aβ aggregation is not clear. However, no published MD simulations had yet been done to study the binding process of Aβ to a model membrane surface and the interactions between Aβ and a model membrane on the surface of the membrane. In the following chapters, MD simulations are described that explore this Aβ-membrane interaction at atomic resolution for both Aβ monomers and Aβ dimers. These simulations provide a detailed portrayal of the different facets of Aβ-membrane interactions and how these interactions combine to promote Aβ aggregation on the membrane surface. By studying specific systems with advanced MD techniques, using carefully chosen controls, and asking limited but poignant questions, these simulations are able to overcome many of the limitations of classic MD simulations and provide results that further our knowledge of the earliest stages of Aβ aggregation that are not yet available to current experimental techniques. The questions and hypotheses raised by these simulations, in combination with previous and future experimental studies, will hopefully provide an appropriate starting point towards achieving a substantial understanding of the earliest stages of Alzheimer's disease. The advancements of the past 20 years in understanding the biochemical cues of Alzheimer's disease, and the current work being performed with advanced experimental and computational methods, provides hope that a cure for Alzheimer's disease is forthcoming and one aspect of the predicted large-scale public health crisis due to the aging of the US population can be averted.

## Advanced Molecular Dynamics Techniques

While the use of MD simulations has become widespread in the biophysics research community, new techniques are being adopted to improve upon the limitations of the current supercomputers used for these large-scale simulations. MD simulations involve the iterative calculation of all forces in a system and use of Newton's laws to advance the system a given step in time depending on this distribution of forces (143-145). Many of the details involved in MD simulations are with respect to the calculation of these forces. Specific force fields are used to describe either bonded interactions, such as allowed bond lengths, bond angles and dihedral angels, or non-bonded van der Waals interactions between atoms (143-145). Various methods are used to calculate electrostatic interactions between particles; however, in the MD simulations described in this thesis, the smooth particle mesh Ewald method (146) is employed for all electrostatics calculations. Various other aspects, such as specific constraints and periodic boundaries, are used in these simulations to improve upon the speed in which the forces can be calculated or improve upon the apparent size of the system (143-145). However, due to the inherent limitations of current computer technology, these simulations still require a significant amount of time to even approach microsecond timescales. Thus, in the simulations performed for this thesis work, two specific methods, umbrella sampling (147, 148) and replica exchange (149) molecular dynamics, were used to improve upon these limitations of MD simulations.

*Umbrella Sampling Molecular Dynamics*

While the introduction sections of each of the remaining chapters of this thesis do introduce details of the MD techniques used, it is important to give a brief introduction to two specific techniques used in these simulations. The first of these two techniques is umbrella sampling (147, 148). Umbrella sampling is a common method used to calculate the free energy change in a specific process, dependent upon the reaction coordinate used. For a given system, a free energy barrier might exist that prevents a particle from undergoing some sort of transformation (Figure 1.6a). An example would be a barrier that prevents an unfolded protein from folding or preventing a peptide from binding to a lipid bilayer. In umbrella sampling, a harmonic potential is placed at specific steps along the reaction coordinate and these harmonic potentials allow the particle to explore the conformational space along the barrier (Figure 1.6b). In a normal MD simulation, the particle would have a very low probability of exploring these barriers because of the high free energy cost required to move up the barrier, so the limitations of computational techniques would prevent the particle from exploring the full conformational space (Figure 1.6a). However, the application of these harmonic potentials, or umbrellas, on top of the normal potential of the system forces the particle to move along the reaction coordinate and explore the conformational space of the barrier (Figure 1.6b). Using a series of these umbrellas between the initial and final state of the transformation, a full description of the transformation process can be obtained. Finally, the weighted histogram analysis method (150) can be employed to computationally reweight the effect of these umbrella potentials on the system and the probability of exploring a given state as a function of the reaction coordinate can be calculated. Using simple thermodynamics,

this probability can be converted to a free energy. Thus, using this umbrella sampling process (147, 148), the free energy along a given path is fully determined. When extended to umbrella sampling along two dimensions, a free energy surface can be calculated, which is even more instructive with regards to the dynamics of the system.

The umbrella sampling process does have its limitations as well. As free energy is calculated along a specific reaction coordinate, choice of that coordinate is crucial to understanding the system and is a necessary aspect for analyzing the results of the work. While some reaction coordinates, such as peptide binding to a lipid surface, can be fairly obvious, other reaction coordinates, such as in protein folding, can be very difficult to determine. Next, it is important the umbrellas along the reaction coordinate overlap. If there is not enough overlap between umbrellas, the particle will not be able to fully explore the entire barrier region and the calculated probability will not be complete. Finally, even within each umbrella, it is important that enough sampling is performed to fully explore that limited area. While conventional MD is commonly used within an umbrella, advanced techniques such as replica exchange are being combined with umbrella sampling (151) to improve sampling even further. Even considering these limitations, the increasingly parallel nature of current supercomputers makes umbrella sampling an ideal method for calculating the free energy change for a variety of biological processes.

*Replica Exchange Molecular Dynamics*

While umbrella sampling MD was used to calculate Aβ binding free energies and other free energy values for this thesis, replica exchange molecular dynamics (149, 152) was used to calculate Aβ structure. On the bilayer surface, specific peptide-lipid interactions can slow down the dynamics of peptide motion. Thus, over the timescales of reasonable MD simulations, the peptide would not have enough time to fully explore its conformational space on the bilayer surface. In order to calculate secondary structure on the bilayer surface and overcome this suppressed structural motion, replica exchange molecular dynamics was used.

Replica exchange molecular dynamics (149, 152) uses temperature or external potentials to overcome free energy barriers in a given process. The most common version of replica exchange used today employs temperature changes to overcome folding barriers (152). In replica exchange, a series of MD simulations are run in parallel at different temperatures. While the low temperature simulations are restricted by local free energy barriers, the energy imparted by the high temperatures in the highest temperature simulations allow the protein to fully explore the conformational space. Then, at a specific time step, the protein structures at adjacent temperatures are compared based on energy of the conformations and exchanged dependent upon a set of thermodynamic criteria usually dictated by the Metropolis conditions (149, 152). In short, as the peptide explores the conformational space at high temperature and finds new, minimum energy structures, the minimum energy structures will be cycled down to the lowest temperature in a thermodynamically consistent process. Thus, by analyzing

the system at the intended low temperature, a more expansive thermodynamic average for a given quantity can be calculated, as the system will explore multiple free energy basins instead of just one in a conventional MD simulation. While a trajectory followed at a specific temperature will not be fully linear as a function of time, a thermodynamic average, such as average secondary structure, will be much more accurate than one calculated for a conventional MD simulation.

Much like umbrella sampling MD, replica exchange MD has limitations due to the nature of its implementation (153). It is necessary that the temperatures are appropriately spaced so that exchanges between systems at adjacent temperatures will occur often to allow for expansive sampling (153). Also, within each replica, conventional MD needs to be run for enough time to allow the system to fully explore the conformational space available at that temperature (153). Finally, while these systems have been adapted for extensive use in solution, the application to membrane systems is limited. As membranes dissolve at high temperatures, it is difficult to have both a fully atomic description of a membrane and a substantial range of temperatures. Previous simulations with explicit membranes (151) have required very stringent constraints that prevent lipid motion within the membrane. In chapter 3, we discuss an implementation of replica exchange with an all-atom membrane that is able to circumvent these limitations. With the use of both umbrella sampling MD and replica exchange MD, the simulations described in this thesis involving Aβ-membrane model systems are able to overcome some of the significant limitations inherent to previously performed MD simulations.

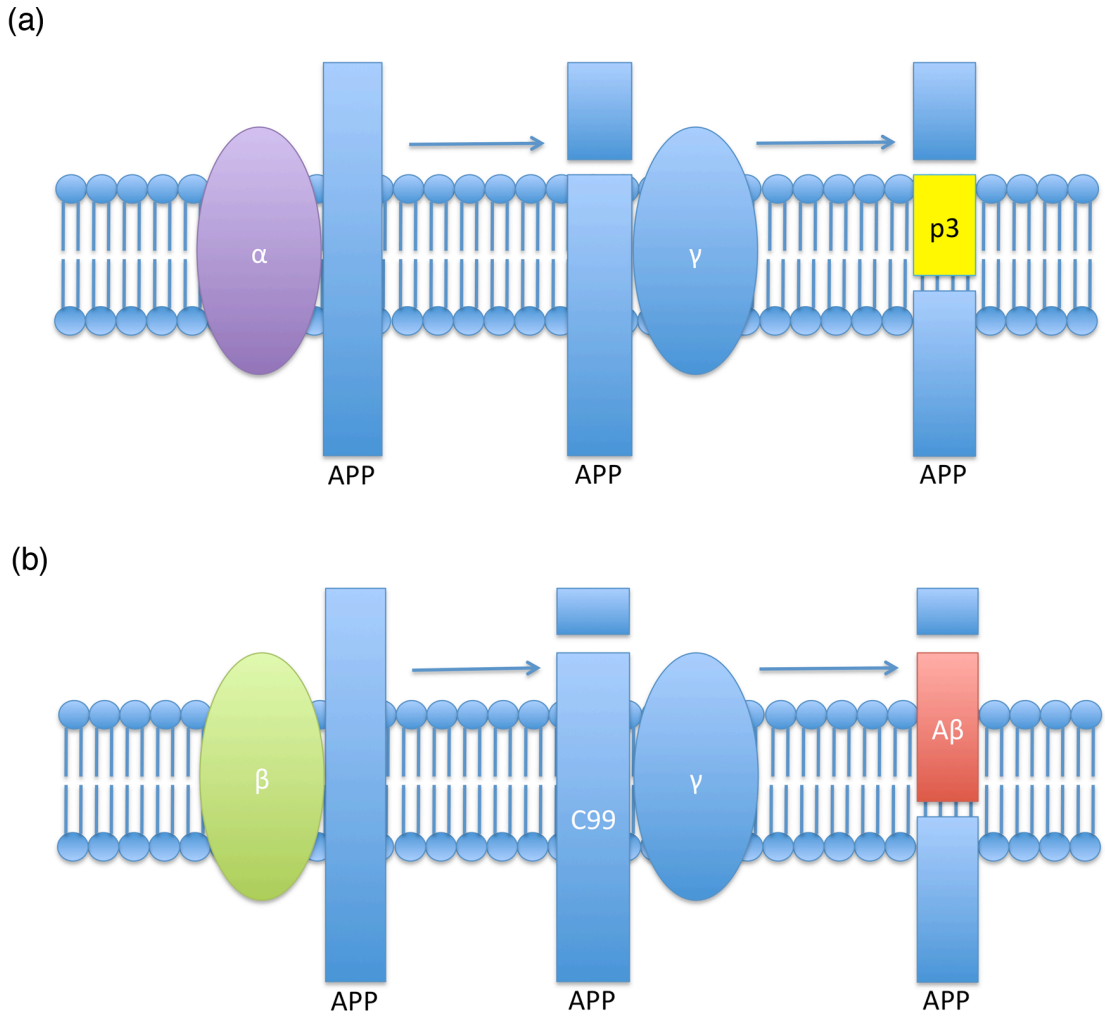


**Figure 1.1** Schematic depiction of Amyloid Precursor Protein processing by secretases in the cell membrane. The normal processing (a) of APP results in production of the non-toxic p3 fragment. Alternative processing (b) of APP results in production of the 38-43 residue Aβ peptide.

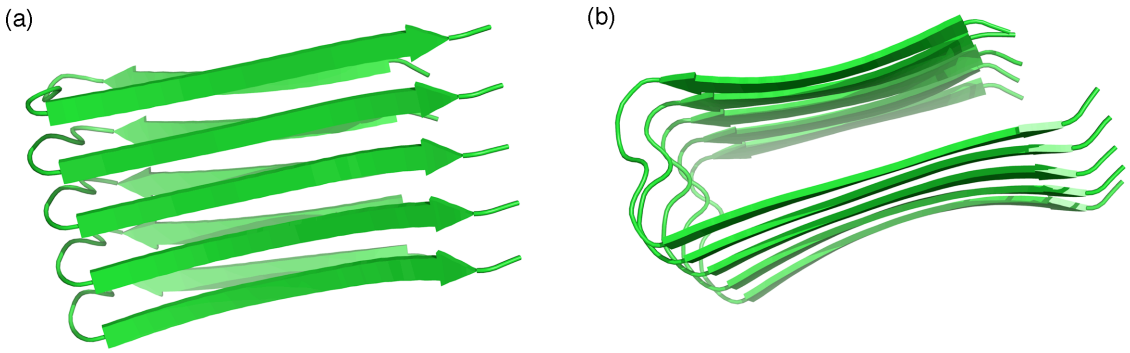


**Figure 1.2** Representation of one proposed structure for a filament within an Aβ fibril determined using NMR depicted as a (a) side and (b) top view. These structures are derived from PDB code 2BEG (49).

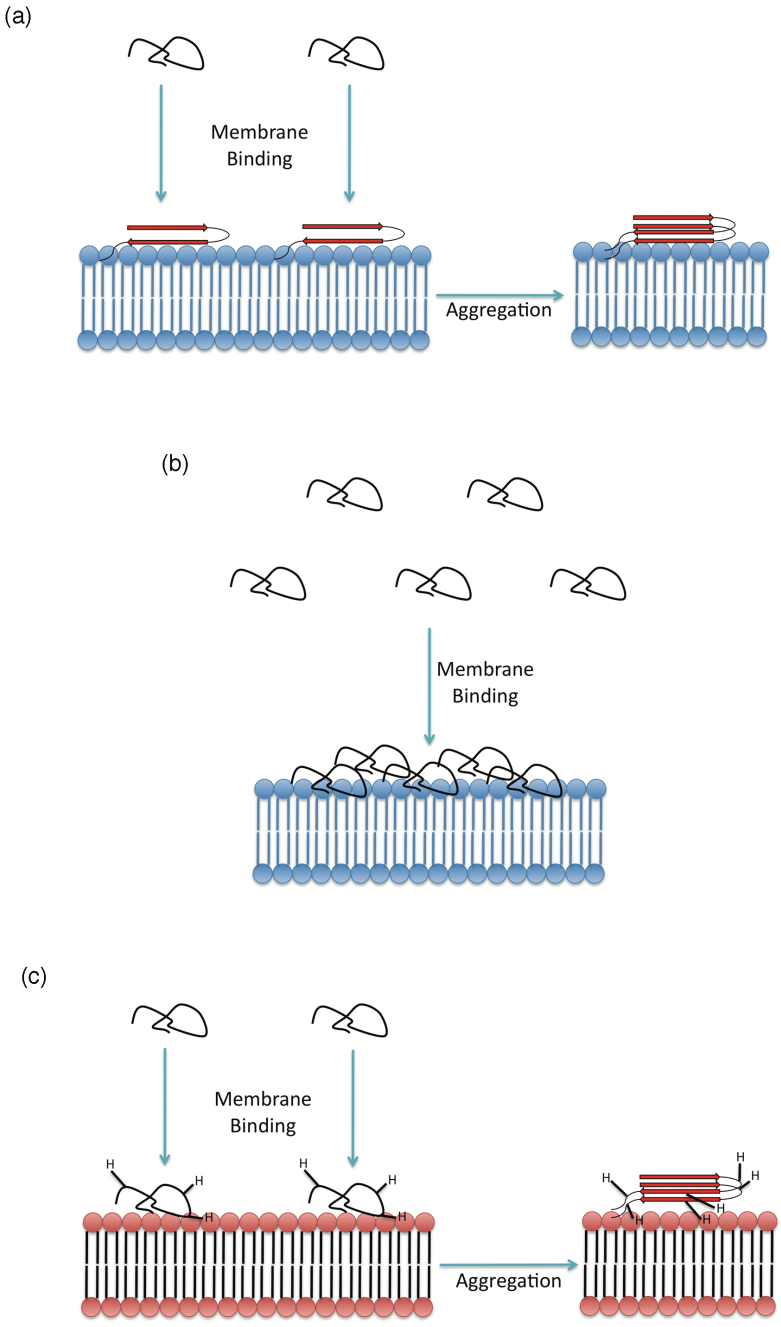


**Figure 1.3** Physical methods in which membranes can effect protein aggregation. (a) The membrane can favor formation of a folded structure from an unfolded monomer that promotes aggregation. (b) Membrane binding locally increases protein concentration by limiting motion to a restricted area. (c) Protein binding to anionic lipids (represented by the red spheres/headgroups) leads to protonation of certain residues due to the local decrease in pH.

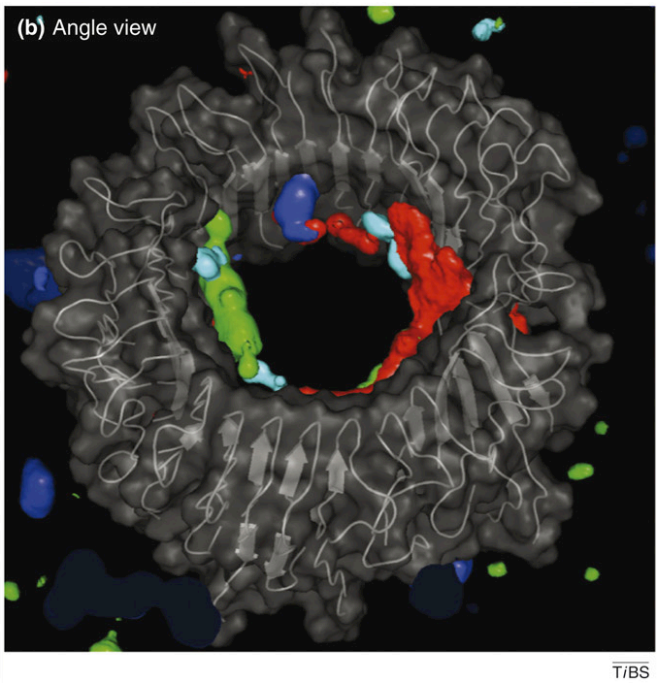


**Figure 1.4** Predicted structure for a transmembrane pore of 24 Aβ(17-42) peptides taken from simulation. The Aβ(17-42) peptides have an imposed β-hairpin structure. Reprinted from Trends in Biochemical Sciences, Vol. 33, Issue 2, H. Jang, J. Zheng, R. Lal, and R. Nussinov, New structures help the modeling of toxic amyloidβ ion channels, pages 91-100, Copyright (2007) with permission from Elsevier.

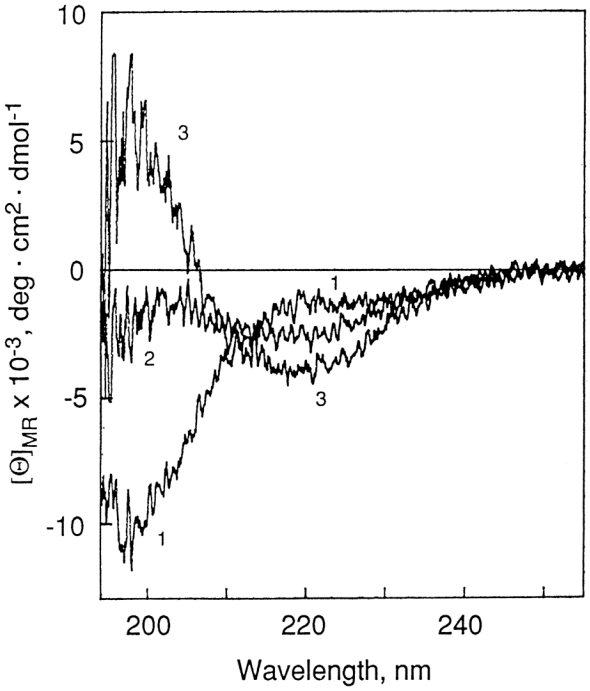


**Figure 1.5** Circular dichroism spectra of Aβ(1-40) mixed with POPC/POPG vesicles (75/25 mol/mol lipid mixture). Curve 1 represents a lipid:peptide ratio of 0 (pure Aβ). Curve 2 represents a lipid:peptide ratio of 22 and curve 3 represents a lipid:peptide ratio of 55. When mixed with the POPC/POPG vesicles, Aβ converts from a random coil to predominantly β structure. Reprinted from Journal of Molecular Biology, Vol. 252, Issue 6, E. Terzi, G. Hölzemann, and J. Seelig, Self-Association of β-Amyloid Peptide (1-42) in Solution and Binding to Lipid Membranes, pages 633-642, Copyright (1995) with permission from Elsevier.

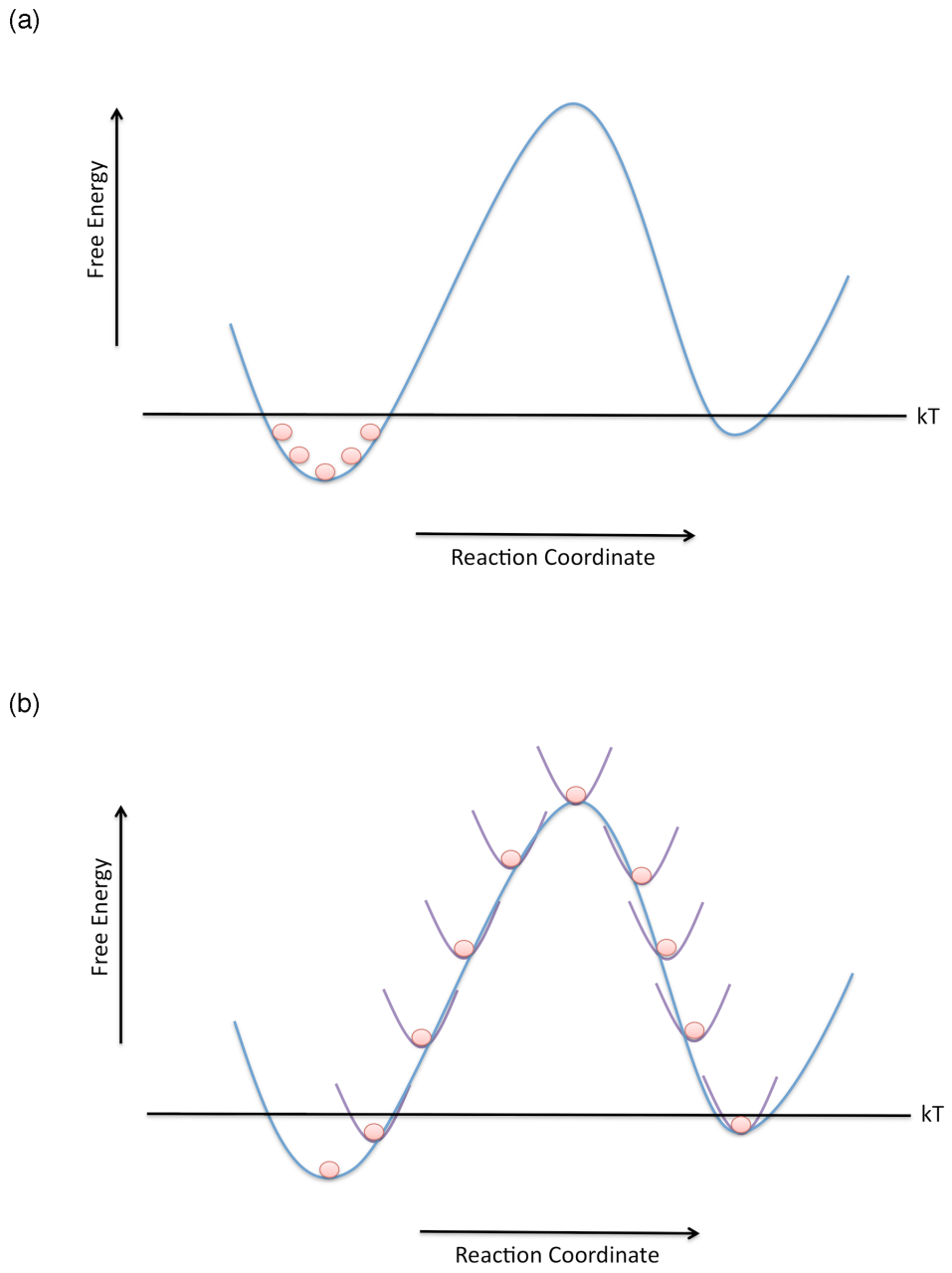


**Figure 1.6** A schematic of the umbrella sampling molecular dynamics technique. In regular molecular dynamics (a), the particle is not able to transverse the barrier and is restricted by the energy provided in kT. Using umbrella sampling (b), the potentials placed along the reaction coordinate allow the particle to explore the reaction coordinate along the entire barrier.

**Chapter 2:**

# Interaction between Amyloid-β (1-42) Peptide and Phospholipid Bilayers: A Molecular Dynamics Study

Charles H. Davis[1] and Max L. Berkowitz[2]

[1]*Department of Biochemistry and Biophysics, University of North Carolina at Chapel Hill, Chapel Hill, North Carolina, 27599*
[2]*Department of Chemistry, University of North Carolina at Chapel Hill, Chapel Hill, North Carolina, 27599*

Published in *Biophysical Journal*, 96, 785-797 (2009)

**Abstract**

The Amyloid-β (Aβ) peptide is a key aggregate species in Alzheimer's disease. While important aspects of Aβ peptide aggregation are understood, the initial stage of aggregation from monomer to oligomer is still not clear. One potential mediator of this early aggregation process is interactions of Aβ with anionic cell membranes. We use unconstrained and umbrella sampling molecular dynamics simulations to investigate interactions between the 42-amino acid Aβ peptide and model bilayers of zwitterionic dipalmitoylphophatidylcholine (DPPC) lipids and anionic dioleoylphosphatidylserine (DOPS) lipids. Using these methods, we determine that Aβ is attracted to the surface of DPPC and DOPS bilayers over the small length scales used in these simulations. We also find supporting evidence that the charge on both the bilayer surface and the peptide affects the free energy of binding of the peptide to the bilayer surface and the distribution of the peptide on the bilayer surface. Our work demonstrates that interactions between the Aβ peptide and lipid bilayer promotes a peptide distribution on the bilayer surface that is prone to peptide-peptide interactions, which can influence the propensity of Aβ to aggregate into higher order structures.

## Introduction

Neurodegenerative disorders, including Alzheimer's disease, share a similar mechanism of toxicity (45, 154), namely aggregation of unfolded peptides into amorphous oligomers that coalesce to form an ordered fibril. It is of great importance to understand both the exact steps behind fibril formation from the monomer state and the means of toxicity in these diseases. By further defining integral steps in the aggregation pathway for neurodegenerative disorders, in particular Alzheimer's disease in this work, greater insight into the toxic mechanisms and potential therapeutic approaches for a host of fatal diseases will be gained.

One of the major aggregate species in Alzheimer's disease is the Amyloid-β peptide (Aβ) (3, 11, 12, 40). Aβ is a 38-42 amino acid cleavage product of the amyloid precursor protein, a large transmembrane protein of unknown function in the cell (3, 11, 12). Aβ contains two domains: a charged domain at the N-terminus and a hydrophobic domain situated at the C-terminus. NMR results (26, 27) show that Aβ has a random coil structure in solution at pH7. Upon onset of Alzheimer's disease, Aβ forms soluble oligomers that aggregate to form ordered fibrils with β-sheet morphology in the hydrophobic domain, as determined through solid-state NMR and electron microscopy (46, 49). In this aggregation process, the steps involved in the initiation of aggregation from monomers to small oligomer structures are not well determined. There are many aspects of cellular function that may play a significant role in the early stages of Aβ aggregation, such as cellular pH (62), salt concentration (63), covalent attachments of Aβ

due to oxidation and interactions of Aβ with metal ions (64). However, one hypothesis (4, 5, 66) that shows promise for explaining both the early steps of aggregation and the effect of certain risk factors in Alzheimer's disease is the interaction between Aβ and cellular membranes. This hypothesis postulates that interactions between Aβ and lipids promote conversion of disordered Aβ into a partially folded intermediate that will aggregate under favorable conditions. The membrane can affect soluble proteins through a variety of ways: electrostatic interactions between amino acids and charged headgroup (4, 5, 66-68), new partially folded or unfolded free energy minima at the surface (4, 5, 66-68), increased aggregation due to faster diffusion over a 2-dimensional surface (4, 5, 66-68) and a lower surface pH due to anionic lipid headgroups (57, 67, 68). In this work, we will investigate these lipid-peptide interactions using molecular dynamics simulations and identify properties of lipid bilayers that may promote peptide-peptide interactions characteristic of aggregation.

Experimental investigations have been able to replicate the aggregation of Aβ peptides *in vitro* quite accurately. Most experimental conditions between *in vivo* and *in vitro* aggregation are in agreement; however, one significant difference is that *in vitro* aggregation requires a much higher peptide concentration (approximately μM) to induce aggregation than *in vivo* aggregation (approximately sub-μM peptide concentration) (58, 59, 82). One potential hypothesis (4, 5, 66) to explain this discrepancy proposes that interactions with the cell membrane are promoting altered function and aggregation *in vivo*. This hypothesis is well founded in biology through signal peptide binding to bilayers during signaling cascades (155, 156) and in peptide-lipid binding in toxin-related

cell death (155, 156). Early experiments using circular dichroism (6) spectroscopy to follow structural changes for Aβ incubated with lipid vesicles demonstrated that zwitterionic lipids headgroups (57, 58, 82), such as phosphatidycholine, did not significantly affect peptide structure. However, when Aβ was incubated with anionic lipid headgroups (57, 58, 82), such as phosphotidylserine, a clear conversion from a random coil to β-structure was observed. Further, imaging experiments demonstrated that Aβ was aggregating into fibrils at concentrations near *in vivo* aggregation conditions in the presence of vesicles (83, 157). $^{31}$P-NMR (81) and x-ray reflectivity (59) results have shown that Aβ peptides are interacting with anionic lipids and leading to significant alteration of properties of the bilayer itself. These results provide a clear demonstration that lipids can fundamentally impact the aggregation pathway for Aβ; yet, they are not able to determine the exact interactions that are occurring on the bilayer surface that force this conformational change. Some controversies (4) also exist regarding the extent of interactions between Aβ and anionic lipids. In some experimental work, a claim is made that Aβ-anionic lipid interactions are weak or non-existent under certain conditions (4). Therefore, detailed understanding of interactions between Aβ and lipids at the bilayer surface will be integral to comprehending the basis for these controversies that exist in experiments.

While most experimental approaches do not have the necessary resolution to determine direct protein-lipid interactions on a single molecule level, molecular dynamics (MD) simulations provide an ideal approach to this system. MD with explicit (158-161) and implicit (159, 162-164) solvent and free energy (160, 162, 164) calculations have

been used previously for studying peptide-lipid interactions with good agreement to experimental results. Further, MD has been used extensively with Aβ (29, 69, 129-131, 136, 165-170). Single peptide MD simulations confirm a random coil structure for Aβ in solution; however, transient β-hairpin structure is seen in longer time (69, 130, 131, 165, 167), replica exchange (29, 170) and low pH (167) simulations. Previous MD simulations of Aβ with lipid bilayers (69, 136) have investigated the stability of a preinserted Aβ in a zwitterionic bilayer and have not investigated the effect of headgroup charge and other bilayer properties on Aβ structure or stability near the bilayer surface. This previous computational work with Aβ further supports the use of MD for investigating unanswered details of Aβ peptide-lipid interactions.

To examine peptide-lipid interactions in this system, we present here calculations of free energies of peptide binding to the bilayer surface for various lipid headgroup charges and peptide charges. The chosen lipids for these studies will have zwitterionic phosphatidylcholine (PC) and anionic phosphatidylserine (34) headgroups. Lipids with PC headgroups are the most abundant lipids in neural membranes (96). Lipids with anionic PS headgroups play an integral role in localization to cell membranes and programmed cellular death mechanisms (99). Anionic lipids decrease local surface pH (57, 67, 68), so varying both lipid charge and peptide charge is essential to understanding the influence of electrostatics on the system. By investigating both electrostatic and hydrophobic aspects of the Aβ-bilayer interaction, a more detailed picture of the influence of membranes on Aβ aggregation will be obtained. The results from this work will help to determine the validity of the cell membrane as a catalytic element in Aβ

aggregation and, with knowledge of the toxic mechanism of this class of similar neurodegenerative diseases, will assist in future treatment and prevention of these diseases.

## Materials and Methods

*Simulations in Solution*

Two structures were chosen for simulations of the 42 amino acid Aβ peptide both in solution and near the bilayer surface. By using two structures, some bias inherent with having an ordered starting structure will be eliminated. The first structure is PDB code 1Z0Q and represents a random coil with some helix content as determined by NMR (27). The structure used in calculations was the first NMR structure (27) given in the file deposited in the PDB. The second structure is PDB code 2BEG, which is one peptide taken from the structure of an Aβ fibril as determined by solid state NMR (49). Residues 1-16 in the N-terminal tail were unstructured and were not included in the PDB file. Therefore, these residues were added using the SYBYL software program (Tripos Inc., St. Louis, MO). This β-hairpin structure is controversial, as it is not universally accepted as the accurate monomer structure in fibrils (46). Recent results (46) have shown that the β-sheet structure detected in fibrils may be shared between two monomers. However, for this work, the β-hairpin structure is used as it represents potential β-structure that can be formed from a monomer of Aβ. All structures from the PDB were edited using GROMACS software to convert the structures to a united atom format described by the GROMACS force field (143, 144). Along with using 2 initial structures for simulations, three charge states of Aβ were used. At pH7, Aβ has a -3 charge due to 6 aspartic and glutamic acid residues and 3 lysine and arginine residues, assuming uncharged termini. At pH~5, three histidine residues become protonated (57) to give Aβ a neutral charge. Then, at low pHs, the aspartic and glutamic acid residues are protonated to give Aβ a +6 charge. The termini were uncharged in these simulations so that the effect of peptide

charge on the peptide-lipid interactions was isolated to the amino acid sidechains only. GROMACS utilities (143, 144) were used to change the protonation state of relevant histidines, aspartic acid and glutamic acid residues to give the appropriate charge for the peptide state. The combination of 2 initial structures and 3 pH states for each structure produced a set of 6 simulations performed in solution.

Each structure was solvated in a 6.4nm x 6.4nm x 8.1nm box, with $Na^+$ or $Cl^-$ counterions added to the system to balance peptide charge and NaCl salt added to produce a near physiological concentration of 0.1M NaCl (Table 2.1a). The system was equilibrated with a 3ns molecular dynamics (MD) simulation, then 80ns MD simulations were performed for analysis. Temperature was held constant at 323K using a Nose-Hoover (171) scheme with a relaxation time of 0.5 ps under constant volume (NVT) conditions. All bonds in the system were constrained with the LINCS algorithm (172), which allowed a time step of 3.5 fs. Long range electrostatics were handled using the SPME algorithm (146) and periodic boundary conditions were used in all three dimensions. The SPC/E model (173) of water was used for all simulations. Secondary structure was calculated using the DSSP package (174) in GROMACS.

*Unconstrained Simulations on DPPC and DOPS*

The 6 conditions used for Aβ simulations in solution were again used for simulations near a dipalmitoylphosphatidylcholine (DPPC) and dioleylphosphatidylserine (DOPS) bilayer. While direct biological considerations would promote use of lipids such as palmitoyloleoylphosphatidylcholine (POPC) and dipalmitoylphophatidylserine (DPPS)

for our simulations, bilayers containing these lipids differ substantially in their area per headgroup. Since surface charge density is an important parameter for studying electrostatics, we decided to choose PC and PS lipids that have very close areas: dipalmitoylphosphatidylcholine (DPPC) and dioleylphosphatidylserine (DOPS). Thus, our model lipid bilayers still contain biologically relevant headgroups.

Initially, both bilayers were brought to an equilibrated state before placing a peptide near the bilayer. For both the DPPC and DOPS bilayers, a single lipid molecule was built using the SYBYL package, which was then used to create a symmetric 128 lipid bilayer. The DPPC bilayer was equilibrated for 30ns with 3,654 water molecules on the bilayer. The computational details for these simulations are similar to the previous simulations with Aβ in solution; however, a constant pressure ensemble (NPT) was used to allow the bilayer to reach an appropriate area per headgroup. The Parrinello-Rahman pressure coupling scheme (175) was used with a barostat relaxation time of 2.0 ps at a pressure of 1atm. Further, the lipid force field parameters were taken from the work of Berger (176). These simulations used a time step of 4fs. The DPPC equilibration resulted in an area per headgroup value of 63.6 $Å^2$, which is in agreement with previous experimental (177) and computational (178) results. The DOPS bilayer was also equilibrated for 30ns with 128 $Na^+$ counterions and 4102 water molecules on the bilayer. The DOPS bilayer equilibration resulted in an area per headgroup value of 63.9 $Å^2$, which is also in agreement with experimental (179) and computational (180) results. Once the bilayers were equilibrated, simulations could be performed with Aβ near the bilayer surface. Both initial starting structures of Aβ at all 3 pH values were solvated

with SPC/E water molecules, $Na^+$ or $Cl^-$ counterions and NaCl salt in a 6.4nm x 6.4nm x 4.5nm box. The solvated peptide box was then placed near the surface of the equilibrated bilayer. To ensure that the system was symmetric except for the peptide, a box of SPC/E water with similar ion concentrations was placed below the DPPC and DOPS bilayers to give 1 peptide with SPC/E water molecules, 128 lipid molecules, and $Na^+/Cl^-$ ions in a 6.4nm x 6.4nm x 16.3nm box for DPPC simulations (Table 2.1b) and 1 peptide with SPC/E water molecules, 128 lipid molecules, and $Na^+/Cl^-$ ions in a 6.4nm x 6.4nm x 16.8nm box for DOPS simulations (Table 2.1c). For these simulations on DPPC and DOPS bilayers, the peptide center of mass was placed at a distance of 6.0nm and 6.2nm, respectively, from the bilayer center of mass. This distance ensured that the peptide was completely surrounded by solvent and that no portion of the peptide would be influenced by short-range interactions with the bilayer surface due to the initial configuration of the simulation. The Aβ-bilayer system was then simulated, after energy minimization, for 80ns. Simulation conditions were similar to previously described simulations. A constant volume (NVT) ensemble was used with a time step of 3fs at a constant temperature of 323K with periodic boundary conditions along all three dimensions. All secondary structure analysis was performed using the DSSP package (174) in GROMACS.

*Umbrella Sampling Simulations with Aβ near DPPC and DOPS*

To calculate free energies of binding of Aβ to the surface of DPPC and DOPS bilayers, umbrella sampling (147, 148) was performed. The previous experimental evidence has demonstrated that Aβ had a random coil structure (26, 27) in solution.

Therefore, only one starting structure was used for umbrella sampling simulations as these calculations were setup to closely replicate an Aβ peptide approaching a bilayer from solution. The final structures from the simulations using the β-hairpin initial configuration of Aβ in solution were all predominately random coil at the end of the 80ns simulation and thus were ideal as starting structures for these umbrella sampling calculations. To improve sampling, three initial configurations were used for the Aβ-bilayer system. First, the peptide was placed so that it was parallel to the bilayer surface and that neither the charged N-terminus nor hydrophobic C-terminus was closer to the bilayer surface. Then, the peptide underwent rigid-body rotation so that either the N-terminus or C-terminus was close to the bilayer surface. While these extra initial conditions cannot fully overcome sampling issues associated with limited timescales of MD simulations, the multiple free energy calculations from the 3 initial conditions at each pH on DPPC and DOPS will improve the validity of the calculated free energy profile. For each initial configuration, the random coil peptide was solvated with SPC/E water molecules, $Na^+$ or $Cl^-$ counterions and NaCl salt in a 6.4nm x 6.4nm x 4.2 nm box. This peptide box was then placed above the equilibrated DPPC or DOPS bilayers and a similar box of SPC/E water and ions without the peptide was placed below the bilayer for symmetry purposes. This resulted in a system of 1 Aβ peptide above a bilayer of 128 lipids with SPC/E water molecules and $Na^+$ or $Cl^-$ ions in a 6.3nm x 6.3nm x 15.8nm box for simulations with DPPC (Table 2.2a) and 1 peptide above a bilayer of 128 lipids with SPC/E water molecules and $Na^+$ or $Cl^-$ ions in a 6.3nm x 6.3nm x 16.1nm box for simulations with DOPS (Table 2.2b). The center of mass separation for Aβ and the DPPC or DOPS bilayer in this initial configuration file was between 6.3nm to 6.6nm.

For each initial configuration, a short 3ns equilibration simulation was performed. In these simulations, the z-dimension of the peptide was constrained so that the peptide-bilayer center of mass separation would remain greater then 6.0nm but the system would still be able to equilibrate. The simulation details of this short equilibration were the same as the previous unconstrained simulations except that a 1fs timestep was used.

For the umbrella sampling (147, 148), 14 windows were chosen. These windows spanned peptide-bilayer center of mass separations from 6.0nm to 2.1nm. Therefore, the spacing between each window was 0.3nm, which would enable sufficient sampling. Further, this range of distance allows the peptide to be pulled from a full solvated, solution-like environment onto the surface of the bilayer then into the interfacial region of the bilayer. The pulling was accomplished by applying a harmonic force with a force constant of 500 kJ/(mol*nm$^2$). For each window with the parallel initial configuration, an 80ns MD simulation was performed. After performing error analysis on the 80ns MD simulations, it was determined that 40ns simulations were sufficient to provide an error of $\pm$4.1kcal/mol for the free energy of binding, which is adequate for the free energies calculated in this work. Error analysis was performed by using a block error analysis scheme. In this scheme, a 40ns simulation was broken into smaller blocks and the average value and standard deviation for the potential of mean force at each center of mass separation was calculated. The maximum standard deviation converged to 4.1kcal/mol after splitting the simulation into blocks up to a total of 30 blocks. Thus, only 40ns MD simulations were performed in each window for the N-terminus down and C-terminus down initial configurations. Computational details of the simulations

performed in each window are exactly the same as in the previous unconstrained simulations except that a 3fs timestep was used. Again, the system utilized a constant volume (NVT) ensemble with periodic boundary conditions along all 3 dimensions with a constant temperature of 323K. For each window, secondary structure was calculated using the DSSP program (174) in GROMACS. Free energy was calculated for each configuration using the Weighted Histogram Analysis Method (WHAM) (150) adapted for in-house code. The center of mass fluctuations from the second 40ns of the parallel initial configuration MD simulations were used for free energy calculations to maintain a consistent 40ns simulation time amongst all initial configurations, while the center of mass fluctuations from the full 40ns MD simulations for the N-terminus down and C-terminus down initial configurations were used for free energy calculations. In order to calculate an averaged free energy of binding for the three initial configurations of Aβ at each pH on either DPPC or DOPS, the center of mass fluctuations for all three initial configurations were combined, then analyzed using WHAM. If the free energies for each initial configuration were calculated with WHAM then averaged by obtaining an unweighted average of the sum of the exponentials of individual potentials of mean force, as previously described (181), one can also get a potential of mean force if enough orientationally dependent potentials are included in the unweighted average, and if the peptide is a rigid body. Since both of these conditions are strongly violated in our case, we expect that this method will produce a large error. Thus, free energies were calculated by combining center of mass fluctuations then analyzing with WHAM. Nevertheless, we also calculated the free energy curves for each initial orientation of the peptide to perform a contact value analysis. A contact value for Aβ binding to the bilayer was calculated for

each umbrella sampling window throughout the umbrella sampling simulations. Contact was defined as a separation of less than 5Å in the Z-coordinate between any atom on a given amino acid and the average position of the phosphate atom in the lipid headgroup, which was calculated using the 64 phosphate atoms on the bilayer leaflet that Aβ was closest to. The residue was given a contact value of 1 if any atom in the amino acid was within 5Å of the average phosphate and a contact value of 0 if it was not. Contact values were calculated for all amino acids in Aβ and averaged over all timesteps in the simulation, which gives contact values between 0 (no contact) and 42 (full contact/binding) for a given umbrella sampling window. The contact values were then used to calculate a two dimensional free energy surface using the unweighted probabilities obtained from the previously-mentioned WHAM calculations on the center of mass separation coordinate and conditional probabilities calculated from the distribution of contact scores within each umbrella sampling window.

## Results

*Simulations in Solution*

Initial simulations were performed with the 42-amino acid Aβ peptide in solution. These simulations were used as a test of the protein force field to determine if experimental solution structures would be obtained during simulations starting from ordered structures. Further, these simulations provide a baseline for comparison with the results from simulations of Aβ-lipid systems. Two initial structures were chosen for these simulations to eliminate any bias due to starting configuration (Figure 2.1, see Methods for further details of structures). Both structures were fully solvated with appropriate counterions and with NaCl salt. The simulations were performed with a 1ns equilibration followed by a full 80ns simulation. The secondary structure of both the helix and β-hairpin starting structures changed drastically throughout simulation. Both the helix and the β-hairpin structures lost the majority of the ordered structure content to become a full random coil (Table 2.3). These results agree with previous experimental NMR (26, 27) and CD (27) results, as well as previous simulations (69, 130, 131, 165, 167, 170), which show that Aβ has a random coil structure in solution at pH7.

In the studies of Aβ interactions with bilayers of various lipid headgroup charge, lipids with anionic headgroups were used as a model system. It has been shown that anionic lipids can lower the pH (57, 67, 68) of solution near the bilayer, which will in turn alter the protonation state of proteins near these bilayers. Calculations (57) fitting experimental data with Aβ bound to anionic palmitoyloleoylphosphatidylglycerol (POPG) lipids show that protonation of the 3 histidine residues upon binding does occur,

thus further supporting the use of multiple pH states for studying Aβ binding. Therefore, we also investigated various protonation states of Aβ near bilayers. Similar to the previous simulations of Aβ in solution at pH7, simulations of Aβ at different protonation states in solution were performed for comparison to simulations of the Aβ-lipid bilayer systems. Aβ can undergo two major protonation events (termed pH5 and pH3 simulations) which result in a neutral and +6 net charge of the peptide (see Methods section for further details). Not only will studies with these 3 pH states provide insight into the effect of pH on Aβ structure in solution and near lipid bilayers, the use of an anionic, neutral and cationic peptide will demonstrate the direct importance of electrostatics on peptide-charged bilayer interactions.

From our simulations, we observed that both initial peptide structures at pH5 and the helical peptide at pH3 lost essentially all secondary structure during the simulation to result in a random coil as the final structure (Table 2.3). For the β-hairpin starting structure at pH3, the final structure was not completely random coil but had some transient turn content. Thus, this final configuration can be considered as having some transient order as a turn (182) is not purely random but is a somewhat intermediate structure between a helix and a sheet. Nevertheless, this amount of ordered structure at pH3 is small and it can be concluded that a random coil was the primary structure for Aβ in solution regardless of the starting structure used in the simulation and the total charge on the peptide.

*Simulations near DPPC and DOPS bilayers*

The results from the simulations of Aβ in solution were then extended to simulations of Aβ with a zwitterionic dipalmitoylphosphatidylcholine (DPPC) bilayer and an anionic dioleylphosphatidylserine (DOPS) bilayer. For simulations on the fluid DPPC and DOPS bilayers, both the helix starting structure and β-hairpin starting structure were again used. Also, simulations were performed at all three charge states for the Aβ peptide. While a DPPC bilayer would not affect local pH (57) and thus not induce protonation state changes on Aβ, performing these simulations of Aβ near neutral lipids will provide insight into the role of the protonation state on the structure of Aβ near a surface it should not interact with extensively. The results of the simulations in solution demonstrated that 80ns was adequate simulation time to allow for the peptide to undergo significant conformational flexibility considering computational restraints. While it was possible for Aβ to pass through the upper periodic boundary and interact with the bottom leaflet of the bilayer in the chosen simulation setup, this did not occur during simulations as Aβ was clearly attracted to the surface of the DPPC bilayer and was near the upper leaflet surface for the majority of the simulation time. Near the DPPC bilayer, the helix starting structure at each peptide pH unfolded into a structure dominated by random coil and turns, while the β-hairpin starting structure unfolded into a full random coil, similar to the simulations performed in solution (Table 2.3). For these simulations, it is clear that, while Aβ was attracted to DPPC near the bilayer surface, the DPPC bilayer is not affecting the overall secondary structure content of peptide. These results agree with previous experimental results (57, 58, 82) that show vesicles composed of neutral lipids do not alter the secondary structure of Aβ when mixed. Near the DOPS bilayer,

analogous to the simulations with DPPC, Aβ was attracted to the surface of the bilayer in all simulations, independent of peptide charge. For simulations involving the helix starting structure at all 3 pHs, the DOPS bilayer strongly enhanced the helical structure, especially near the N-terminus of the peptide (Table 2.3). For the β-hairpin starting structure, the β-hairpin configuration was mostly retained at pH7 and pH5 with some turn structure also developing. At pH3, the β-hairpin did unfold slightly into a structure dominated by turns. Therefore, it appears that the DOPS bilayer is influencing the secondary structure of Aβ so that the random coil observed in solution or near a zwitterionic bilayer is not formed. These results agree to an extent with previous experimental measurements (57, 58, 82), which show significant secondary structure in Aβ near anionic lipids; however, the time restrictions inherent in MD simulations prevent observation of any significant secondary structure change on the surface of DOPS bilayers. These previous experimental measurements demonstrated that a random coil Aβ in solution will be converted to a β-sheet dominated structure upon addition of anionic vesicles (57, 58, 82, 183), which can be converted to an α-helix upon further addition of anionic vesicles. While the time constraints of these simulations do limit potential structural conversion for a single peptide, they show the anionic bilayer stabilizes both β-structure and helix structure. The qualitative results of simulations with Aβ near DPPC and DOPS prompted us to further study this system using a more quantitative method to help understand why Aβ appeared to be attracted to the bilayer surface regardless of the peptide charge or bilayer charge.

*Umbrella Sampling Simulations*

To describe the Aβ-bilayer interactions using a quantitative method, umbrella sampling techniques were used. Umbrella sampling (147, 148, 150) determines a free energy of binding of Aβ to the surface of the lipid bilayer using a systematic routine. For these simulations, the initial Aβ structure was taken to be the final structure of the Aβ simulations in solution from starting β-hairpin structures. The final structures of the Aβ β-hairpin simulations in solution had very little ordered structure and were predominantly random coil. Therefore, the use of these random coil starting structures for umbrella sampling simulations will closely mimic the experimental conditions of an Aβ peptide in solution, which has a mostly random coil structure (26, 27), approaching a cell membrane. Further, for each starting structure, three initial configurations of Aβ with respect to the bilayer surface were used; one with the N-terminus of Aβ close to the bilayer surface, one with the C-terminus of Aβ close to the bilayer surface and one in which Aβ is parallel to the bilayer surface so neither terminus is closer to the bilayer. The use of three initial configurations will improve the sampling of the free energy calculations (See Methods section for further details). From these simulations, a free energy of binding for Aβ from solution to the bilayer surface can be calculated and compared to experimental predictions.

Calculated average free energies of binding are listed in Table 2.4 and presented as free energy profiles in Figure 2.2. As was predicted from the unconstrained molecular dynamics simulations, Aβ was attracted to the bilayer surface independent of Aβ charge or bilayer headgroup charge. For calculations on the DPPC bilayer, Aβ at all pH values

had $\Delta G_{binding} \approx$ -16kcal/mol to -19kcal/mol ($\Delta A$ was actually obtained in our calculations, but, as common for condensed systems, $\Delta G \approx \Delta A$). This reduces to a $\Delta G_{binding} \approx$ -0.4kcal/mol*residue, which is close to previous experimental predictions for peptide-lipid binding interactions (183). For calculations on the DOPS bilayer, the free energy of binding did depend significantly on the Aβ charge. The free energy of binding for the pH5 and pH3 Aβ were within error, $\pm$4.1kcal/mol as described in the Methods section, of free energies of binding for Aβ with DPPC. However, the free energy for binding of the anionic pH7 peptide to DOPS was less then half of the binding free energy of the pH5 and pH3 peptide to DOPS. This discrepancy in binding free energies is likely due to the interplay of electrostatic interactions with lipid headgroups and interactions between the hydrophobic residues of Aβ and the interfacial region of the bilayer. For the highly negative free energies of binding on DPPC or DOPS, the majority of favorable interactions between the peptide and bilayer, which lead to the large, negative free energy of association, are derived from these interactions between the hydrophobic residues of Aβ and the interfacial region of the bilayer. However, for the pH7 peptide binding to DOPS, while the hydrophobic C-terminus of the peptide allows for a negative free energy of association for Aβ to DOPS, the anionic DOPS headgroups, even partially screened by $Na^+$ counterions, interact strongly with the charged N-terminus of Aβ and prevent the full association of the peptide with the interfacial portions of DOPS.

Along with magnitude of the free energy of binding, the free energy profiles from these umbrella sampling calculations provide further information about the system (Figure 2.2). The free energy profiles supply some insight into the length scales for

binding events. In the profiles, the free energy decreases smoothly as the peptide approaches the bilayer. For some of the Aβ-bilayer combinations, such as Aβ at pH3 approaching a DOPS bilayer, small barriers are present in the free energy profiles. These barriers have values in the range of 0.1 kcal/mol to 0.2 kcal/mol and are therefore insignificant at the considered temperature. Thus, the point in the free energy curve in which the free energy begins to decrease marks the distance where Aβ becomes significantly attracted to the bilayer surface. For Aβ binding to the DPPC bilayer and the pH7 peptide binding to the DOPS bilayer, this distance is at a center of mass separation of 4.5nm. For, the pH5 and pH3 peptide binding to the DOPS bilayer, this distance is at a center of mass separation of 5.1nm. Considering a bilayer leaflet thickness of ~2-2.5nm, the center of mass of the peptide is separated from the bilayer surface by over 2nm at these center of mass distances, which is a significant length and not appropriate for the interactions with the interfacial region of the bilayer that may be driving this binding. Thus, to better understand this binding and to demonstrate that this center of mass separation can be a deceiving coordinate, a contact value was calculated during the binding process (see Methods for details). In short, a value of 1 is assigned to any residue of Aβ that is bound to the interfacial region of the bilayer while a value of 0 is assigned to any residue that is not bound. This value is calculated for each residue and averaged over the full simulation. The contact value is calculated for every window in the umbrella sampling and a two dimensional free energy surface as a function of center of mass separation and number of contacts was determined (Figure 2.3). The plot shown in Figure 2.3 for the parallel initial configuration of the pH7 Aβ peptide binding to DPPC is characteristic of most free energy profiles for binding. At large center of mass

separations, there is no contact between any amino acids and the bilayer surface. Then, at the distances of approximately 4nm to 4.5nm, the first amino acids of Aβ come in contact with the interfacial region of the bilayer, as seen in snapshot 1. As free energy begins to decrease significantly, more amino acids come into contact with the bilayer surface, as seen in snapshot 2. Finally, at the free energy minimum, 90-95% of amino acids are in contact with the bilayer surface and the peptide is clearly bound to the interfacial region of the bilayer, as seen in snapshot 3. Snapshot 3 also demonstrates the parallel binding of the Aβ peptide to a DPPC bilayer, mentioned previously as a causative factor in the large, negative free energy of binding of Aβ to DPPC. Further, the free energy surface shows that the most probable path taken for binding is that the Aβ peptide will approach the bilayer surface without making significant contact. Then once the peptide is close to the bilayer surface at center of mass separations around 4nm (Snapshot 1), the peptide will begin to quickly make contacts with the bilayer surface and the free energy will drop drastically as the peptide approaches the surface (Snapshot 2) and tightly binds with the surface (Snapshot 3). An alternate path where the peptide creates contacts monotonically as it approaches the bilayer surface is not favored as it requires many more contacts at a given center of mass separation, which will force the peptide to extend and expose hydrophobic residues to solvent in order to have a similar free energy to the more favored binding path. Interestingly, the pH7 Aβ peptide has a lower number of total amino acids in contact with the DOPS bilayer surface at the free energy minimum, with only 36 of 42 amino acids in contact instead of ~40 of 42 amino acids in contact in the other systems. This lower extent of contact between the anionic peptide and DOPS, due to electrostatic repulsion on the bilayer surface, helps to explain the smaller free energy of binding of

pH7 Aβ to DOPS even though the contact of 36 amino acids to the bilayer surface provides a favorable free energy of binding and drives the binding process. Further, the use of this contact score demonstrates that the large center of mass separations described by the free energy profiles are still compatible with binding driven by association of the peptide with the interfacial region of the bilayer. Finally, the radius of gyration of Aβ was calculated as a function of center of mass separation (Data not shown). For all peptide-bilayer combinations, the radius of gyration was constant until the peptide began to make contact with the bilayer surface. The radius of gyration then increased and peaked as the peptide made extensive contacts with the bilayer surface. Once the peptide had made a significant number of contacts with the bilayer surface, the radius of gyration decreased to a value slightly less then the pre-binding level and remained constant as the peptide finished the binding process. These radius of gyration calculations demonstrate that, similar to the contact score calculations, the peptide is altering its structure to make extensive contacts with the bilayer as it begins to interact with the bilayer surface.

Along with inspecting quantitative aspects of Aβ binding to the bilayer surface by using umbrella sampling, the secondary structure of Aβ could be analyzed throughout the process. As each umbrella involved a molecular dynamics simulation with a restrained center of mass separation (147, 148, 150), secondary structure analysis could be performed at each window for the entire simulation time. In these simulations, only the earliest stages of binding could be investigated due to the temporal limitations of simulations. In the Aβ-membrane binding process, we expect that the majority of conformational change will occur after significant binding has occurred. Therefore, the

secondary structure analysis will provide insight towards the earliest stages of conformational change and may help to predict any significant secondary structure change after binding. For all bilayer and Aβ combinations, the secondary structure was not greatly affected until the peptide came in full contact with the bilayer surface. Upon full contact with the bilayer surface, the secondary structure was influenced by the bilayer. For the simulations on a DPPC bilayer, the secondary structure remained a random coil. This is exactly as expected for the zwitterionic DPPC based on the unconstrained simulations previously mentioned and in experimental results (57, 58, 82). For simulations on the DOPS bilayer, both turn and β-structure content increased upon contact with the bilayer for all Aβ pH regimes, similar to the previous unconstrained simulations near the DOPS bilayer. However, these resultant transient β-structures were not nearly as well ordered as the β-hairpin (49) used in the initial unconstrained simulations and thus only represent an intermediate Aβ structure. The DOPS bilayer was able to introduce some ordering of the Aβ peptide, but not enough to fully structure a single peptide. Similar to the unconstrained simulations, the time restrictions imposed by all-atom MD simulations prevent observation of significant secondary structure changes on the timescales analyzed here. Potentially, other methods such as parallel tempering are required to observe any structural change, or perhaps the structural change observed in experiments are due to protein-protein interactions formed in oligomers and not stable on the single peptide level.

*Unconstrained Simulations at Free Energy Minima*

To study the effect of peptide-lipid interactions occurring on the bilayer surface of the Aβ-bilayer system, we performed the density profiles analysis presented in Figure 2.4. Density profiles for the system were calculated using GROMACS utilities (143, 144). To ensure that the center of mass constraints did not influence the distribution of the peptide on the bilayer surface, unconstrained MD simulations were performed. For each of these simulations, the final structure from the umbrella sampling simulation in the window that was closest to the free energy minima was chosen. For all three Aβ-DPPC simulations, the 2.1nm center of mass separation window was closest to the free energy minimum and was thus used for the initial structure of unconstrained simulations. For the Aβ-DOPS simulations, the 2.4nm center of mass separation window final structures were used. The computational details of these simulations were exactly the same as the previous umbrella sampling simulations except that the harmonic potential restraint was removed and each simulation was performed for 80ns. The density profiles that are plotted on Figure 2.4 are taken from the initial configuration with a free energy profile closest to the average free energy profile, which indicates that this initial configuration is the heaviest weighted initial configuration for the calculations. Thus, the density profiles plotted with DPPC are: pH7 – parallel initial configuration, pH5 – N-terminus down initial configuration, pH3 – C-terminus down initial configuration, and with DOPS: pH7 – C-terminus down initial configuration, pH5 – parallel initial configuration, pH3 – parallel initial configuration.

Aβ was separated into two segments for density calculations: residues 1-22, which are primarily charged and hydrophilic residues, and residues 23-42, which are primarily hydrophobic residues. In these density plots, both the charged and hydrophobic sections of Aβ on DPPC appear to be clearly bound to the bilayer where interactions with the interfacial regions of the bilayer dominate. At all pH's on DPPC, the charged section of Aβ and the hydrophobic section of Aβ overlap significantly with the interfacial portions of the DPPC density, creating an Aβ distribution wherein Aβ is parallel to the bilayer surface at the interface of the hydrophobic sections of the bilayer. While these possible hydrophobic interactions with the bilayer may not involve hydrophobic insertion of the peptide into the bilayer core, binding to the interfacial region of the bilayer will lead to removal of water from the peptide and subsequent interactions with the interface of the hydrophobic core of the bilayer, which drives the binding. For Aβ on DOPS, it is clear that electrostatic interactions are influencing the distribution of the peptide on the bilayer surface due to different peptide density distributions concurrent with pH. At pH7, the charged section of the peptide is repelled from the bilayer surface and remains outside of the bilayer density while the hydrophobic section of Aβ is clearly distributed in the interfacial region of the bilayer. This creates a peptide distribution where Aβ at pH7 is situated almost perpendicular to the bilayer surface, with the hydrophobic region interacting with the bilayer interfacial region and the charged section repelled from the surface (Figure 2.5). For the pH5 and pH3 Aβ on DOPS, the charged and hydrophobic sections of the peptide both clearly overlap with the DOPS density. However, overlap of the hydrophobic section of Aβ with the interfacial region of the bilayer is still more extensive then overlap of the charged section of Aβ with the interfacial region of the

bilayer (Figure 2.4). Also, in comparison to the distribution of Aβ on the DPPC bilayer, pH5 and pH3 Aβ is more solvent exposed and less tightly bound to the interfacial surface of the bilayer, as seen from both the lower overlap of either region of the peptide with the DOPS bilayer in comparison to the significant overlap of both regions of Aβ with the DPPC bilayer and in snapshots from the simulations (Figure 2.5). These peptide and lipid charge-dependent density distributions of Aβ on the bilayer surface clearly demonstrate the effect of both electrostatic and interfacial interactions with this region of the bilayer and may play a role in the availability of Aβ for peptide-peptide interactions near the bilayer surface, which drives aggregation.

**Discussion**

The results obtained from simulations with the 42 amino-acid Aβ peptide provide insight into the detailed interactions occurring between Aβ and lipids on the surface of a pure lipid bilayer. The unconstrained simulations both in solution and near a DPPC or DOPS membrane demonstrate that the molecular dynamics techniques used for this study are effectively able to replicate various experimental results. During the simulations in solution, Aβ unfolds into a random coil peptide from ordered starting structures. Near bilayers, Aβ is attracted to both the DPPC and DOPS bilayer over the short length scales used in these simulations with the DOPS bilayer stabilizing secondary structure to a greater extent then the DPPC bilayer. These results support previous experimental work using CD and NMR spectroscopy (57, 58, 82) which demonstrate that addition of anionic vesicles to a solution of random coil Aβ peptides will lead to a significant change in the secondary structure of the peptide while the addition of zwitterionic vesicles does not affect the peptide structure.

The most insightful results from this work are derived from the umbrella sampling simulations on DPPC and DOPS bilayers. Not only did these calculations provide quantitative details for the extent of attraction of Aβ to the bilayer surface through free energies of binding, the setup of these simulations allowed for detailed analysis of peptide structure and distribution as Aβ systematically approached the bilayer surface. From this analysis, intriguing aspects of the Aβ-bilayer system were revealed. The umbrella sampling simulations provided insight into the distribution of Aβ on the bilayer

surface dependent upon peptide and lipid headgroup charge. From the density profiles in Figure 2.4 and the simulations snapshots in Figures 2.3 and 2.5, it is apparent that electrostatic interactions at the bilayer surface greatly influence peptide distribution. On the DPPC bilayer, Aβ, independent of peptide charge, sits nearly parallel to the bilayer surface near the interface between the headgroup and hydrophobic core regions of the bilayer. This orientation maximizes interactions with the interfacial region of the bilayer throughout the peptide without completely burying hydrophilic and charged residues found on the N-terminus of the peptide in the bilayer core. On DOPS, Aβ does not adopt this parallel arrangement and instead promotes a much more superficial interaction with the bilayer surface for the neutral (pH5) and cationic (pH3) Aβ peptides. Further, for the anionic pH7 peptide, an almost perpendicular arrangement is observed wherein the hydrophobic C-terminus of the peptide interacts with the hydrophobic core of the bilayer while the hydrophilic N-terminus becomes solvent exposed. This configuration is due to the interplay of interfacial association of C-terminal tail of the peptide with the hydrophobic core of the bilayer and electrostatic repulsion between the anionic N-terminal tail and anionic lipid headgroups. Thus, for the neutral and cationic Aβ bound to DOPS, the energetically favorable electrostatic interactions between the peptide and the lipid headgroups prevent the extreme solvent exposure of the N-terminus. However, these electrostatic attractions between the charged headgroups and the N-terminus amino acid side chains prevent the tight association of the N-terminus with the interfacial region of DOPS, in comparison to the peptide distributions on DPPC. This attraction near the headgroup region of DOPS with the pH5 and pH3 peptides promotes a more solvent exposed distribution of the N-terminus of the peptide, which forces the entire peptide to

be bound less tightly to the bilayer interface and thus more exposed for protein-protein interactions that may drive oligomerization on the bilayer surface. Therefore, the charge on Aβ during binding to an anionic bilayer surface will significantly influence the distribution of the peptide upon nonspecific binding.

Further, secondary structure analysis during the binding process provides some insight into the computation approach to this system. Any peptide secondary structure change required that the peptide be in full contact with the bilayer, which occurred near the free energy minima presented in Figure 2.2. Even though the peptide began to make contact with the bilayer at large center of mass separations, secondary structure change was only seen when the peptide was in full contact with the bilayer at center of mass separations of 2.1nm to 2.4nm. Further, this secondary structure change was not very extensive. Only in the extreme case of a pH3 peptide on a DOPS bilayer was any secondary structure change observed. For the more physiologically feasible pH5 peptide on DOPS, there was some transient stabilization of β-structure, but not to the extent of formation of distinct β-structure as in the predicted fibril structure of Aβ. Therefore, our results appear to support the hypothesis that the bilayer cannot fully order a single peptide into a fibril-like structure but likely acts to stabilize an intermediate state that is aggregation-prone. Further, recent results have implicated that the β-structure observed in Aβ fibrils is not formed from a single peptide but is β-structure shared between two Aβ peptides (46). If these structural predictions hold true, we are unlikely to see any physiologically relevant formation of a β-hairpin in these simulations, as β-structure formation would be due to peptide-peptide interactions, which the bilayer surface may

facilitate. It is also possible that the 40ns timescales used in this simulation are not adequate for observing significant secondary structure change. The 80ns unconstrained MD simulations at the free energy minima were also analyzed for secondary structure change and very little structural change was observed. Through 120ns of combined unconstrained and constrained MD simulations at the free energy minima, secondary structure change was transient at best. Thus, approaches such as replica exchange, similar to some previously performed work (151), or coarse-grained MD will likely be required to adequately explore Aβ secondary structure formation on the bilayer surface.

The results of this work have lead to a rough mechanism for elucidating how the detailed balance between electrostatic and hydrophobic forces on the bilayer surface may affect Aβ aggregation. Initially, the Aβ peptide is brought close to the surface of a bilayer due either to diffusion, through interaction with sugar groups on lipids such as gangliosides or after cleavage from the amyloid precursor protein. Once the peptide is close enough to the surface, it will favorably bind with the lipids. If this binding is on a mostly zwitterionic bilayer, the peptide will strongly interact with the interface at the hydrophobic core of the bilayer, as seen in the density profiles of Figure 2.4, thus precluding extensive interactions with other nearby peptides and preventing any secondary structure change, in agreement with previous experiments (57, 58, 82). However, if this binding occurs on an anionic bilayer, the peptide will not be as strongly associated with the bilayer core and more exposed to the solvent and other bound peptides. If the anionic headgroups on lipids are able to lower the local pH by 1-2 units, the hydrophobic portion of the peptide will become exposed, as demonstrated in density

profiles in Figure 2.4, and more likely to interact with other nearby peptides, thus driving oligomerization. Also, previous research (62) has shown that fibrilization occurs more rapidly in solution at a lower pH≈5. Therefore, lowering pH near the anionic lipid surface may also promote aggregation by intrinsically increasing protein-protein interactions through reducing electrostatic repulsion between peptides, which along with altering peptide distribution on the bilayer, will promote oligomer formation. Based on previous structural determination (46), it is likely that the resulting peptide-peptide interactions on the bilayer surface will drive the secondary structure changes observed in experiment (57, 58, 82) and promote fibrilization. Therefore, an anionic lipid membrane appears to promote aggregation by (1) increasing peptide diffusion by altering diffusion from a 3D to 2D process, (2) locally increasing Aβ concentration on the bilayer surface due to the highly favorable free energy of binding and (3) decreasing the local pH on the bilayer surface to promote an Aβ configuration that would be amiable to protein-protein interactions that can drive oligomerization.

Many aspects of this system are still open for future MD simulations. As mentioned previously, work with replica-exchange MD for analyzing Aβ secondary structure change will be very interesting for determining the direct role of the bilayer on peptide secondary structure near the bilayer surface. Further, simulations using multiple peptides on the bilayer may provide insight into the role of peptide-peptide interactions on early oligomer formation near the bilayer surface. Finally, a study similar to previous replica exchange MD work (151) using the WALP peptide on the DPPC bilayer, where both bilayer surface binding and peptide insertion into the bilayer core was simulated

with subsequent calculation of a 2D free energy surface, would be very informative for this system. For the current study on only Aβ binding to the bilayer surface, a 2D free energy surface calculation using a second reaction coordinate similar to extent of helix formation used in the WALP-DPPC study is not applicable. However, Aβ binding and insertion could be studied using a similar order parameter and a free energy surface for the full process could be calculated. Performing such a study on the full insertion process would provide great insight into a full range of Aβ-bilayer interactions that would only be available on the detailed scale of MD simulations. Thus, future experimental and computational endeavors with Aβ on the bilayer surface will be integral to confirming that the structural change observed in experiment is due to protein-protein interactions occurring during the early stages of oligomerization and also essential to further characterizing the influence of anionic membranes on Aβ aggregation in Alzheimer's disease.

**Table 2.1** Simulation contents for unconstrained simulations

**a) Simulations in Solution** – 6.4nm x 6.4nm x 8.1nm box

| Starting Structure | Aβ pH | SPC/E | $Na^+$ | $Cl^-$ |
|---|---|---|---|---|
| Helix | pH7 | 10534 | 22 | 19 |
| | pH5 | 10539 | 19 | 19 |
| | pH3 | 10530 | 19 | 25 |
| β-Hairpin | pH7 | 10521 | 22 | 19 |
| | pH5 | 10523 | 19 | 19 |
| | pH3 | 10515 | 19 | 25 |

**b) Simulations with DPPC** – 6.4nm x 6.4nm x 16.3nm box

| Starting Structure | Aβ pH | SPC/E | $Na^+$ | $Cl^-$ |
|---|---|---|---|---|
| Helix | pH7 | 15587 | 27 | 24 |
| | pH5 | 15588 | 24 | 24 |
| | pH3 | 15585 | 24 | 30 |
| β-Hairpin | pH7 | 15576 | 27 | 24 |
| | pH5 | 15580 | 24 | 24 |
| | pH3 | 15569 | 24 | 30 |

**c) Simulations with DOPS** - 6.4nm x 6.4nm x 16.8nm box

| Starting Structure | Aβ pH | SPC/E | $Na^+$ | $Cl^-$ |
|---|---|---|---|---|
| Helix | pH7 | 15906 | 155 | 24 |
| | pH5 | 15907 | 152 | 24 |
| | pH3 | 15904 | 152 | 30 |
| β-Hairpin | pH7 | 15896 | 155 | 24 |
| | pH5 | 15899 | 152 | 24 |
| | pH3 | 15888 | 152 | 30 |

**Table 2.2** Simulation contents for umbrella sampling simulations

**a) Simulations with DPPC** - 6.4nm x 6.4nm x 15.8nm box

| Starting Structure | Aβ pH | SPC/E | $Na^+$ | $Cl^-$ |
|---|---|---|---|---|
| Random Coil | pH7 | 14764 | 27 | 24 |
| | pH5 | 14762 | 24 | 24 |
| | pH3 | 14759 | 24 | 30 |

**b) Simulations with DOPS** - 6.4nm x 6.4nm x 16.1nm box

| Starting Structure | Aβ pH | SPC/E | $Na^+$ | $Cl^-$ |
|---|---|---|---|---|
| Random Coil | pH7 | 15083 | 155 | 24 |
| | pH5 | 15081 | 152 | 24 |
| | pH3 | 15078 | 152 | 30 |

**Table 2.3** Average structures for unconstrained Aβ simulations. Starting structure refers to if the peptide was originally the 1Z0Q (Helix) or 2BEG (β-Hairpin) derived structure. Aβ pH refers to the charge on the peptide during the simulation.

| **Initial Conditions** | | **Final Structure** | | |
|---|---|---|---|---|
| Starting Structure | Aβ pH | In Solution | On DPPC | On DOPS |
| Helix | pH7 | Coil | Coil/Turn | Helix |
| Helix | pH5 | Coil | Coil/Turn | Helix |
| Helix | pH3 | Coil | Coil/Turn | Helix |
| β-Hairpin | pH7 | Coil | Coil | β-Hairpin |
| β-Hairpin | pH5 | Coil | Coil | β-Hairpin |
| β-Hairpin | pH3 | Coil/Turn | Coil | β-Hairpin/Turn |

**Table 2.4** Calculated free energies for binding of Aβ to the bilayer surface

| Bilayer Type | Aβ pH state | Free Energy (kcal/mol) |
|---|---|---|
| DPPC | pH7 | -16.0 kcal/mol |
| | pH5 | -18.4 kcal/mol |
| | pH3 | -18.9 kcal/mol |
| DOPS | pH7 | -6.6 kcal/mol |
| | pH5 | -14.1 kcal/mol |
| | pH3 | -15.6 kcal/mol |

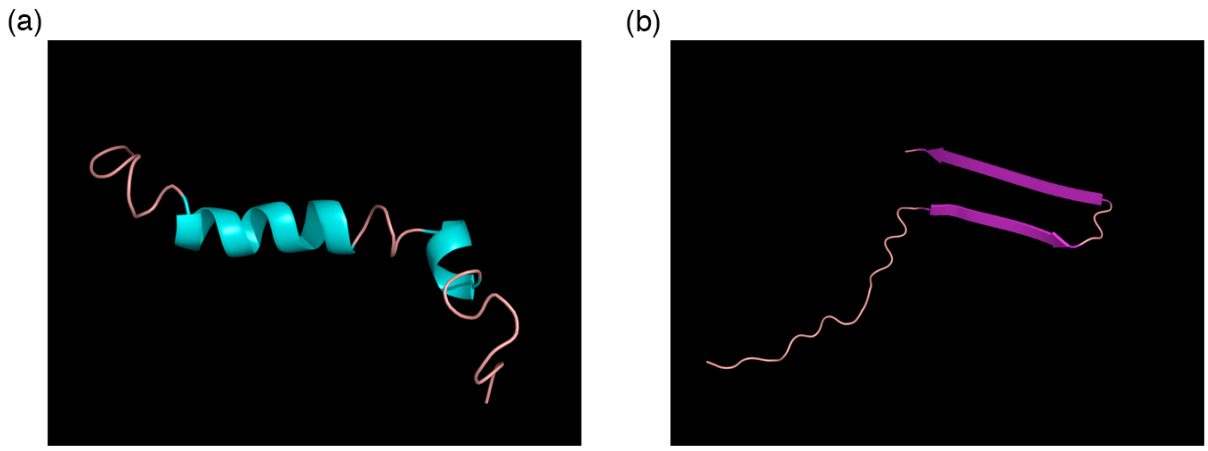


**Figure 2.1** Initial configurations of Aβ used for simulations. Figure 2.1a, PDB code 1Z0Q is a coil-dominated structure (27) while Figure 2.1b, PDB code 2BEG, is a preformed β-hairpin (49).

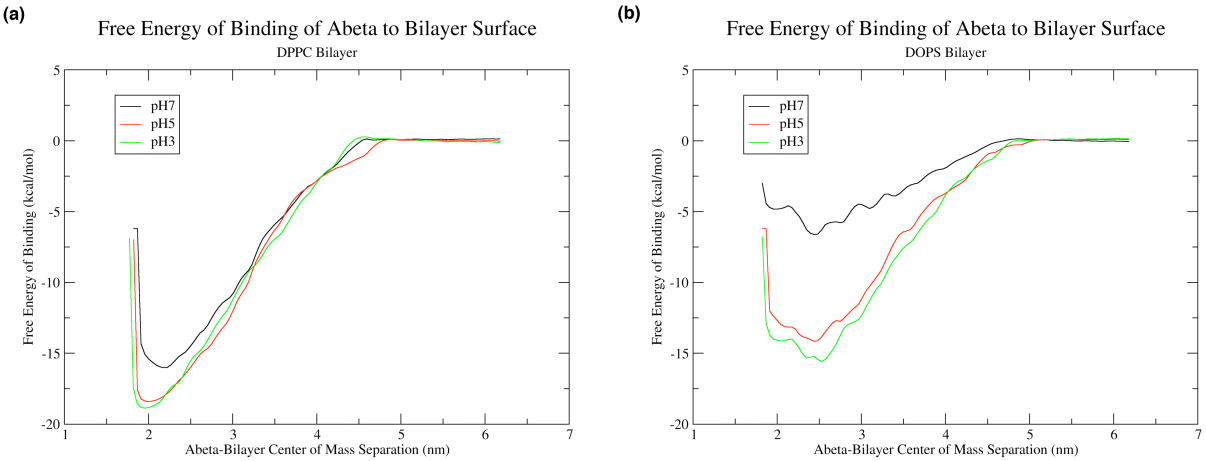


**Figure 2.2** Free energy profiles for binding of Aβ to the surface of the (a) DPPC or (b) DOPS bilayer. The error associated with the minimum of these potentials is 4.1kcal/mol.

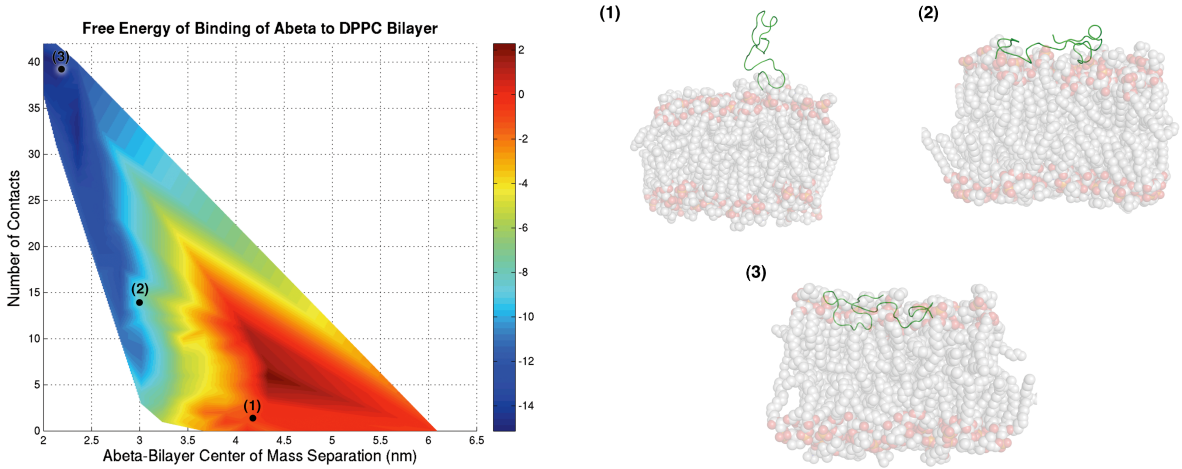


**Figure 2.3** Free energies of binding of Parallel pH7 Aβ to DPPC bilayer as a function of Aβ-bilayer center of mass separation and number of contacts. The surface shows, using the color scale next to the figure, the relative free energy change as the peptide binds to the bilayer surface. Other peptide-bilayer combinations showed a similar free energy surface. The snapshots represent points along the binding trajectory and show the extent of contact at (1) 4.2nm, (2) 3.0nm and (3) 2.1nm center of mass separations.

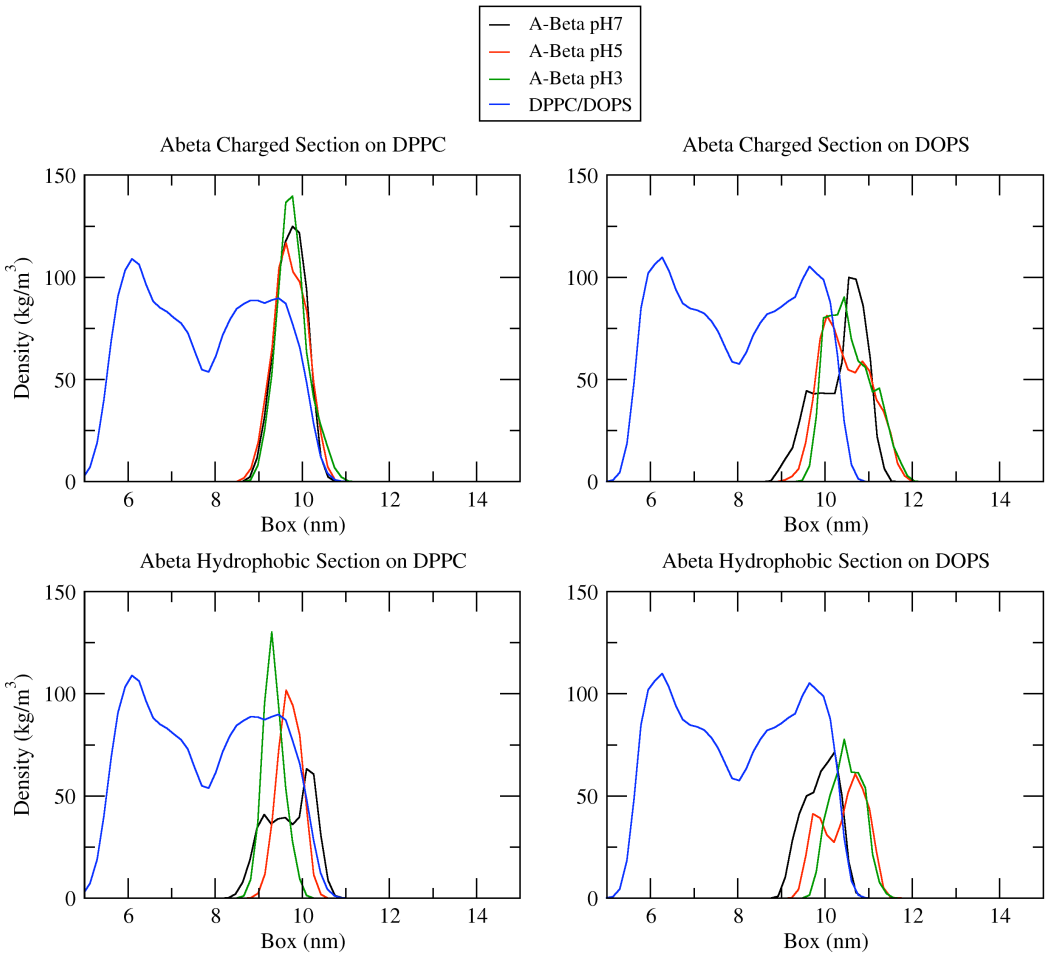


**Figure 2.4** Density profiles of Aβ on DPPC and DOPS bilayers calculated from 80ns simulation at center of mass separation closest to the free energy minima of profiles in Figure 2.2. All plots on DPPC are at a COM separation of 2.1nm. All plots on DOPS are taken from simulations at a COM separation of 2.4nm. The "Abeta Charged Section" is with reference to residues 1-22 of the peptide and the "Abeta Hydrophobic Section" is with reference to residues 23-42.

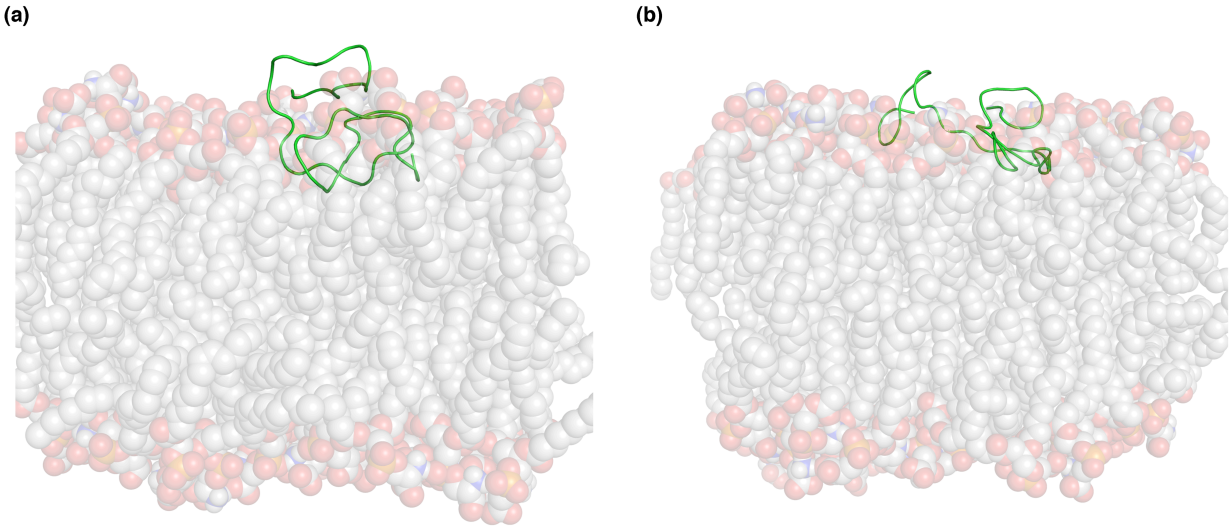


**Figure 2.5** Comparison of simulation snapshots from 80ns unconstrained MD simulations of (a) pH7 Aβ and (b) pH5 Aβ on DOPS at the free energy minima center of mass separation.

**Chapter 3:**

# Structure of Amyloid-β (1-42) Monomer Absorbed to Model Phospholipid Bilayers: A Molecular Dynamics Study

Charles H. Davis[1] and Max L. Berkowitz[2]

[1]*Department of Biochemistry and Biophysics, University of North Carolina at Chapel Hill, Chapel Hill, North Carolina, 27599*
[2]*Department of Chemistry, University of North Carolina at Chapel Hill, Chapel Hill, North Carolina, 27599*

Published in *Journal of Physical Chemistry B*, 113, 14480-14486 (2009)

**Abstract**

The Amyloid-β (Aβ) peptide, the 39 to 43 amino acid peptide that plays a substantial role in Alzheimer's disease, has been shown to interact strongly with lipids both in vitro and in vivo. Aβ-lipid interactions have been proposed as a considerable factor in accelerating Aβ aggregation through the templating role of membranes in aggregation disorders. Previous work has shown that anionic lipids are able to significantly increase Aβ aggregation rate and induce a structural conversion in Aβ from a random coil to a β-structure that is similar to the monomer structure observed in mature fibrils. However, it is unclear if this structural change occurs with the Aβ monomer due to direct interactions with the lipids or if the structural change results from protein-protein interactions during oligomerization. We use extensive replica exchange molecular dynamics simulations of an Aβ monomer bound to a homogeneous model zwitterionic or anionic lipid bilayer. From these simulations, we do not observe any significant β-structure formation except for a small, unstable β-hairpin formed on the anionic dioleylphosphatidylserine bilayer. Further, we see that the Asp23-Lys28 salt bridge that plays a role in β-hairpin formation is not substantially formed on the bilayer surface and that Lys28 preferentially interacts with lipids when bound to the bilayer. These results suggest that the structural conversion seen in experiments are not due to the ordering of monomeric Aβ on the bilayer surface but are a result of protein-protein interactions enhanced by Aβ binding to the cell membrane.

## Introduction

The Amyloid-β (Aβ) peptide is an amyloidogenic protein whose aggregation has been linked to neural degeneration (3, 11, 12, 40) that is a hallmark of Alzheimer's disease. Due to the association of Aβ with Alzheimer's disease, Aβ has been extensively studied (3, 11, 12, 40) over the past 20 to 30 years. In particular, the structure of the Aβ peptide, through its passage from monomer to small aggregate to fibril, has been a subject of great interest for both experimental (4, 5, 57-59, 81, 85, 87, 91, 95, 157, 184) and computational (27-29, 69, 121, 123-131, 136) researchers. Knowledge of the structure of Aβ at each step of the aggregation pathway will provide insight into the mechanism of aggregation that can hopefully be exploited for therapeutic benefits. Previous research has already made significant progress on this front as the dogma of Aβ neurotoxicity has been shifting away from mature fibrils and towards small oligomers as one of the main neurotoxic species in Alzheimer's disease (4, 5, 37). This knowledge places even further impact on gaining a fundamental understanding of the earliest stages of Aβ aggregation as a major target for prevention of extensive neurodegeneration.

While it is clear that the first stages of Aβ aggregation are vital to the progress of Alzheimer's disease, it has not yet been determined what factors influence this initial conversion from monomer to oligomer. While oligomerization does occur naturally in solution, there are other possible factors that may catalyze this reaction. Recent work (4, 5, 57-59, 81, 85, 87, 91, 95, 157, 184) has demonstrated that cell membranes may play a significant catalytic role in increasing Aβ aggregation rates. The Aβ peptide is derived

from the transmembrane Amyloid Precursor Protein (APP) (3, 11, 12). Upon cleavage from APP, the C-terminus (3, 11, 12) of Aβ maintains a significant portion of the transmembrane region of APP. Extensive experimental work (4, 5, 57-59, 81, 85, 95) has shown that Aβ, when mixed with lipid vesicles of various structure and headgroup charge, will aggregate at a much faster rate then in solution. Further results have demonstrated that this interaction between Aβ and lipids will induce a structural conversion (4, 5, 57-59, 81, 85, 87, 91, 95, 157, 184) from a disordered peptide into a peptide dominated by β-structure. Mixing Aβ peptide with anionic lipids, in the form of vesicles or bilayers, induces a substantial increase in both aggregation rate and secondary structure formation (4, 57-59, 81, 87, 91, 184). Also, it has been shown that extensive interactions with cell membranes can lead to pore formation and disruption of ion balance (157, 185) across the bilayer, which may play a role in Aβ neurotoxicity.

While experimental results have demonstrated an extensive interaction of Aβ with lipid bilayers, these same experimental techniques are limited in resolution. Circular dichroism, nuclear magnetic resonance, electron microscopy and other common techniques (5, 57-59, 81, 85, 87, 91, 95, 157, 184) require a low concentration to study Aβ without immediate aggregation, which prevents these techniques from being able distinguish if Aβ is in a monomeric or small oligmeric state. This subtle shortcoming due to the nature of Aβ does cloud one aspect of these results: Is the secondary structure change observed in experiment inherent to the Aβ monomer or does the structural conversion occur due to peptide-peptide interactions that are enhanced on the lipid

surface? Thus, molecular dynamics (MD) simulations would be ideal to determine the structure of Aβ as a monomer on an atomic level.

MD simulations have been extensively performed on the Aβ peptide. Simulations on the full length monomer (27-29, 69, 121, 136), on monomer fragments (124, 126-128, 130), on small oligomers (125, 126, 131) and on full fibrils (129) using all atom (27-29, 69, 121, 123-125, 127-131, 136) or coarse grain techniques (126, 131) in both explicit (27, 29, 69, 123, 124, 127-131, 136) and implicit (28, 121, 125, 126) solvent have produced significant insight into the structure of Aβ at each step of aggregation. Replica exchange MD simulations (28, 29, 121, 123-125), which allows for much more extensive motion of the peptide through its configurational space by effectively overcoming barriers on the conformational free energy surface, have been particularly insightful for Aβ structure studies. These replica exchange studies (28, 29, 121, 123-125) on Aβ have shown that the peptide does have a predominantly random coil structure in solution but can still form stable secondary structure, such as β-hairpins or small helices, that may help to accelerate aggregation. However, these same studies have not yet been extended to Aβ in an explicit membrane environment. Previous studies have investigated the stability of a preinserted (69, 136) Aβ into either an explicit or implicit membrane environment, but these works did not concentrate on Aβ structure when bound to the membrane surface. A previous work of ours (138) investigated Aβ binding free energies to various bilayers of differing headgroup charge, but we did not investigate Aβ structure due to lack of sampling without replica exchange. In this work, we use the replica exchange method to study Aβ structure and the effect of both peptide charge and lipid

charge on peptide structure. As anionic lipids bilayers are able to decrease local pH (57, 68), it is necessary to study the effect of lipid binding on Aβ with different total charges. The results of this work will help to elucidate the mechanism of structural change experimentally observed in Aβ aggregation at a molecular level not available to many current experimental techniques.

## Materials and Methods

### *Initial Conditions*

The initial structures used for replica exchange simulations were obtained from a previous work (138) by our group. In that work, a random coil structure of the 42 amino acid Aβ peptide was systematically pulled to the surface of an equilibrated 128 lipid dipalmitoylphosphatidylcholine (DPPC) or dioleylphosphatidylserine (DOPS) bilayer using the umbrella sampling technique, and a free energy of binding was calculated. The initial conditions for the replica exchange simulations presented here were obtained from the final snapshots of MD simulations at the bound free energy minimum, as determined from the calculated free energy profiles for binding. These final snapshots from the simulations occurred at an Aβ-bilayer center-of-mass separation of 2.1nm with DPPC and 2.4nm with DOPS. Thus, the initial structures chosen for the replica exchange simulations described here represent configurations where the 80ns of restrained MD simulations allowed for extensive simulation time to equilibrate the Aβ-bilayer system. The Aβ-bilayer center-of-mass restraint used in the previous work was removed for replica exchange, ensuring that the Aβ was not restrained to the bilayer surface.

### *Peptide and Lipid Parameters*

Replica exchange simulations were performed using the GROMACS 4.0 simulation package (143, 145, 149, 186). The Aβ peptide was described using the united-atom GROMOS96 force field (143, 145, 186). The DPPC and DOPS lipids were described using the Berger (176) force field parameters. These force fields were chosen

to match our previous work (138) and because of the extensive use of each force field in previous molecular dynamics studies. The system was solvated with SPC/E model (173) water and included counter-ion and co-ion Na+/Cl- salt. As the local pH near anionic lipid bilayers is lower then bulk (57, 68), it was important to perform these simulations at physiological pH and also at a lower pH to determine if peptide protonation state could affect Aβ structure near lipids. Thus, simulations were performed with Aβ at a -3 total charge, which is the physiological charge of Aβ, and with a net 0 total charge due to protonation of three histidine residues. This 0 total charge state would be a close approximation of the charge on Aβ at pH5, which is a feasible pH for Aβ bound to an anionic bilayer surface. Therefore, the -3 total charge simulations are termed the pH7 simulations and the 0 total charge simulations are termed the pH5 simulations throughout, for simplicity. The N-terminus was represented by NH3+ and C-terminus was represented by COO- to match the most likely charge state at physiological pH. Thus, four total replica exchange simulations are performed with two peptide charge states on either a DPPC or DOPS bilayer. Exact contents of the simulation are given in Table 3.1. For each replica, temperature was held constant using a Nose-Hoover (171) scheme with a relaxation time of 0.5ps under constant volume (NVT) conditions. All bonds were constrained using the LINCS algorithm (187), which allowed for a time step of 3fs. Long range electrostatics were maintained using the SPME algorithm (146) with periodic boundary conditions in all three dimensions. Secondary structure was calculated using the DSSP algorithm (174) within GROMACS and all other analysis was performed using GROMACS utilities. As a clarification note for the tables and figures, a discontinuous trajectory refers to a system trajectory obtained at a fixed temperature

during the replica exchange, while a continuous trajectory refers to a trajectory obtained by reordering the set of discontinuous trajectories so that one initial structure is followed through the temperature space during the full simulation time.

*Replica Exchange Details*

The temperature exchange simulations involved 83 replicas spaced between 325K and 502K. The exact temperatures of all replicas are provided in Table 3.2. The temperatures were chosen using the Temperature Generator for REMD-simulations (188) associated with the GROMACS package. Thus, 80ns (pH7) or 110ns (pH5) molecular dynamics simulations were performed for each of the 83 replicas at random initial velocities with exchanges attempted every 3ps and coordinates written every attempted exchange. The pH5 simulations were extended to 110ns to determine the stability of secondary structure formed at the end of the 80ns simulation. With a minimum of 80ns total simulation time and 3ps exchanges, over 26,000 exchange attempts are made during the span of the simulation. Further, results from the simulations showed an exchange probability of 0.2 - 0.35 over all temperatures. The combination of a rate of exchange greater then 1ps and over 20,000 exchange attempts should guarantee at least one full transit for the replicas through the temperature space and, subsequently, a well-mixed (153) replica exchange simulation. All details involving the replica exchange and the replica temperatures were the same for the four initial conditions.

*Bilayer Constraint*

At the high temperatures used in this simulation, neither the DPPC or DOPS bilayer was stable. Thus, a restraint was necessary to keep the fidelity of the bilayer while still allowing the peptide significant conformational flexibility. Further, it was important to maintain individual lipid flexibility within the bilayer as lipid-protein interactions may play a significant role in Aβ structure. A restraint was chosen to keep the average separation along the Z-axis between the phosphate groups of the two leaflets of the bilayer constant. In order to impose this restraint, the 64 phosphate atoms from each leaflet were grouped together and a harmonic constraint was applied to the average distance along the Z-axis between the center-of-mass of these two groups. By imposing the constraint on the center-of-mass separations of the group instead of each phosphate individually, it allows for each lipid to fluctuate significantly as long as the average Z value for each leaflet remains relatively constant. To calculate the average constraint distance for the DPPC and DOPS bilayers, we used the final 20ns of the umbrella sampling simulations of our previous work (138). From these previous simulations, we calculated that the average phosphate-phosphate distance on DPPC was 3.90nm and the average distance on DOPS was 4.16nm. It was necessary to impose a force constant of 4kJ/ (mol*$nm^2$) to prevent the bilayer from breaking apart and to prevent exceptional amounts of water from penetrating the bilayer. However, visual inspection of the trajectories at 502K show that the bilayer remains together throughout the 80ns simulation and the extent of bilayer fluctuations are not significantly different in comparison to the simulation at 325K. Further, we calculated the number of water molecules that interact with the hydrophobic core of the bilayer. At 502K, the number of

water molecules interacting with the bilayer core is three times larger then the number of water molecules interacting with the bilayer core at 325K and both values are stable over the length of the simulation. Both the leaflet to leaflet restraint and the constant volume (NVT) simulation condition, which also acts as a restraint on the system, prevent this increase in water molecules near the hydrophobic core from disrupting the bilayer structure, which would, in turn, force more water molecules into the hydrophobic core and eventually dissolve the bilayer. As previously mentioned, the leaflet to leaflet restraint on the bilayer was the only specific restraint applied on the system and the peptide was not restrained to the bilayer surface during replica exchange.

## Results

*Aβ-Bilayer Replica Exchange MD Setup*

In order to properly assess the structure of monomeric Aβ at the surface of the bilayer, replica exchange simulations were performed for the 42 amino acid form of the Aβ peptide at pH7 (-3 total charge) or pH5 (0 total charge) on either a homogeneous DPPC or DOPS bilayer. The initial structures for each of the four replica exchange simulations were taken as the final equilibrated structures at the membrane-bound free energy mimima determined in a previous work (138). Figure 3.1 is a representative example of one of the initial configurations for Aβ bound to the bilayer surface. The initial configurations for Aβ represent an Aβ structure where the peptide is strongly bound to the interfacial region of the bilayer with some amino acid sidechains inserted into the bilayer hydrophobic core and some sidechains either fully solvent exposed or interacting with the lipid headgroups.

MD simulations using the replica exchange methodology were then performed using these 4 initial configurations over a temperature range of 325K to 502K. As demonstrated in Figure 3.2, the replica exchange setup employed in this work allows each replica to adequately explore the temperature space during the duration of the simulation, which was consistent over all 4 initial conditions. In combination with the 3ps exchange rate of these simulations, the extensive motion through the temperature space should allow these replica exchange simulations to be considered well mixed and the configurational space well sampled (153). Further analysis at the lowest temperature (325K) should provide an appropriate estimate to the conformational space of Aβ while

bound to a bilayer surface. The use of a weak restraint between the average positions of the phosphate groups from each leaflet of the bilayer allows for some natural fluctuations of the bilayer surface without allowing the bilayer to dissolve. Allowing the bilayer to be more flexible may play a significant role in the dynamics of a protein bound to the bilayer surface.

*Aβ Secondary Structure on the Bilayer Surface*

Secondary structure content of the protein was calculated at 325K for all 4 systems as a means of determining how the membrane surface influences Aβ structure (Figure 3.3). From these calculations, it is clear that Aβ remains in a predominantly random coil configuration throughout the duration of the simulation. In particular, at pH7, the protein contains almost no ordered structure except for a small amount of β-sheet formed near the end of the simulation of pH7 Aβ on DOPS. However, at pH5, Aβ is able to adopt structures containing more ordered secondary structure. Most notably, the pH5 protein on DOPS develops a turn/ β-sheet structure from residues 21-34 beginning at 76ns of the simulation, which can be seen more clearly in Figure 3.4a. This structure is reminiscent of a β-hairpin, which has been postulated to be the building block (47, 48) of Aβ fibrils. On DPPC, it appears that a similar structure is formed, also at 75ns, but this structure spans fewer residues and is more transient. The replica exchange simulations at pH5 on DPPC and DOPS were both extended 30ns to test the hairpin stability. From Figure 3.3, it is obvious that this structure is still not stable over the length of the simulation and has quickly disappeared after 86ns of total simulation time. This β-hairpin structure only appears for 10ns of the 110ns of total simulation time and

does not significantly influence the average structure of the peptide during simulation. Finally, a turn and some β-sheet structure are transiently formed in the last 5 residues of the pH5 Aβ during the simulation on DOPS. This small turn has been previously seen (29) in studies of Aβ, due to Gly37 and Gly38, which have been predicted to strongly favor formation of turns. These replica exchange simulations confirm that this turn is feasible, yet it is not stable in the interfacial membrane environment.

*Asp23-Lys28 Salt Bridge Stability*

The salt bridge that can be formed between Asp23 and Lys28 has previously been implicated (47, 124, 127, 128, 189) to be a major factor in fibril formation by Aβ and has been observed in structures of Aβ fibrils (47). A recent experimental work (189) has demonstrated that a covalent lactam bridge created between Asp23 and Lys28 substantially increases the Aβ aggregation rate. Further, many computational studies (124, 127, 128) have shown that this salt bridge is significant in the formation of a β-hairpin in monomeric Aβ. However, it is still a point of contention if this salt bridge is necessary for fibril-like β-sheet formation Aβ or if hydrophobic interactions drive this sheet formation and the salt bridge is a secondary effect of β-sheet formation. To understand the properties of the salt bridge in our system, we calculated the distance between the $C_\gamma$ group of Asp23 and the $N_\zeta$ group of Lys28 during the pH5 Aβ replica exchange simulations at 325K from 75ns to 81ns on the DOPS bilayer, where the hairpin is transiently stable (Figure 3.4a). Salt bridges between these two residues have previously (124) been described as close-contact salt bridges for separations less than 4.5Å and mediated salt bridges for separations within 4.5Å - 7Å. The snapshots shown in

Figure 3.4b and the $N_\zeta$-$C_\gamma$ distance plot in Figure 3.4c demonstrate that Aβ tends to adopt one of two structures depending on the Asp23-Lys28 distance. When Asp23 and Lys28 are separated by a significant distance (labeled (1) in the Figure), Aβ adopts a β-hairpin structure with a turn between residues 21-24 (Ala-Glu-Asp-Val). However, when a mediated salt bridge is formed between Asp23 and Lys28 (labeled (2) in the Figure), the turn is shifted from residues 21-24 to approximately residues 18-22 (Val-Phe-Phe-Ala-Glu) and a new, smaller turn is created between Asp23 and Lys28 to accommodate this salt bridge formation. From Figure 3.4c, Aβ appears to fluctuate between these two strand-loop-strand structures over the time period studied and that neither structure appears to be significantly more stable then the other. Further, no close-contact salt bridges appear to be formed between Asp23 and Lys28, in contrast to simulations (124) performed in solution that investigated this salt-bridge formation. It is important to note that these ordered β-structures were not significantly stable over the full simulation time and were only formed with the pH5 peptide interacting with either bilayer.

*Aβ Distribution on the Bilayer Surface*

While the secondary structure and salt-bridge calculations did not show a significant difference between Aβ structure on the two bilayers, we also performed density distribution calculations to determine if regions of the Aβ peptide interacted differently with the zwitterionic or anionic lipids. For this analysis, Aβ was separated into a charged section (residues 1-23) and a hydrophobic section (residues 24-42) to see how the peptide interacted with the charged headgroups on the bilayer surface. In Figure 3.5, the left panel shows the pH5 Aβ density distribution on DPPC. This plot shows that

both the hydrophobic and charged sections of Aβ are interacting with the interfacial region of the bilayer. Further, the density of the phosphate atoms in DPPC is also shown, which further supports an interfacial distribution for the peptide. The charged and hydrophobic sections of the peptide appear to be distributed very similarly, both in the peak location and the width of the distribution. It also appears that the hydrophobic section of the peptide is not significantly inserted into the bilayer core. For the distribution on the DOPS bilayer given on the right panel of Figure 3.5, a similar pattern is observed. Both sections of the peptide appear to be sitting in the interfacial region of the bilayer and the distributions from both the charged and hydrophobic sections overlap. However, one significant difference is that the hydrophobic section of the peptide appears to have a broader distribution on DOPS, including significant tails on both sides of the distribution indicating either partial insertion of the hydrophobic section into the bilayer core or more solvent exposure of the hydrophobic residues at the C-terminus. Further, the charged section of the peptide also is able to become significantly solvent exposed by being distributed outside of the DOPS density, which is not seen in the DPPC bilayer. Thus, while Aβ on the DPPC bilayer has an almost parallel arrangement with both sections of the peptide bound to the interfacial region of the bilayer, Aβ bound to DOPS is able to adopt a larger range of distributions on the bilayer surface, including a distribution with a more exposed hydrophobic C-terminus, which may play a significant role in peptide-peptide interactions that drive aggregation.

Finally, we investigated the distribution of various amino acids on Aβ with respect to the bilayer. In particular, we looked at Lys28, which has been shown to be

integral to bilayer association (81, 184, 185), as well as its importance in the Asp23-Lys28 salt bridge described previously. As shown in Figure 3.5, Lys28 tends to distribute on the interfacial region of the bilayer near the hydrophobic core, independent on the charge of the lipids. Interestingly, while the Lys28 density does overlap somewhat with the phosphate density from the lipid headgroups, the lack of complete overlap and different density peaks for Lys28 and the lipid phosphate atoms demonstrates that Lys28 is likely not bonding strongly to these atoms throughout the entirety of the simulation. Further, the Lys28 distribution near the lower end of the Aβ hydrophobic density distribution indicates that Lys28 may be playing a role in anchoring the peptide to the interfacial region of the bilayer through interactions with the glycerol backbone or hydrophobic tails of the lipids. These results of the Lys28 density distribution studies are evidence that the role of Lys28 in Aβ interactions with the bilayer surface is to stabilize the interaction of Aβ with the interfacial region of the bilayer, thus contributing to the strong binding free energies predicted (138) for Aβ binding to either the DPPC or DOPS bilayer surface.

**Discussion**

The results of the replica exchange simulations of the Aβ 1-42 peptide on the zwitterionic DPPC or anionic DOPS bilayer surface provides insight into the structure of the monomeric peptide when bound to a membrane. These simulations appear to be well-mixed replica exchange simulations and the weak restraints applied to prevent the bilayer from dissolving at high temperature allow for significant bilayer motion, which may influence peptide structure or distribution on the bilayer surface. Bilayer restraints were also used in a previous all-atom replica exchange study (151) with a peptide-bilayer system, although those restraints were much more constricting since the temperatures used in the replica exchange simulations were over a much larger range (350K – 800K).

The secondary structure results from these simulations show that, even when bound to the bilayer surface, monomeric Aβ does not adopt a stable secondary structure. Many replica exchange simulations (28, 29, 121, 123-125) have previously been performed using full-length (28, 29) Aβ or Aβ fragments (123, 124) in both explicit and implicit solvent. These studies (28, 29, 121, 123-125) have shown that Aβ prefers a random coil structure in solution, but it is able to form stable secondary structure, which can range from strand-loop-strand structures to small helices, for times during the simulation. One of the most important aspects of these previous studies is that Aβ is able to adopt a multitude of structures and is a highly flexible peptide in solution, considered an integral aspect of Aβ aggregation, over timescales comparable to the simulations performed in this work. However, our results indicate that the interactions of Aβ with the

lipid bilayer do not promote structural ordering similar to observations made in aqueous solution and that conformational motion is likely restricted due to direct protein-lipid interactions. At pH7, Aβ does not form any stable secondary structure on either bilayer, while at pH5, Aβ is able to form some transient β-hairpin structure, especially when bound to the DOPS bilayer. Further, our results show that different β-hairpin structures are formed when bound to DOPS and the Asp23-Lys28 salt bridge interaction may play a significant role in determining which structure is stabilized. These results may appear contrary to experimental results (4, 57-59, 81) showing a significant increase in β-structure when Aβ is mixed with anionic lipid vesicles. It is important to note that these studies are not able to distinguish between Aβ monomers and those small Aβ oligomers on the lipid surface and our results imply that the β-structure seen in experiment is due to peptide-peptide interactions that occur during oligomerization, which are promoted when Aβ is bound to the anionic lipid surface.

The results from the Aβ density distribution analysis also illustrate important aspects of Aβ interactions with lipid bilayers. The density distributions show that the peptide interacts strongly with the interfacial region of the bilayer. Further, residues such as Lys28, when not engaging in intrapeptide salt bridge interactions, are likely interacting with the glycerol backbone or carbon tails of lipid molecules, which stabilizes this binding. The extent of contact between the bilayer surface and Aβ was also calculated at the extreme of the replica exchange simulation, 502K (Figure 3.6). Even at 502K, at least 25 of the 42 residues of Aβ maintain strong contact with the bilayer surface and on average greater then 35 residues remain in contact, independent of bilayer or peptide

charge. These results are not surprising in light of our previous calculations of significant binding free energies for Aβ to the bilayer surface, which are substantially larger than kT even at a system temperature of 502K. These results also agree with previous molecular dynamics studies of pre-inserted Aβ which show either partial or full removal of a transmembrane Aβ from a DPPC bilayer over simulation time due to favorable interactions of Aβ with the interfacial region (69, 136, 138) of the bilayer. Further, previous experimental work (85) has observed favorable interactions of Aβ with the interfacial region of the bilayer both in full length Aβ and Aβ fragments.

The results of these replica exchange molecular dynamics simulations provide significant insight towards the role of cell membranes in Aβ aggregation. While the bilayers used in this study are only simplified models of the complex lipid and cholesterol mixtures that cellular membranes are composed of, these model bilayers do provide an appropriate system for testing Aβ-bilayer interactions on the atomic levels available to molecular dynamics simulations. Further, even though the replica exchange techniques used in this work do improve upon sampling of the conformational free energy surface of Aβ when bound to the bilayer, there are still limitations to the ability of MD to overcome significant free energy barriers over the course of a simulation. It is unknown, solely from this work, if Aβ is able to fully explore its conformational space over the temperature range and time scales adapted for this study and it is likely that large barriers do exist which prevent our study from being able to fully explore this surface over reasonable simulation timescales. Nevertheless, in comparison to previous replica exchange simulations (28, 29, 121, 123-125) of the Aβ peptide in solution with similar

temperature ranges and timescales that show significant peptide flexibility, the motion of the Aβ peptide is severely retarded when bound to the bilayer surface. This comparison between similar replica exchange studies of Aβ in solution and on the bilayer surface implies that Aβ interactions with the bilayer surface substantially affect Aβ dynamics in comparison to Aβ dynamics in solution.

Further, the results of this work imply that the role of the bilayer in Aβ aggregation may be multi-fold, as has been previously postulated (4, 5, 66). First, due to the strong binding of Aβ to the bilayer surface, Aβ peptides will accumulate on the surface of the bilayer. This will transiently increase local peptide concentration and increase diffusion by limiting motion to two dimensions, which will speed up aggregation in comparison to aggregation rates in solution. Next, when bound to the anionic bilayer, the local pH will drop. As has been observed in vitro, Aβ aggregation rates increase in solution at lower pH (62) and the same pattern may hold on the bilayer surface. Finally, the results imply that the hydrophobic section of Aβ is more exposed and accessible on the bilayer surface, which will promote protein-protein interactions through mutual hydrophobic regions of adjacent Aβ monomers that will drive the earliest stages of aggregation. However, these results do not observe any significant structure formation of the monomeric Aβ peptide on the surface of the bilayer, which had been postulated as playing a role in the increased aggregation rate due to lipid interactions. Our results predict that the strongly promoted secondary structure formation in Aβ when mixed with lipids observed in experiment is likely due to the peptide-peptide interactions that are greatly enhanced by interactions with the bilayer. Thus, experimental studies using

highly precise methods for determining Aβ structure both in monomer and small oligomer (dimer, trimer, tetramer) form when bound to a lipid surface will be necessary to determine where the secondary structure formation observed previously is originating. Further, future all-atom or coarse-grain MD studies using a similar replica exchange setup employed in this work with multiple Aβ peptides bound to a bilayer in which direct peptide-peptide interactions and potential secondary structure change are followed would also be very insightful for determining if protein-protein interactions are the cause of the secondary structure change seen in experiment during Aβ aggregation near a membrane surface.

**Conclusions**

In this work, replica exchange MD simulations were performed on all-atom representations of the 42 amino acid Aβ peptide on model lipid bilayers using novel restraints to maintain bilayer integrity at high temperatures. The replica exchange simulations appear to be well mixed and allow for significant conformational freedom for the peptide on the bilayer surface in comparison to MD simulations previously performed at 323K (138). The results of these simulations show that no stable secondary structure if formed by the Aβ monomer at either pH7 or pH5 when bound to the homogeneous DPPC or DOPS bilayers. A salt bridge between Asp23 and Lys28, which may play a significant role in Aβ aggregation, is formed on the DOPS bilayer when the peptide has a net neutral charge, and the formation of the salt bridge imposes a β-hairpin like structure on the peptide. However, this salt bridge is not stable and this secondary structure is not

maintained due to the extensive peptide-lipid interactions that are precluding the intrapeptide interactions necessary for stable secondary structure. In particular, Lys28 substantially interacts with the phosphate moiety and glycerol backbone of the lipid, which stabilizes protein binding to the lipid even at 502K. It appears, from these results, that the strong lipid-protein interactions which force the tight binding of Aβ to the bilayer surface also prevent the internal interactions which would promote the secondary structure change observed during Aβ aggregation in experiment.

The results of this work raise interesting questions regarding the earliest stages of Aβ aggregation near the bilayer surface. Experimental techniques have observed significant β-structure formation when Aβ is incubated with anionic lipid. Our observations tend to indicate that this β-structure formation is not due to structuring at a monomer level but is potentially due to peptide-peptide interactions that are enhanced on the bilayer surface. Further, the lack of secondary structure for monomeric Aβ bound to the bilayer surface may also shed some insight into the large diversity of oligomers that have been observed during Aβ aggregation. As the Aβ monomer is more extended in its membrane-bound, unstructured form, aggregation on the bilayer surface may lead to oligomer structures that are less compact then oligomers observed in solution. In the least, oligomers formed on the bilayer surface should be less structured then oligomers in solution that are forced to have a more compact, ordered structure due to interactions with water. Our work demonstrates that interactions with a membrane significantly effects structural dynamics of the Aβ monomer in comparison to Aβ in solution, which may in turn considerably alter the pathway of Aβ aggregation near the cell membrane.

**TABLE 3.1** Contents of the initial conditions for replica exchange simulations.

**Simulations on DPPC** - 6.4nm x 6.4nm x 15.8nm box

| Aβ pH | DPPC | SPC/E | $Na^+$ | $Cl^-$ |
|---|---|---|---|---|
| pH7 | 128 | 14764 | 27 | 24 |
| pH5 | 128 | 14762 | 24 | 24 |

**Simulations on DOPS** - 6.4nm x 6.4nm x 16.1nm box

| Aβ pH | DOPS | SPC/E | $Na^+$ | $Cl^-$ |
|---|---|---|---|---|
| pH7 | 128 | 15083 | 155 | 24 |
| pH5 | 128 | 15081 | 152 | 24 |

**TABLE 3.2** Temperatures for all replicas used in replica exchange simulation.

| Replica | Temperature (K) | Replica | Temperature (K) |
|---|---|---|---|
| 1 | 325.00 | 43 | 407.85 |
| 2 | 326.81 | 44 | 410.01 |
| 3 | 328.63 | 45 | 412.17 |
| 4 | 330.45 | 46 | 414.35 |
| 5 | 332.29 | 47 | 416.53 |
| 6 | 334.13 | 48 | 418.72 |
| 7 | 335.97 | 49 | 420.92 |
| 8 | 337.82 | 50 | 423.13 |
| 9 | 339.69 | 51 | 425.35 |
| 10 | 341.56 | 52 | 427.58 |
| 11 | 343.44 | 53 | 429.82 |
| 12 | 345.32 | 54 | 432.07 |
| 13 | 347.22 | 55 | 434.33 |
| 14 | 349.12 | 56 | 436.59 |
| 15 | 351.03 | 57 | 438.87 |
| 16 | 352.94 | 58 | 441.16 |
| 17 | 354.87 | 59 | 443.44 |
| 18 | 356.80 | 60 | 445.75 |
| 19 | 358.75 | 61 | 448.06 |
| 20 | 360.69 | 62 | 450.39 |
| 21 | 362.65 | 63 | 452.72 |
| 22 | 364.62 | 64 | 455.07 |
| 23 | 366.59 | 65 | 457.42 |
| 24 | 368.58 | 66 | 459.79 |
| 25 | 370.57 | 67 | 462.22 |
| 26 | 372.57 | 68 | 464.61 |
| 27 | 374.57 | 69 | 467.01 |
| 28 | 376.59 | 70 | 469.40 |
| 29 | 378.62 | 71 | 471.81 |
| 30 | 380.65 | 72 | 474.24 |
| 31 | 382.69 | 73 | 476.65 |
| 32 | 384.74 | 74 | 479.09 |
| 33 | 386.80 | 75 | 481.55 |
| 34 | 388.87 | 76 | 484.02 |
| 35 | 390.94 | 77 | 486.50 |
| 36 | 393.02 | 78 | 488.99 |
| 37 | 395.10 | 79 | 491.24 |
| 38 | 397.21 | 80 | 493.74 |
| 39 | 399.32 | 81 | 496.27 |
| 40 | 401.44 | 82 | 498.78 |
| 41 | 403.57 | 83 | 501.32 |
| 42 | 405.70 | | |

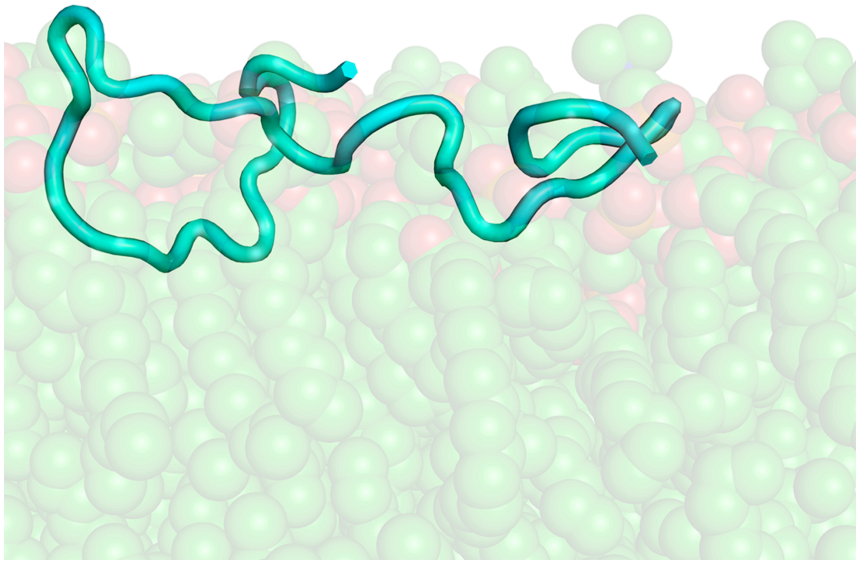

**Figure 3.1** Initial structure of pH7 Aβ peptide on DPPC bilayer. Solvent and ions were removed for clarity.

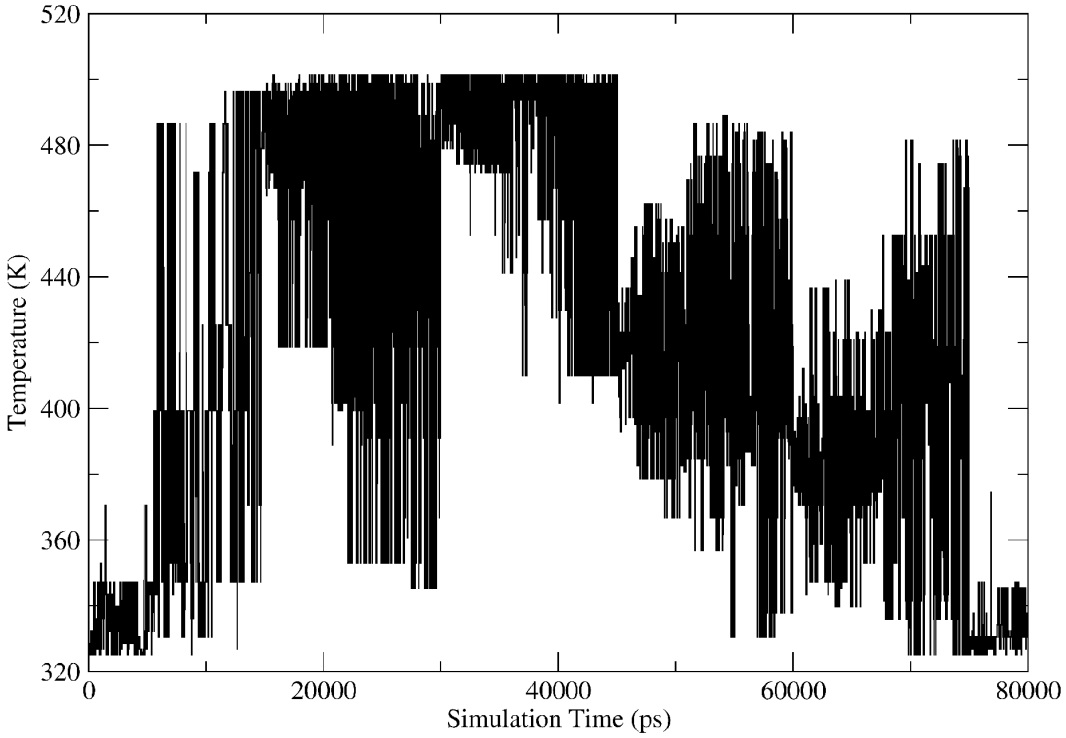


**Figure 3.2** Time series of temperature exchange for replica starting at 325K for the pH7 Aβ peptide on a DPPC bilayer.

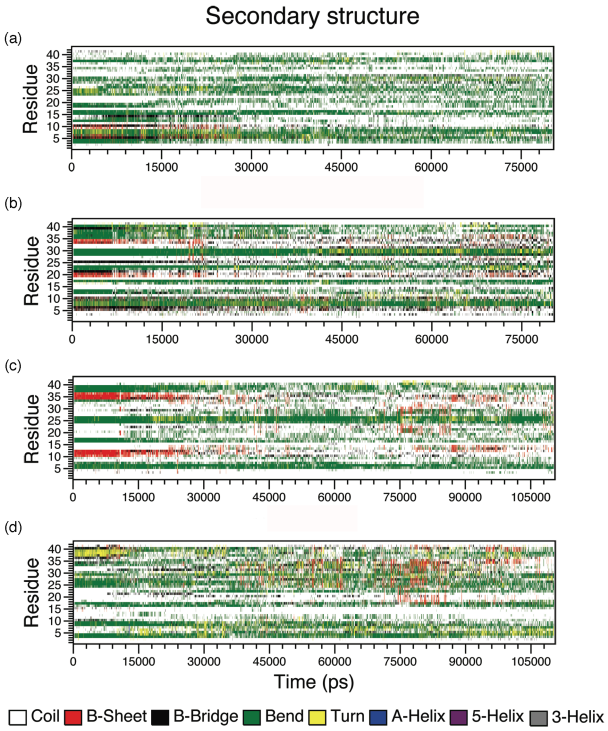


**Figure 3.3** Secondary structure for each residue at 325K for the discontinuous simulations of (a) pH7 Aβ on the DPPC bilayer, (b) pH7 Aβ on DOPS bilayer, (c) pH5 Aβ on the DPPC bilayer and (d) pH5 Aβ on the DOPS bilayer. The secondary structure calculations are for the full 80ns simulations for pH7 Aβ and the full 110ns for pH5 Aβ. Secondary structure readout was produced using DSSP within GROMACS.

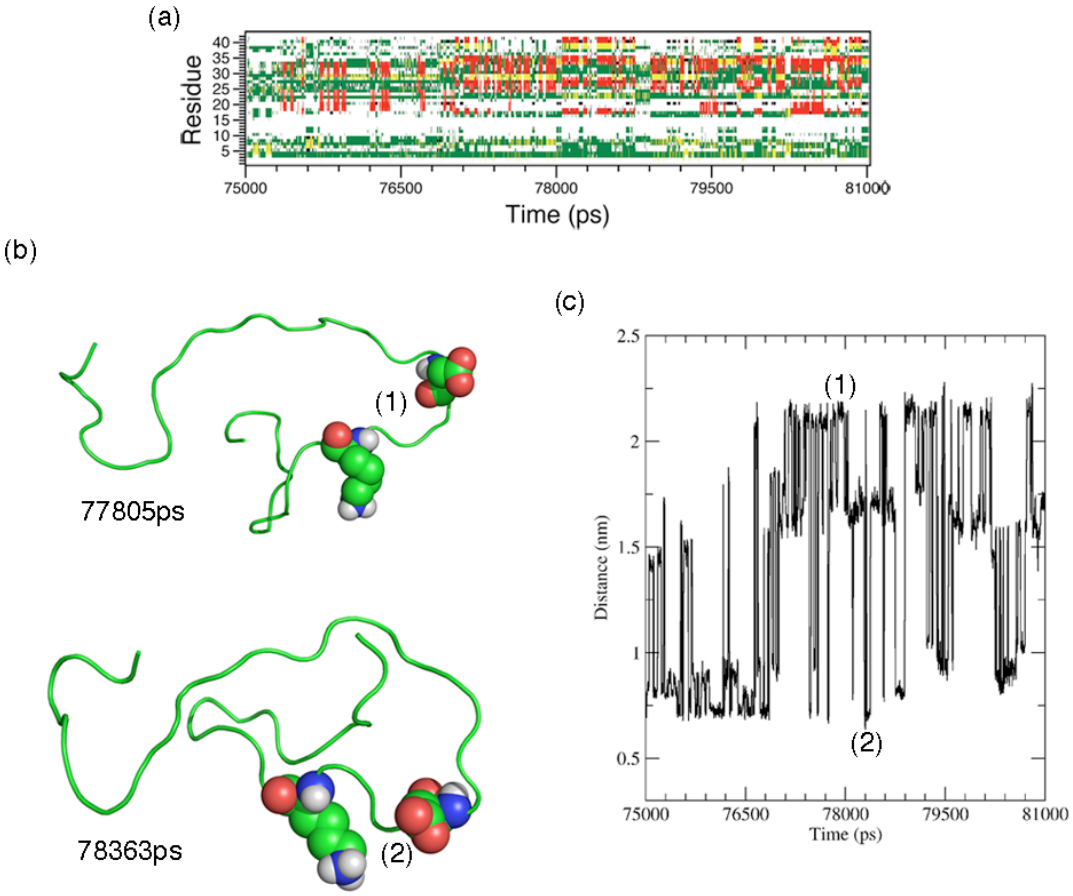


**Figure 3.4** (a) Secondary structure for pH5 Aβ on the DOPS bilayer for the discontinuous simulations at 325K from 75ns to 81ns of simulation time. (b) Aβ structure at timepoints of 77.805ns and 78.363ns showing the average protein structure. Residues Asp23 and Lys28 are shown in space filling mode. (1) and (2) on the snapshots are labels for the salt bridge that could be formed between these residues. (c) Plot of the distance between the $C_\gamma$ of Asp23 and $N_\xi$ of Lys28 over simulation from 75ns to 81ns. The labels (1) and (2) on the plot represent the Asp-Lys distance shown in the snapshots from (b).

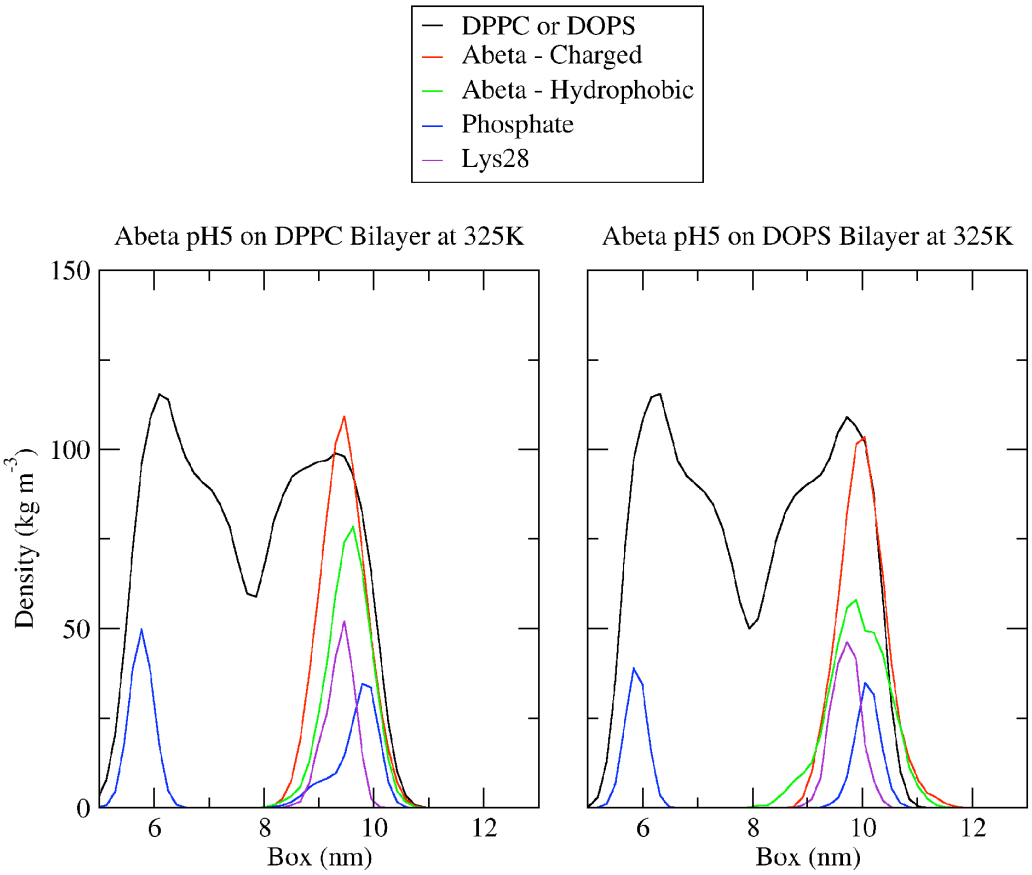


**Figure 3.5** Density distribution of Aβ on DPPC or DOPS bilayer at 325K. The Abeta - Charged density distribution represents residues 1-23 of the Aβ peptide while the Abeta – Hydrophobic density distribution represents residues 24-42. The phosphate density distribution represents the distribution of P8 atoms on the individual DPPC or DOPS lipids within the bilayer.

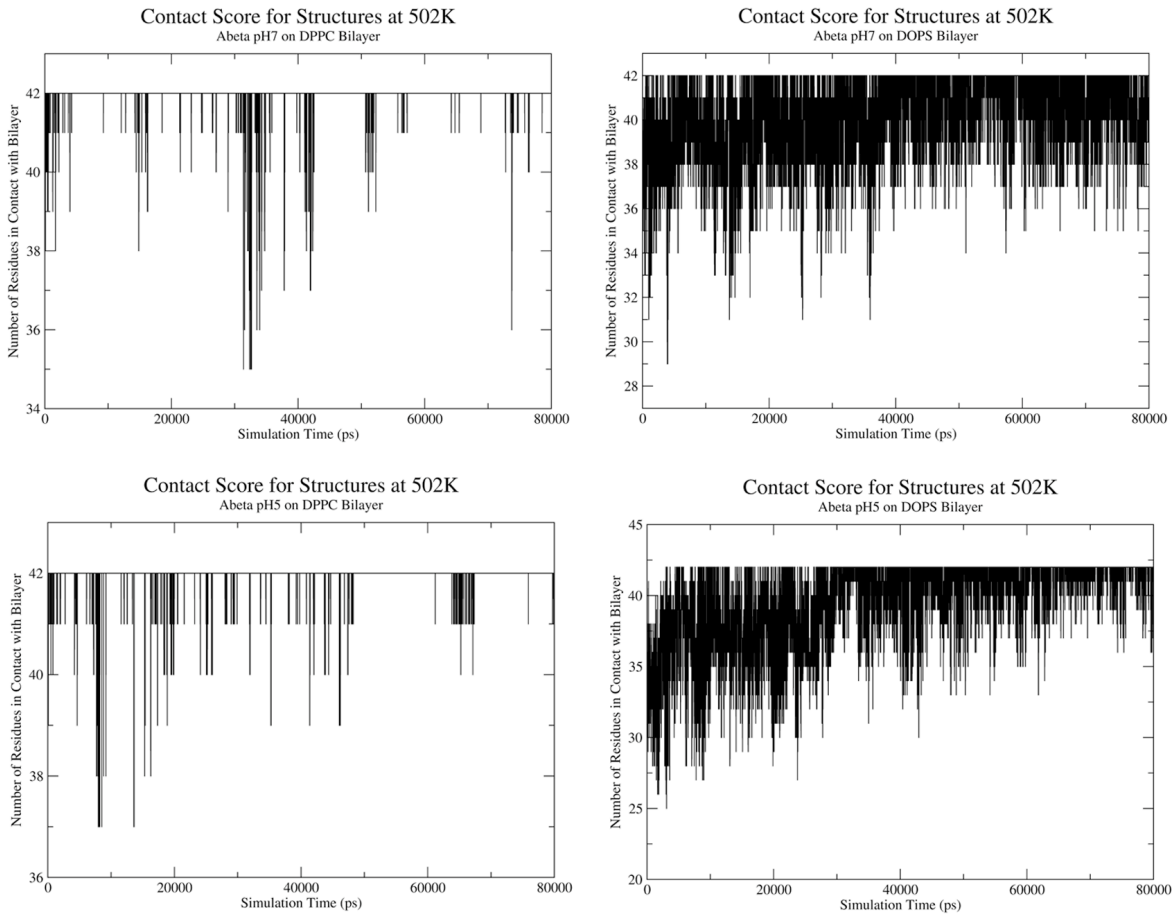


**Figure 3.6** Plots of contact score between Aβ and the bilayer during the replica exchange simulation at 502K. The contact score was calculated so that a given residue had a contact value of 1 if any atom of the residue was within 5Å of the average center-of-mass of the 64 phosphate atoms on the leaflet of the bilayer closest to the peptide. The contact value was zero if there were no atoms within 5Å of the phosphate center-of-mass. As Aβ is 42 amino acids long, the contact score can range from 0 to 42.

**Chapter 4:**

# A Molecular Dynamics Study of the Early Stages of Amyloid-β(1-42) Oligomerization: The Role of Lipid Membranes.

Charles H. Davis[1] and Max L. Berkowitz[2]

*[1]Department of Biochemistry and Biophysics, University of North Carolina at Chapel Hill, Chapel Hill, North Carolina, 27599*
*[2]Department of Chemistry, University of North Carolina at Chapel Hill, Chapel Hill, North Carolina, 27599*

Submitted for publication in *Proteins: Structure, Function and Bioinformatics* on Feb. 19, 2010.

**Abstract**

As research progresses towards understanding the role of the amyloid-β (Aβ) in Alzheimer's disease, certain aspects of the aggregation process for Aβ are still not clear. In particular, the accepted constitution of toxic aggregates in neurons has shifted towards small oligomers. However, the process of forming these oligomers in cells is still not fully clear. Even more interestingly, it has been implied that cell membranes, and, in particular, anionic lipids within those membranes, play a key role in the progression of Aβ aggregation, but the exact nature of the Aβ-membrane interaction in this process is still unknown. In this work, we use a thermodynamic cycle and umbrella sampling molecular dynamics to investigate dimerization of the 42-residue Aβ peptide on model zwitterionic dipalmitoylphosphatidylcholine (DPPC) or model anionic dioleoylphosphatidylserine (DOPS) bilayer surfaces. We determined that Aβ dimerization was strongly favored through interactions with the bilayer. Further, our calculations showed that the DOPS bilayer promoted Aβ release upon dimerization, while DPPC favored tight dimer binding. By promoting dimer formation and subsequent dimer release into the solvent, the DOPS bilayer acts as a catalyst in Aβ aggregation through converting Aβ monomers in solution into Aβ dimers in solution without substantial a free energy cost.

## Introduction

Aberrant protein aggregation and function are the hallmark of a variety of neurodegenerative disorders found in humans. In Alzheimer's disease, the neural degeneration that characterizes this disease has been linked to the aggregation of the amyloid-β (Aβ) peptide, among other potential aggregate species in neurons (3, 11, 12, 40, 45, 154). Because of this direct link between properties of the Aβ peptide and progression of Alzheimer's disease, the Aβ peptide has been at the center of extensive biological research over the last 30 years (3, 11, 12, 40). In particular, both experimental (4, 5, 57-59, 81, 82, 85, 87, 91, 95, 157, 184) and computational (27-29, 69, 74, 121-139) biophysics approaches have focused on this peptide. Along with many other aspects of Aβ function and activity, the underlying processes connected to Aβ aggregation have been of substantial interest to researchers. A more thorough and clearer understanding of the aggregation pathway from Aβ monomer to full Aβ fibril is considered to be crucial to development of any targeted therapeutic against this aspect of Alzheimer's disease.

As our understanding of the aggregation pathway of Aβ has progressed, our view of Aβ toxicity in Alzheimer's disease has evolved (4, 5, 10, 37). Initially, it was believed that full Aβ fibrils or possibly protofibrils were the toxic species in Alzheimer's disease. However, further investigation into this process shifted the focus from full fibrils to Aβ oligomers as the toxic species in neurons (4, 5, 37). Research has shown that these oligomers were able to disrupt cell function and also disrupt homeostasis across the cell membrane (10, 52, 98, 157, 185). Further, it has been postulated that these oligomers

could form ion channels that would allow unregulated flow of ions such as calcium across the cell membrane (79, 98, 185, 190). Recent work has also shown that amyloid fibrils are not harmless but can act as reservoirs of oligomers that can be released if the fibrils are placed under stress (35, 36). Another interesting aspect of this system is the underlying structure of oligomers and fibrils. Aβ monomers have been shown to be mostly random coil in solution (26, 27) with some transient β-sheet or α-helical structure. The Aβ monomer structure can be altered by placing the protein in different environments, promoting either a α-helical or predominantly β-sheet structure (191). However, for Aβ oligomers, the predicted structures of Aβ units are not as clear. The structures of Aβ oligomers have been shown to be highly variable (52-56). Structures that are fibril-like have been observed (55, 56), as well as completely amorphous structures (52-56), or cylindrical structures inserted in cell membranes (74, 79, 80). Thus, it is expected that Aβ oligomer formation is highly heterogeneous and that ordered structure for Aβ is not locked until the protein begins to aggregate into a fibril. Even at the fibril level, there is substantial heterogeneity both on the scale of the fibril as a whole (50, 51), considering the size and shape of the fibril, and the predicted underlying structure of the Aβ units within a fibril (46-49). Thus, a better understanding of the physical processes that dictate Aβ oligomerization and impart such a heterogeneous class of structures to the smallest oligomeric units is essential.

Aβ is a 38-43 amino acid cleavage product of the transmembrane Amyloid Precursor Protein (3, 11, 12). Thus, the Aβ peptide contains significant portions of hydrophobic and hydrophilic residues and shows favorable interactions with cell

membranes (4, 5, 57-59, 81-83, 87, 91, 95, 157). Further, the phenomena dictating the earliest stages of Aβ oligomerization are still not clear. While experimental work is able to replicate most aspects of in-vivo Aβ aggregation with in-vitro methods, these studies still require orders-of-magnitude higher Aβ concentrations to match the aggregation rate of Aβ in cells (58, 82). While many physical attributes of the system, such as cellular pH (62), salt concentration (63), and oxidation of methionine and other residues (64), may play a role in promoting Aβ aggregation in vivo, interactions with cell membranes have been postulated to assist in this process. Cell membranes can affect peptide aggregation through direct electrostatic, hydrophobic or hydrogen bonding interactions with residues of the peptide (4, 5, 66-68), new partially folded free energy states at the bilayer surface (4, 5, 66), faster aggregation rates over a two dimensional lipid surface (4, 5, 66), higher transient peptide concentration as proteins are restricted to the surface and, through lower surface pH due to the attraction of $H^+$ ions in solution to anionic lipid headgroups (57, 67, 68). All of these factors may play a role in Aβ aggregation on the bilayer surface. Previous experimental work (4, 5, 57-59, 81, 85, 87, 157) has demonstrated that interactions between Aβ peptides and lipid vesicles strongly promote a conversion to an amyloid-like structure. Further research (4, 5, 57-59, 81, 87, 91) has shown that mixing anionic lipids with Aβ peptides leads to a substantial increase in aggregation rate. Finally, extensive interactions with cell membranes can lead to Aβ pore formation and disruption of ion balance across the membrane (74, 79, 80, 185). While these results demonstrate the importance of protein-lipid interactions in Aβ aggregation, one shortcoming of these methods is the lack of resolution that results from the low concentration of Aβ necessary to prevent substantial aggregation during the experiment.

Thus, it is unclear what the aggregation state of Aβ is during these investigations using cell membranes. Further work with more detailed methods will be necessary to understand the particulars of atomic-level interactions during Aβ aggregation at the membrane surface.

Towards this end, we use molecular dynamics (MD) simulations to study the earliest step in Aβ aggregation: formation of a dimer. Computational studies have been used with great success to study Aβ structure at the monomer (27-29, 54, 69, 121, 123, 124, 126-128, 130, 132, 135-139), small oligomer (54, 122, 125-127, 131-133, 135), and fibril level (129, 134, 135), using either full-length Aβ (27-29, 69, 121, 122, 125, 131, 133, 135-139) or Aβ fragments (54, 123, 124, 126-130, 132, 134, 135). These studies have used all-atom (27-29, 54, 69, 121-125, 127-130, 133-139) and coarse-grained (126, 131, 132) techniques in various explicit (27, 29, 54, 69, 123, 124, 127-131, 133, 136-139) or implicit (28, 121, 122, 125, 126, 132, 134, 135) solvents to understand this system. More recent works use advanced computational techniques such as replica exchange for even more encompassing studies (28, 121-125, 132, 135, 139). However, the extent of computational research (69, 74, 80, 136-139, 141) on Aβ-lipid interactions is more restricted. Most research that has been previously performed on an Aβ-lipid system has involved use of Aβ monomers (69, 136-139, 141). These works have also been heavily biased towards studying pre-inserted Aβ over interactions between Aβ and the bilayer surface. Our previous work with this system has investigated both the properties of Aβ binding to a model bilayer surface (138) and the structure of Aβ on the bilayer surface (139). Nevertheless, it is of upmost importance to begin to expand these studies to the

small oligomer structure of Aβ. Work has been done towards predicting Aβ pore structure within the bilayer (74, 80), but there is a substantial dearth of investigations in the specific interactions between Aβ and the surface of cell membranes that may promote Aβ dimerization. Recent works (52, 53) have demonstrated the fundamental role that the Aβ dimer plays as a unit of Aβ aggregation. A more complete understanding of the physical processes that dictate Aβ dimer formation at the cell surface is necessary to fully appreciate Aβ aggregation. In this work, we use a thermodynamic cycle to calculate the free energy of dimerization on a model lipid bilayer for two specific Aβ dimers. The results of this work, including comprehensive information gleaned from each process of the thermodynamic cycle, provide molecular level details of Aβ aggregation that can be utilized towards a greater understanding of the earliest stages of aggregation and the toxic role of cell membranes in this process.

## Materials and Methods

*Initial Dimer Structures*

For the calculations presented in this work, two initial dimer structures were selected. These two structures are termed the "extended" and "hairpin" structures throughout the paper. Both structures are derived from possible configurations of 2 Aβ units within a full fibril structure. All Aβ structures used in this work are the 42 residue peptides. The structure of Aβ peptides within a fibril is still controversial as there appears to be a significant amount of heterogeneity in fibril structure (46, 47, 49). . The extended dimer represents a separate dimer unit that has been observed within fibrils (46) where two C-terminal units of adjacent Aβ peptides are shared in an antiparallel structure with non-interacting N-termini. As a crystal structure for the fibril did not exist at the time of these simulations, an idealized structure was manually created from a 42 residue monomer unit within the 2BEG (49) NMR structure. To create the extended C-terminal region, the monomer was placed in a vacuum and a constraint was placed between residue 17 and residue 42 of the peptide. GROMACS 4.0 (143, 145, 186) was used to increase the length between these residues to 7.0nm along the x-axis. A second monomer was created by translating and rotating the first monomer and the two monomers were placed in the appropriate position to create an idealized, antiparallel extended dimer, as shown in Figure 4.1a. The hairpin dimer represents what is believed to be the more consensus structure for a dimer unit within a fibril. The hairpin unit is taken as two monomers from the Protein Database (PDB) code 2BEG fibril structure (49) as edited to include the full N-terminal residues as described in our previous work and pictured in Figure 4.1b of that work (138). In order to create the ideal hairpin dimer structure, we

added the appropriate N-terminal residues to a monomer from the 2BEG structure, then spaced two 42 residue Aβ monomers to exactly reproduce a 2 unit structure from within the 2BEG file (Figure 4.1b). For all structures used in this work, the N-terminus was represented by $NH_3^+$ and the C-terminus was represented by $COO^-$. Further, a united atom GROMOS96 forcefield (143, 145, 186) was used in all calculations to represent the dimer.

As mentioned in our previous works (138, 139), anionic lipids are able to decrease the local pH near the bilayer surface due to attraction of $H^+$ ions from solution to the headgroups at the bilayer surface (57, 68). For Aβ it has been shown that binding of the peptide to a purely anionic palmitoyloleoylphosphatidylglycerol membrane is sufficient to protonate the three histidine residues on Aβ (57). At a physiological pH, Aβ has a net charge of -3. However, upon binding to anionic lipids, the protonation of these three key histidine residues changes the net charge to neutral. Thus, it is important to study Aβ at both the charged and neutral states. We repeated the above procedure for dimer creation for both the charged and neutral states of Aβ. The charge on the histidines was changed using utilities within GROMACS (143, 145, 186).

Once the idealized dimers were created, it was clear that they were unlikely to be stable in their ideal structures and required significant equilibration. Both dimers were solvated in a large box of SPC/E water molecules (173), a steepest descent energy minimization was used to remove clashes in the system, and a short 8ns MD simulation was performed under constant pressure (NPT) conditions to equilibrate the structure. For

the charged system, 6 $Na^+$ ions were added for charge neutrality. For the neutral system, no ions were added. After the short equilibration, a full 150ns MD simulation was performed under the same conditions in order to compare the stability of these idealized structures in solution versus on the bilayer surface during equilibration. For these simulations and all future simulations, including the umbrella sampling simulations, temperature was held constant at 323K using a Nosé-Hoover scheme (171) with a relaxation time of 0.5ps. All bonds were constrained using the P-LINCS algorithm (187). For the full MD steps during all production runs, both during equilibration and umbrella sampling, this constraint allowed for a 3ps time step. Long-range electrostatics used the SPME algorithm (146) with periodic boundary conditions applied in all three dimensions. SPC/E water (173) was used for all simulations. For the systems described under NPT conditions, a Parrinello-Rahman pressure coupling scheme (175) was used with a barostat relaxation time of 0.5ps at a pressure of 1atm. For all umbrella sampling simulations, a constant volume (NVT) constraint was used. If the system was not specifically described as being under NPT conditions, then the system was under a constant volume (NVT) constraint. Secondary structure during the full MD simulations in solution was calculated using the DSSP algorithm (174) with GROMACS.

*Thermodynamic Cycle Calculations*

The goal of this work is to study Aβ dimerization on the bilayer surface. As described in more detail in the Discussion section, direct calculation of this value through umbrella sampling MD simulations would be exceptionally cumbersome and fraught with potential sources of error. Thus, we have decided to use a thermodynamic cycle to

calculate this dimerization free energy indirectly. As demonstrated in Figure 4.2, we are able to calculate a value for $\Delta G_{Dimerization}$ through use of the relationship:

$$2*\Delta G_{Binding} + \Delta G_{Dimerization} + \Delta G_{Release} + \Delta G_{Dissociation} = 0 \quad (4.1)$$

As long as the final structures for the dimer dissociation process results in two equilibrated, non-interacting monomers in solution, the above relationship should hold. The values for $\Delta G_{Binding}$ were calculated for an equilibrated Aβ monomer in a previous work (138). Further, values for $\Delta G_{Release}$ and $\Delta G_{Dissociation}$ can be calculated directly using umbrella sampling techniques (147, 148). The process of dimer release and dimer dissociation does not have as significant of sources of error as the direct calculation of $\Delta G_{Dimerization}$. Thus, the use of this thermodynamic cycle allows us to study the dimerization of Aβ using a more accurate technique considering the current restrictions of computational power available today. Of note, the dimerization free energy is being calculated for only two specific dimer structures. This choice was made so that we could directly investigate how properties of the dimer structure affect the oligomerization process. Thus, the value of $\Delta G_{Dimerization}$ calculated in this work is not a generic dimerization free energy, as would be expected in experiment, but a specific dimerization free energy for a idealized structure at a given charge state.

*Dimer Equilibration on the Bilayer Surface*

In order to perform the umbrella sampling simulations required for our thermodynamic cycle calculations (Figure 4.2), it was necessary for the dimer structures to be extensively equilibrated on the bilayer surface. For the dimer release step of the cycle, the initial structure should be a well-equilibrated, specific dimer structure on the

bilayer surface. Structures for the dimers after the short 8ns equilibration in solution were used for the initial structures for equilibration on the bilayer surface. In our previous work (138, 139), we used a 128-lipid bilayer system. However, because the dimer is larger, we decided to use a 200-lipid system for this study in order to prevent virtual interactions through the periodic boundaries along the bilayer surface. For a model zwitterionic system, we used a dipalmitoylphosphatidylcholine (DPPC) bilayer and, for a model anionic system, we used a dioleylphosphatidylserine (DOPS) bilayer. DPPC was chosen as the zwitterionic system due to its preponderance both in neurons (96) and in simulation studies (178) and DOPS was chosen in part because of its importance to biology (99), but also because of a similar area per headgroup value to DPPC. As we are studying protein-lipid interactions at the bilayer surface, area per headgroup is an important physical parameter with regards to charge density. These same lipids were used for our previous investigations, so bilayer equilibration was exactly as described in a previous work (138, 176). Both lipids were described using the Berger force field parameters (176).

Starting with both the equilibrated bilayer and equilibrated dimer structures, the dimer was solvated and placed at a distance away from the bilayer surface. Only the charged dimer was used in simulations with DPPC and only the neutral dimer was used in simulations with DOPS. This pairing created 4 initial conditions: charged Aβ/DPPC for the extended and hairpin dimers and neutral Aβ/DOPS for the extended and hairpin dimers. For the charged Aβ/DPPC system, $30Na^+$ and $24Cl^-$ ions were added to approximate a 0.1M NaCl system. For the neutral Aβ/DOPS system, $224Na^+$ and $24Cl^-$

ions were added. The extra 200 $Na^+$ ions were necessary to counteract the charge on the DOPS lipids and were already included in the equilibration process for the DOPS bilayer. A more detailed description of exactly how a similar system was built using an Aβ monomer instead of Aβ dimer is provided in a previous work (138). After the system was built and energy minimization was applied, a short 500ps simulation was performed under NPT conditions to allow the peptide-bilayer system to reach a transient equilibration. Because of the constraints that the bilayer surface places on building a peptide-bilayer system, the dimer was originally placed in solution at approximately 2nm above the bilayer surface. A 4ns equilibration under NVT conditions was then performed with an umbrella constraint placed between the dimer center of mass and bilayer center of mass. This equilibration forces the dimer to bind to the bilayer surface without creating any significant clashes. For the simulations on DPPC, the constraint minimum was at a center of mass separation of 2.1nm while, with DOPS, the constraint minimum was at 2.4nm. A force constant of 500 kJ/(mol*$nm^2$) was used. After the 4ns simulations with the constraint, the umbrella constraint was removed and another 4ns equilibration simulation was performed. Once these equilibration steps were finished, the dimer was strongly bound to the bilayer surface. However, the dimer had not been given adequate time to reach equilibration on the bilayer surface. The equilibration under NVT conditions was then extended for another 150ns to allow for an extensive dimer equilibration. The secondary structure of the dimer during equilibration was calculated using the DSSP algorithm.

*Dimer Release from the Bilayer Surface*

To calculate the free energy for dimer release from the bilayer surface, an umbrella sampling procedure (147, 148) was utilized. Umbrella sampling allows us to directly calculate this free energy while providing full MD trajectories within each umbrella that are available in order to understand the dimer removal process in a stepwise fashion. We initially attempted to pull the equilibrated dimer from the bilayer surface using the final structure of the 150ns dimer equilibration on the bilayer surface. However, upon placing a constraint on the dimer and removing the dimer from the surface, strong protein-lipid interactions led to significant bilayer disruption. To overcome this issue, we decided to model dimer release as the negative free energy of dimer binding. Using enough umbrellas and a long enough MD simulation within each umbrella, dimer binding should be similar to dimer release with regards to the potential of mean force profiles calculated using the Weighted Histogram Analysis Method (WHAM) (150). As long as the initial dimer structure is the same as the equilibrated dimer on the bilayer surface, the dimer will not have enough time during the quick pulling process for any substantial internal motion to change the equilibration it shared with the bilayer. The dimer structure from the final snapshot at the end of the 150ns equilibration on the bilayer surface was used for this process. Similar to the procedure for initially creating the dimer-bilayer system, the dimer was placed at a significant distance away from the pre-equilibrated lipid bilayer and solvated with SPC/E water and either $30Na^+/24Cl^-$ (charged Aβ) or $224Na^+/24Cl^-$ (neutral Aβ) ions. After energy minimization, a short 4ns equilibration was performed under NVT conditions with an umbrella restraint between the dimer center of mass and bilayer center of mass. For the

charged/DPPC systems, the constraint minimum was 7.0nm and, for the neutral/DOPS system, the constraint minimum was at 8.0nm. This constraint was necessary during the equilibration to prevent any dimer-bilayer interactions. Once the system was equilibrated, umbrella sampling could be performed.

For umbrella sampling, the reaction coordinate used for the pulling process was the dimer – bilayer center of mass separation. Thirteen windows were placed between center of mass separations of 1.8nm to 6.9nm along the reaction coordinate. This results in a 0.3nm distance between windows, which allowed for adequate sampling in our previous umbrella sampling calculations (138). A spring constant of 500 kJ/(mol*nm$^2$) was placed on each center of mass separation. Starting from the same initial condition, 150ns MD simulations were performed within each window. In our previous work (138) investigating Aβ monomer binding to lipid bilayers, 80ns simulations were performed in each window. However, because of the larger size of the dimer and the use of a larger bilayer, the lengths of MD simulations performed within each window were extended to improve upon sampling. Within each window, analysis was performed using either GROMACS code or the DSSP algorithm within GROMACS. Once the MD simulations within each window were finished, a potential of mean force was calculated using the WHAM methodology adapted for in-house code. The potential of mean force curves calculated for this process are given in Figure 4.4a. The difference between the minimum and maximum on the potential of mean force curve are given in Supplementary Information. Further, block error analysis was used to calculate the error in this process. Using the charged Aβ/DPPC system for the extended dimer, the error converged to

7.0kcal/mol after separating the system into 40 blocks. While this error appears to be rather large, it is similar to the error calculated for Aβ monomer binding to the bilayer surface. For both procedures, the error is 25% of the value calculated for the minimum-maximum separation on the potential of mean force curve. Further, a $\Delta G_{Release}$ could be calculated from the potential of mean force curve as described previously (192). In short, the following equation was used for this calculation, where W(z) represents the potential of mean force curve:

$$\exp\left(\frac{-\Delta G_{\text{Release}}}{k_b T}\right) = \frac{1}{l_0}\int_0^{\infty}\left(\exp\left[-\beta W(z)\right]-1\right)dz \qquad (4.2)$$

In obtaining $\Delta G_{Release}$, $l_0$ was determined as the reaction coordinate value where the potential of mean force reached a value of zero once appropriate shifting of the potential of mean force curves was performed. However, in performing these calculations, we observed that the values for $\Delta G_{Release}$ were resistant to the value chosen for $l_0$; thus, $\Delta G_{Release}$ was fairly robust. Values for $\Delta G_{Release}$ are provided in Table 4.1. Also, since the values that were reported in our previous work (138) for $\Delta G_{Binding}$ were the difference between the minimum and maximum values of the potential of mean force curves, we recalculated $\Delta G_{Binding}$ from these curves using equation 4.2. These values are also reported in Table 4.1. Comparing these $\Delta G_{Binding}$ values to the values reported in the previous work (138), it is clear that there is not a significant difference between the two values and all patterns presented in the previous work hold for $\Delta G_{Binding}$.

*Dimer Dissociation*

To calculate the final necessary step in the thermodynamic cycle, umbrella sampling simulations were performed to approximate the dimer dissociation process. For these simulations, it was necessary to separate the two monomers from a well-equilibrated dimer in solution and allow the two monomers to reach equilibration in solution without interacting. Due to the procedure used in the dimer release calculations, a well-equilibrated dimer in solution was already available. The final dimer structure from the 6.9nm center of mass separation umbrella after 150ns of MD simulation was isolated and used as the initial structure for the dimer dissociation calculations. The isolated dimer was solvated in a large box of SPC/E water with either $30Na^{+}/24Cl^{-}$ (charged Aβ) or $24Na^{+}/24Cl^{-}$ (neutral Aβ) ions. Again, this procedure was repeated for both the extended and hairpin dimers, creating 4 initial conditions for umbrella sampling. Further, the water box was quite large (12.0 nm) along the z-axis, which was the chosen axis for the reaction coordinate, to prevent the monomers from interacting through periodic boundaries. After energy minimization, a short 1ns MD simulation was performed to allow the system to come to equilibration. After equilibration, umbrella sampling was performed. For the reaction coordinate of this system, the center of mass separation along the z-axis of the box was chosen. This coordinate ensured a final system of two separated, non-interacting monomers. Twenty umbrellas were placed between center of mass separations from 0.1nm to 5.8nm, providing a separation of 0.3nm between umbrellas. A spring constant of 500 kJ/(mol*$nm^2$) was placed on each center of mass separation. For the neutral Aβ hairpin dimer system, an extra umbrella was added at 6.1nm to provide further data for the largest center of mass separations. Within each

umbrella, 150ns of MD simulations were performed. Similar to the dimer release step, analysis was performed using GROMACS utilities and potential of mean force curves for dimer dissociation wers calculated using WHAM adapted for in house code. The potential of mean force curves are provided in Figure 4.3b, the difference between the minimum and maximum values of the potential of mean force are provided in Supplementary Information, and the $\Delta G_{Dissociation}$, calculated using equation 4.2, is given in Table 4.1. The error in the potential of mean force curves for dimer dissociation was calculated in the same manner as for the dimer release step, using the charged Aβ extended dimer to calculate an error of 5.0 kcal/mol. Similar to the binding and release steps, this was close to an error of 25%. Finally, $\Delta G_{Dimerization}$ was calculated from equation 4.1 and provided in Table 4.1.

## Results

*Equilibration Simulations*

As described in the Methods section, two initial dimer structures (Figure 4.1) were used to calculate a specific dimerization free energy for each Aβ dimer on the bilayer surface. The first of these structures, the extended dimer (Figure 4.1a), represents shared C-termini between two Aβ monomers as predicted from electron microscopy data (46). The other structure, the hairpin dimer (Figure 4.1b), represents two monomer units from within an Aβ fibril as determined by x-ray crystallography (49). Thus, intense equilibration is necessary in order to bring each structure to an equilibrated state on the bilayer surface from which our thermodynamic cycle calculations could begin. Initially, each structure was equilibrated in solution for a short time to remove any clashes due to the placement of each monomer in the dimer. Then, the dimer was placed on the surface of a model lipid bilayer and 150ns MD simulations were performed. These simulations allowed the dimer adequate time to equilibrate to the bilayer environment with the intention that this long equilibration time will reduce the bias due to initial conditions in the free energy calculations for removal of the dimer from the bilayer surface.

However, aside from just equilibration, these 150ns simulations provided an ideal opportunity to study the stability of the idealized dimer structures on the bilayer surface versus in solution. Along with the 150ns equilibration on the bilayer surface, we also continued the short equilibration in solution for an analogous 150ns. By comparing the evolution of the dimer secondary structure over these equilibration events, it is possible to study the stability of these specific, ideal dimer structures in either environment.

Representative plots of the DSSP secondary structure readout are given in Figure 4.3. As can be seen for all four plots shown, the dimer structure is not exceptionally stable and does tend to fluctuate in all cases. In comparing the extended charged dimer in solution (Figure 4.3a) versus on the surface of a DPPC bilayer (Figure 4.3b), it is clear that the dimer in solution maintains its structure to a greater extent then the dimer on the bilayer surface. It appears that the only secondary structure feature that is maintained throughout both simulations is the turn on the second monomer approximately near residue 20 (residue 62 on the plots). In solution, a much stronger beta sheet region is formed between residues 30 and 40 on both monomers. For the extended dimer structure, this represents the region of overlap between the two monomers, where the monomers can strongly interact with each other. When this dimer is in solution, the almost entirely hydrophobic section of each monomer preferentially interacts with the other monomer over being fully exposed to the solution, thus forcing the more stable secondary structure. However, when bound to the surface of DPPC, the hydrophobic C-terminus of each monomer can preferentially interact with the interfacial region of the lipid bilayer, thus providing favorable options outside of protein-protein interactions for each monomer, which decreases the stability of the dimer secondary structure. For residues 1-20 of both monomers, which are more hydrophilic and are not able to undergo interprotein interactions between monomers due to the geometry of the dimer, the residues are mostly unstructured in either environment.

Figures 4.3c and 4.3d demonstrate the secondary structure comparison for the uncharged hairpin dimer in solution versus on the surface of the DOPS bilayer. Similar

to the extended dimer, the presence of the lipid bilayer alters the stability of certain elements of secondary structure. Unlike the extended dimer, all regions of the hairpin dimer are able to undergo interprotein interactions as the two monomers are stacked on one another. In comparing dimer stability in the two environments, it is clear that β-sheet structure is stabilized to some extent both in solution and on the bilayer surface. In both environments, though, the β-sheet structure does tend to dissipate over time and the amount of dimer secondary structure decreases. This is not surprising as the secondary structure of the hairpin is largely derived from the very regular arrangement of Aβ within a fibril. By removing stabilizing interactions on both sides of the dimer unit by removing it from a fibril, it would be expected that the peptide would become more disordered. Interestingly, in solution, a turn is formed between residues 25-29 in one of the monomers that quickly dissipates on the bilayer surface. It appears that the hydrophobic residues in this turn region, such as glycine or alanine, plus the positive charged lysine 28 begin to interact with aspects of the lipid bilayer that tend to unfold this turn and disrupt the dimer structure. Further, it is also of note that the ordered, stacked β-sheet structure is maintained for longer on the bilayer surface. It is possible that the bilayer acts to replace one of the missing surfaces that is lost when the dimer structure was removed from the fibril. From the plots, though, it appears that the bilayer surface is not an ideal replacement of the fibril as the β-structure is still largely lost by the end of the 150ns simulation. For all four initial conditions that were investigated, the effects described here are consistent. The comparison of these simulations demonstrates that the lipid bilayer does play an interesting role in dimer stability and that neither of these ideal dimer structures are fully stable with regards to secondary structure either in solution or

on the bilayer surface. Nevertheless, for all equilibration simulations, the two monomers do stay tightly bound to each other during the extent of the equilibrations.

*Thermodynamic Cycle Calculations*

Once the dimers were appropriately equilibrated on the bilayer surface, the thermodynamic cycle calculations could be performed, as demonstrated in Figure 4.2. The thermodynamic cycle allowed us to calculate a quantity, $\Delta G_{Dimerization}$, that would be very difficult to calculate directly due to bias created from the choice of reaction coordinate for the pulling procedure. By calculating quantities with more obvious reaction coordinates that are less affected by this initial bias, we are able to have more confidence in this free energy calculation. Further, by calculating $\Delta G_{Dimerization}$ for two specific dimers instead of one generic dimer calculation, we can draw more specific conclusion regarding the effect of the bilayer on this process. A more detailed description of our logic for using a thermodynamic cycle for these calculations is included in the Discussion.

The results of these calculations are summarized in Table 4.1. The dimerization free energy is calculated using the results as shown in equation 4.1. The free energies presented in Table 4.1 are calculated from the potentials of mean force as described in equation 4.2. The errors presented in the Materials and Methods section are calculated using block error analysis from the potentials of mean force on the charged Aβ + DPPC free energy calculations for dimer release or the charged Aβ in solution free energy calculations for dimer dissociation. All data for step 1 is taken from a previous work

(138). For a thorough discussion of the monomer binding process, please see our previous work (note that Aβ charged is referred to a pH7 and Aβ neutral is referred to as pH5 in the previous work). To better understand the results in Table 4.1, it is best to present each step individually and then investigate the calculated dimerization free energy.

*Dimer Release from the Bilayer Surface*

The release of the Aβ dimer from the bilayer surface is the third step in our cycle. The potentials of mean force calculated for this process are given in Figure 4.4a. From examining both the potential of mean force curves and the calculated free energies, it is clear that the largest source of distinction between systems is the charge on the lipid. For the charged peptide on DPPC, the structure of the dimer does not affect the dimer release free energy to any extent. The free energies for release are similar and the shapes of the potentials are also similar. Further, the release free energy of the dimer is quite large, implying a very strong attraction of the dimer to the bilayer surface. It is interesting that the magnitude of the release free energy is very close to twice the magnitude of the binding free energy of the monomer. Also, the potential curve for dimer release is remarkably similar to the monomer binding curves presented in our earlier work (138). This implies that the Aβ dimer is still preferentially interacting with the interfacial region of the lipid bilayer and the protein-protein interaction within the dimer is not particularly strong. The minimum of the potential of mean force curve also implies a strong interaction with the interfacial region of the bilayer surface. Thus, as the dimer is

removed from the bilayer surface, the peptide-lipid interaction becomes weaker and the peptide-peptide interaction becomes dominant in order to retain the fidelity of the dimer.

For the neutral Aβ dimer interacting with the DOPS bilayer, the structure of the dimer also does not effect the dimer release process. Both the extended and hairpin free energies of dimer release and the potentials of mean force curves are very similar. However, in contrast to the calculations on DPPC, the release free energy on DOPS is much smaller. Further, the potential of mean force curves are also more rugged near the free energy minimum. For the calculations on DPPC, there is a sharp drop in potential when approaching the minimum on the surface. Yet, on DOPS, there is no sharp drop in the potential and the dimer center of mass can explore approximately anywhere within a 2nm range of the free energy minimum without a substantial gain in free energy. All of these aspects of the potential of mean force curves imply a weaker interaction between the dimer and the bilayer surface. Also, the location of the free energy minimum provides evidence towards a weaker interaction. While the free energy minimum is sharply centered around a dimer-bilayer center of mass separation of 2nm on DPPC, the free energy minimum on DOPS is closer to a 3-3.5nm center of mass separation. A one-dimensional center of mass separation reaction coordinate can be a very deceiving coordinate, but visual inspection and analogies to our previous work (138, 139) do show that the DOPS dimer is not strongly interacting with the interfacial region of the bilayer, as in the case of the dimer on DPPC, but is only transiently interacting with the head group region of the bilayer. Further, the weak free energy of dimer release demonstrates that the DOPS bilayer biases the system towards strong peptide-peptide interactions due to weaker protein-lipid interactions. This is in direct contrast to the strong peptide-lipid

and weak peptide-peptide interactions observed on the surface of the DPPC bilayer. This result may have implications for the biological differences in Aβ interactions between zwitterionic and anionic lipids as described in more detail in the Discussion section.

Along with the analysis of the free energies for dimer release and potential of mean force curves, we also investigated secondary structure change during the dimer release process. Use of umbrella sampling for free energy calculations provides 150ns simulations at a series of dimer-bilayer center of mass separations. By analyzing secondary structure content within each umbrella, we are able to obtain some insight into how secondary structure changes as the dimer is released from the bilayer surface. Figure 4.5a shows the average β-structure for each of the dimers studied as a function of center of mass separation. For these calculations, β-content is termed as any residue with β-bridge or β-sheet structure as determined by DSSP calculation. From this plot, it appears that the amount of β-content slowly increases as the dimer is removed from the bilayer surface. For the charged and neutral extended dimer and the neutral hairpin dimer, the average β-content is approximately the same, between 10-20 residues. For the charged hairpin dimer, the average β-content is somewhat higher than the same structure with a neutral charge. However, it is important to note that this average is very deceiving. The average value for β-content does increase as the dimer is pulled from the surface, but it is not clear if these averages are due to a population of a few structures centered on one average structure or if the average is due to a large range of structures over a significant variation in β-content. To investigate this discrepancy, we calculated free energy surfaces as shown in Figures 4.5b and 4.5c. Figures 4.5b and 4.5c show the

free energy surface for either the charged extended dimer (Figure 4.5b) or the charged hairpin dimer (Figure 4.5c) as a function of bilayer-dimer center of mass separation and the number of β-residues. What is obvious from these plots is how similar these two surfaces are. In both cases, there are no substantial free energy wells at a given bilayer-center of mass separation. Actually, if the value of bilayer-center of mass separation is fixed, there appears to be no favored number of β-residues. This implies that the secondary structure content for either the extended dimer or the hairpin dimer is very fluid and there is not a "dominant" structure throughout this process. Also, this demonstrates that the apparent slight increase in average β-structure as the dimer is removed from the surface is not significant. It appears that the averages shown in Figure 4.5a are a numerical value with little physical significance as the average is not representative of the expansive population of potential secondary structures available to the dimer at any dimer-bilayer center of mass separation. These results are consistent for the dimer release process neutral dimer from the DOPS bilayer as well. What can be concluded from these plots is that neither lipids in bilayer surface or water molecules in solution greatly bias the dimer towards a specific secondary structure but allow for substantial structural flexibility. What does appear to effect secondary structure more substantially is the dimer structure. Yet, because of the wide range of available secondary structures for both extended and hairpin dimers, it would be difficult to draw any strong conclusion. We also investigated other secondary structure elements, such as helix content, as it has been predicted that Aβ can adopt a helical shape when inserted near the bilayer interface (69). However, as the initial dimer structures were heavily biased towards β-sheets, the extent of helix structure was negligible and any helix

structure that appeared was transient. For the dimer release process, it appears that the nature of the lipid headgroup significantly affects the energetics of the release process, but does not bias the system towards a favored secondary structure content during release.

*Dimer Dissociation*

The fourth step in the thermodynamic cycle involved calculation of the free energy required to dissolve the specific Aβ dimer structure in solution, leaving two non-interacting Aβ monomers. For this calculation, the final Aβ structure from step 3 at the largest bilayer-center of mass separation was used as the initial structure for step 4. The dimer was placed in a water box large enough so that periodic images would not interact at the largest monomer-monomer center of mass separation. Again, as in the dimer release calculation, umbrella sampling was used to calculate the potential of mean force curves (Figure 4.4b) and the $\Delta G_{Dissociation}$ was calculated.

From both the $\Delta G_{Dissociation}$ values and the potential of mean force curves, it is apparent that a significant amount of free energy is required to dissolve both dimer structures. In solution, the protein-protein interactions for both dimer structures are very strong, thus leading to the high free energy of dissociation. Further, the potentials of mean force for all four structures show a similar shape. The curves are smooth until close to the free energy minimum, where a sharper drop occurs until a broad free energy minimum is reached. The basis behind such a free energy profile is reminiscent of a dock-and-lock mechanism similar to those proposed for monomer addition to an amyloid

fibril (134). However, this is a very tenuous comparison as the dock-and-lock mechanism has a very ordered pathway with important intermediate steps while this dimer dissolution seems to be much more fluid. Yet, it still appears that the two monomers quickly form an ordered structure once the two monomers are close enough together. Once the monomers are separated enough to break this ordered structure, the profile shows a smooth release of one monomer from another, as peptide-peptide interactions are smoothly and consistently broken as the center of mass separation increases.

For the charged extended, neutral extended and charged hairpin dimer structures, both the $\Delta G_{Dissociation}$ and the potential of mean forces curves are very similar. This is not surprising considering the interactions that are stabilizing the dimer. For both extended dimer structures, the monomers are overlapping from approximately residues 28 – 42 on the C-terminus. The majority of residues in this region of Aβ are hydrophobic and derive from the transmembrane portion of the APP peptide before secretase cleavage. As there are no histidines in this region of the peptide, there should be no difference within the overlapping regions of the monomer for the charged and neutral dimer. The difference in charge between these two species is at the N-terminus of the peptide and these regions of the dimer do not participate in any extensive interprotein interactions. This information also provides an important baseline for the strength of the hydrophobic interaction at the C-terminus of the peptide. With $\Delta G_{Dissociation}$ values between -15kcal/mol and -20kcal/mol, the hydrophobic interactions and potential hydrogen bonding interactions

between the two C-termini of the monomers provide a substantial stabilizing force for this dimer structure.

The hairpin dimer also shows a very interesting pattern in the potential of mean force profiles. For the charged hairpin dimer, the $\Delta G_{Dissociation}$ and potential of mean force profiles are very similar to the extended dimers. This implies a very similar peptide-peptide interaction to the interactions observed for the extended dimers. However, the neutral hairpin dimer is very different from the three other conditions. While the potential of mean force curve is similar in its shape, the $\Delta G_{Dissociation}$ for the neutral dimer is more then 50% larger than the $\Delta G_{Dissociation}$ of the charged peptide. Thus, extra interactions are occurring in the neutral dimer that are not available to charged dimer. As mentioned previously, the difference between the charged and neutral dimer are the protonation of three histidines (His 6, His 13 and His 14) on the N-terminal tail of Aβ. While, for the extended dimer, the geometry of the dimer prevents the two N-terminal tails from interacting, the hairpin dimer almost promotes N-terminal tail interaction due to the geometry. As mentioned in more detail in the Methods section, high temperatures are used in the equilibration of the hairpin dimer to randomize the structure of the N-terminal tails and prevent any bias due to the initial structure of the N-terminus. However, once the dimer is placed on the bilayer surface, it is possible for these tails to interact. Further, because of the strong interactions occurring between residues 28 – 42 of the two monomers, as demonstrated by the large $\Delta G_{Dissociation}$ of the extended dimers, the N-terminal tails are restricted in their motion. It is also a fallacy to state that these tails are fully charged or hydrophilic. While the tails do contain the majority of charged or hydrophilic residues in the peptide, a significant number of amino acids in the N-

terminus are still hydrophobic. Thus, strong interactions could occur between the two N-terminus tails.

To investigate if the N-terminus residues are the cause of the significant difference between the $\Delta G_{Dissociation}$ of the charged and neutral hairpin dimers, we calculated center of mass distances between residues of the two monomers (Figure 4.6). The reasoning behind these calculations was to see if specific interactions were occurring for the neutral peptides that were not occurring for the charged peptides due to the protonation of the three histidines. Figure 4.6 shows four representative plots for these distances. Also, for each pair of residues, the distance was calculated for three different windows. Each window corresponds to the free energy minimum and the use of three different windows shows that these effects are not due the choice of a specific simulation. It can be observed for three of these plots that the two analyzed residues are much closer for the neutral dimer and the separation between them fluctuates much less, implying a more stable dimer structure. For $His6_1$ and $Asp7_2$ (where the subscripts identify the monomer) and $His6_1$ and $Glu3_2$, there is a much larger fluctuation for the charged tails. This demonstrates that the far N-terminal tails of the charged dimer show some electrostatic repulsion between the two tails which prevents them from coming close enough to form stable electrostatic or hydrogen bonding interactions. For $His14_2$ and $Glu11_1$, the fluctuations are less extreme than the first two examples for the charged dimer, but the extent of fluctuations is still larger than for the neutral dimer. The smaller fluctuations for these two residues for the charged dimer are likely due to the geometric restrictions of being closer to the "fixed" points of the hydrophobic region of the peptide. Further, the neutral dimer shows a smaller distance between the two residues, implying

that a direct electrostatic interaction is formed. Once again, this shows that electrostatic interactions are occurring between residues of the N-terminal tails that act like a glue to stick to the tail together, which helps to form hydrophobic or hydrogen-bonding interactions that are not seen between the two N-terminal tails for the charged dimer. The interaction between $His13_1$ and $Asp11_2$ is included to show that this pattern does not hold for all pairs of charged residues on the N-terminal tails. However, analysis of all pairs of nearby charged residues with His6, His13 and His14 in the N-terminal tails shows patterns closest to the first three plots shown in Figure 4.6 for the majority of pairs. Further, similar analysis was done with some hydrophobic pairs within the N-terminus. While the results were not as dramatic as the pair distance plots shown in Figure 4.6, the neutral dimer did show closer pair distances and less fluctuation then the charged dimer. These results imply that the much stronger $\Delta G_{Dissociation}$ for the neutral hairpin dimer is due to interactions between the N-terminus of the two monomers. They also emphasize the importance of the N-terminus and the role of pH and protein charge in the Aβ aggregation process.

*Dimerization on the Bilayer Surface*

The value for $\Delta G_{Dimerization}$ is calculated using equation 4.1 from the free energy values calculated in this work and a previous work (138). Further, in Table 4.1, a value for $\Delta G_{Dimerization} + 2*\Delta G_{Binding}$, which can be termed the total dimerization free energy, is also provided. This second value represents the free energy gain in binding two non-interacting Aβ monomers in solution into a specific dimer structure on the bilayer surface. The values for $\Delta G_{Dimerization}$ show that dimerization on the bilayer surface is

strongly favorable for all conditions except the neutral extended dimer. For this structure, the weak $\Delta G_{Release}$ is not compensated for by a strong $\Delta G_{Dissociation}$, as in the case of the neutral hairpin dimer, which results in an unfavorable dimerization free energy. For the other three conditions, the $\Delta G_{Dimerization}$ is similar, demonstrating that an interaction with the bilayer can act to drive dimerization. For all conditions, the total dimerization free energy ($\Delta G_{Dimerization} + 2*\Delta G_{Binding}$) is very favorable. Even for the neutral extended dimer, the large free energy gain upon monomer binding is able to drive a favorable dimerization process. It is important to consider this total dimerization free energy in comparison to the directly calculated $\Delta G_{Dimerization}$ as binding of the monomer to the bilayer surface may be one of the key aspects of membrane-assisted Aβ aggregation. A discussion of the role of the membrane in this process and the information contained in $\Delta G_{Dimerization}$ versus the total dimerization free energy has been reserved for later in the Discussion section. Overall, these results of the calculations from the thermodynamic cycle presented in this work demonstrate the effect of the membrane on multiple aspects of Aβ dimerization process.

**Discussion**

The results from this work using thermodynamic cycles to calculate dimerization free energies for the Aβ peptide on a membrane provide a wealth of insight into the early stages of the Aβ oligomerization process on lipid membranes. One of the first, and most fundamental, points of discussion in this work is the choice of two specific dimer structures. The two dimer structures which we used for this work are derived from a theoretical dimer structure within a fibril as predicted through electron microscopy (46) and a structure obtained directly from a x-ray crystallography structure of an Aβ fibril (49). For this work, we are deriving no actual conclusions as to which of these structures is correct or which structure is most likely within a fibril. Previous work has demonstrated that the small oligomer structures of Aβ are very heterogeneous, including structures containing significant β-sheet, α-helix and unstructured sections. Further, it has been proposed that the ordered structures seen in fibrils are not a function of the smallest oligomer structures but get locked in depending on the aggregation pathway a given oligomer takes (52, 53). Thus, our choices for dimer structures were not motivated by pure predictive power of the method, but more for the structural differences between these dimers that do have some basis in biology. The extended dimer is a much more exposed dimer with the N-terminal sections of the peptide not able to interact. The hairpin dimer is more compact, has N-terminal sections that are able to interact and has a different potential β-structure as the two monomers are parallel versus antiparallel in the extended dimer. Further, the hairpin dimer has an important biological function when considering its interaction with membranes. Computational studies on potential Aβ pores

created by inserted Aβ oligomers commonly use β-hairpins as a stable building block for the oligomer subunits of the pore (74, 80). Thus, these two dimer structures provide enough diversity in their structures to allow us to investigate fundamental aspects of the peptide-lipid interaction at the dimer level.

In concert with the importance of choosing the two dimer structures is the use of the thermodynamic cycle to calculate $\Delta G_{Dimerization}$. In principle, it would be feasible to take two equilibrated Aβ monomers on a bilayer surface and bring these two monomers together using umbrella sampling to calculate a dimerization free energy. However, the problems with this calculation would be with the reaction coordinate and with the sampling of the system. First, the reaction coordinate that is chosen for the pulling would highly bias the system to a particular dimer structure. If the center of mass separation between two monomers was chosen as the reaction coordinate, the initial configuration of the monomers would effect what portions of each peptide are in contact during the pulling process, thus effecting dimer structure. If other positions are chosen for the reaction coordinate, such as N- or C-terminus position, pulling with this coordinate will also dictate final structure. Thus, with the current restrictions to sampling in all-atom molecular dynamics, pulling together two monomers on the bilayer surface will not give a global $\Delta G_{Dimerization}$ but give a path-dependent $\Delta G_{Dimerization}$ for a specific structure. Within our thermodynamic cycle, the choice of reaction coordinate is more obvious. The reaction coordinate for monomer binding is explained in a previous work (138). Much like the monomer binding, the use of dimer-bilayer center of mass separation is also a clear reaction coordinate for dimer release. For dimer dissolution, the reaction coordinate

of monomer-monomer center of mass separation also appears to be fairly apparent. Because the end point of dimer dissolution is two non-interacting Aβ monomers, which should be able to reach equilibration in the simulation time, using monomer-monomer center of mass separation is an appropriate reaction coordinate. Thus, by using a thermodynamic cycle with more explicit reaction coordinates, we can calculate a $\Delta G_{Dimerization}$ for a specific dimer that is reaction coordinate independent and more general then a $\Delta G_{Dimerization}$ calculated by directly pulling two monomers together.

As mentioned, another reason for utilizing the thermodynamic cycle was sampling issues. In a previous work, we observed that interactions with a cell membrane slow down structural transitions for monomeric Aβ (139). This would imply that directly calculating $\Delta G_{Dimerization}$ through pulling two monomers together would suffer from this same sampling issue, where the restrictions of all-atom molecular dynamics would not allow enough conformational sampling in reasonable simulation times. For the other steps of the thermodynamic cycle, the conformational sampling issue is not as substantial. The free energy surfaces of dimer release (Figure 4.5b and 4.5c) show that the dimer is not restricted in sampling a variety of secondary structures. Further, our calculations are for a specific dimer structure, not the generic dimer, so full equilibration for all possible structures is less necessary. For dimer dissolution, the monomeric Aβ peptide in solution is mostly a random coil and that is what we observe in this calculation. Thus, while more sampling would be ideal for all steps of this calculation, the penalties for lacking of complete sampling for dimer release and dimer dissolution are much less significant than if a direct dimerization free energy was calculated through an umbrella sampling scheme

on the bilayer surface. Finally, of note, our calculations have been developed in order to calculate $\Delta G_{Dimerization}$ for a specific dimer. Our intention was not to calculate a generic $\Delta G_{Dimerization}$ of Aβ on a bilayer surface, such as would be measured in experiment. This would require substantial sampling due to the heterogeneous nature of Aβ oligomer structure that would only be obtained through extensive coarse-grained or replica exchange methods. While these methods are becoming more common for protein-lipid systems, our goal has been to use all-atom simulations to investigate the details of this process. Thus, we have strived to use two specific, different structures to investigate protein-lipid interactions at the Aβ dimer level and to use the $\Delta G_{Dimerization}$ as a tool to differentiate the effects of lipid and peptide charge on this process.

Within the thermodynamic cycle, each step reveals interesting aspects of this process. As mentioned, a detailed analysis of monomer binding is provided in our previous work (138). For the dimer release process, the potentials of mean force and $\Delta G_{Release}$ are very insightful. What appears to be the deciding factor in this process is the charge on the bilayer surface and not the specific dimer structure. On the DPPC surface, both the extended and hairpin dimer are tightly bound with a very large $\Delta G_{Release}$. Similar to the results seen with monomeric Aβ, both the hairpin and extended dimer interact strongly with the interfacial region of the bilayer. Because of the zwitterionic nature of the phosphatidylcholine headgroup, charges within the N-terminus of each monomer are able to interact favorably with the headgroup and glycerol backbone of the lipids, which allows the hydrophobic portions of the dimer to interact with the interfacial region of the lipids. Further, comparison of the $\Delta G_{Binding}$ and $\Delta G_{Release}$ shows that, as $\Delta G_{Release}$ is very

close to $2*\Delta G_{Binding}$ in magnitude, the monomers within the dimer are still acting very much like monomers and the strong peptide-peptide interactions reflected in $\Delta G_{Dissociation}$ do not occur until the dimer is in solution. Thus, peptide-lipid interactions are still dominant on DPPC. However, on DOPS, the dimer is much more weakly bound to the bilayer surface. On a pure DOPS bilayer, it is possible for the three histidines in Aβ to become protonated due to the higher concentration of $H^+$ ions near the phosphatidylserine headgroups (57). Thus, our simulations with DOPS use a neutral Aβ peptide. From analysis of the potential of mean force curves, both the neutral hairpin and extended dimer are bound near the free energy minimum at a larger dimer-bilayer center of mass separation. While it can be difficult to determine the dimer location just from a dimer-bilayer center of mass separation as the dimer can tumble around a fixed separation, visual analysis of trajectories confirms that the dimer is associating with the headgroup region of the bilayer. It is possible for the dimer to interact with the interfacial portion of the bilayer, but this is not a strong, stable interaction. Because the dimer is not interacting strongly with the core of the bilayer, the interaction with the bilayer is weaker and $\Delta G_{Release}$ is much smaller. Further, in comparison to the dimers on DPPC, $\Delta G_{Release}$ is much smaller then $2*\Delta G_{Binding}$. Because the values for $\Delta G_{Dissociation}$ are large for the neutral dimer, we can assume that peptide-peptide interactions are favored on DOPS over much weaker peptide-lipid interactions. On DOPS, the dimer is not acting as two monomers but is acting as a unit that binds more weakly to the lipid surface.

Along with the information obtained from free energy profiles of dimer release, we also investigated secondary structure change as a function of dimer-bilayer center of

mass separation. By analyzing at the average β-structure of each dimer as a function of the reaction coordinate, it appears that the β-content slightly increases as the dimer is pulled into solution. This might seem appropriate as water molecules would force a more ordered structure in the hydrophobic region of the peptide that was not required on the lipid surface due to the lipid-protein interactions. However, looking closely at the data through free energy surfaces (Figure 4.5), it appears that this trend is deceiving. These free energy surfaces provide a more general perspective of the interplay between β-structure and center of mass separation by demonstrating the probability (or free energy) of the dimer having a particular β-structure at a specific center of mass separation. At a given center of mass separation, there is not any favored value for the extent of β-content. The dimer is able to freely move and change secondary structure as it is released. Again, it does not appear that there is a favored β-structure for any dimer and structural flexibility is a hallmark of these dimers. This also harkens back to the notion of heterogeneous dimer structure and lack of a dominant single structure for small Aβ oligomers.

In the dimer dissociation step of the thermodynamic cycle, the role of dimer structure in this process becomes more apparent. From both the $\Delta G_{Dissociation}$ and free energy profiles, it is clear that the neutral hairpin dimer has a drastically different dissociation free energy than the extended dimer. Further, the neutral hairpin dimer dissociation also differs from the charged hairpin dimer, while the charged hairpin dimer dissociation is almost exactly the same as the two extended dimer calculations. While this does appear to be a contradiction at first, further analysis shows the importance of the

N-terminus in this process. For the two extended dimer conditions, the N-termini are physically separated and are not able to interact. The only difference between the charged and neutral dimer is the protonation of three histindines that reside in the N-terminal tail of Aβ. Thus, there is no significant difference in the dissociation calculations for the charged and neutral dimers as the regions of the two monomers that are able to interact in the dimer are the same for both systems. However, for the hairpin dimer, this is not the case. Due to the parallel β-sheet structure of the overlapping hairpins in the dimer, the N-terminal sections of both monomers are restricted to being near each other. Even though these N-terminal tails are extensively equilibrated to prevent initial structure bias, they are able to interact if favorable. For the charged hairpin dimer, electrostatic repulsion between the tails prevents extensive interaction. Thus, the interactions, either electrostatic, hydrophobic or hydrogen-bond, that bind the two monomers together for the charged hairpin are isolated to the C-terminal half of the peptide, which is the same region of interaction as the extended dimer. This is clearly seen in the similarities of the $\Delta G_{Dissociation}$ and free energy profiles of the charged hairpin and two extended dimers.

However, for the neutral hairpin dimer, the charged histidines in the N-terminal tail of each monomer are now available for favorable electrostatic interactions with the anionic residues with the opposing monomer. These more favorable interactions are demonstrated by the closer and more stable center of mass distance measurements presented in Figure 4.6. By changing the N-terminal interaction from unfavorable to favorable and allowing for extensive electrostatic and hydrophobic interactions amongst

the tails, the monomers are more tightly bound and the magnitude of $\Delta G_{Dissociation}$ increases significantly. These calculations show the importance of the N-terminal tail charge state when studying Aβ peptide oligomerization. When Aβ is at physiological pH, the N-terminal tail is negatively charged and the dimerization energy is strongly based on mutual hydrophobic or hydrogen-bonding interactions between the C-terminal tails. Because of this interaction, the structure of the dimer is somewhat irrelevant as long as the C-terminal regions are interacting. At a lower pH such as pH 4 of pH 5, when histidine becomes protonated, the N-terminal tails no longer mutually repel to such a significant extent. Monomer interactions are no longer dominated by only the C-terminal end of the peptide and dimer structure becomes more critical. From the $\Delta G_{Dissociation}$ of the extended and charged hairpin dimer calculations, it is clear that hydrophobic or hydrogen-bonding interactions on the C-terminus of the dimer are strong enough to tightly bind the two monomers. However, N-terminal interactions can provide extra free energy towards binding by increasing $\Delta G_{Dissociation}$ by over 50%. These results raise an important caveat to future experimental and computational studies of this system. While studies using Aβ fragments, especially C-terminal fragments, have been very important and necessary to extending our knowledge of this system, it is important to note that the N-terminal half of Aβ can play a significant role in this process. If studies are performed to investigate effects of peptide charge on aggregation, use of the full Aβ peptide will be crucial to obtaining a full understanding of this system.

Using the thermodynamic cycle presented in this work, we have been able to estimate a dimerization free energy, $\Delta G_{Dimerization}$, as presented in Table 4.1. From this

calculation, it appears that the formation of a dimer on the bilayer surface for three different conditions, the charged extended dimer and both hairpin dimers, is favorable while formation of the neutral extended dimer is not. However, we believe that this $\Delta G_{Dimerization}$ is a somewhat misleading number. While this number would provide insight for dimerization of nascent Aβ peptides after APP cleavage but before membrane release, it does not describe the effect of a cell membrane on soluble Aβ. To determine this value, it is best to look at the sum of $\Delta G_{Dissociation} + 2*\Delta G_{Binding}$. Considering this value, dimerization is highly favorable for all potential dimer structures. There are discrepancies in these values and it appears that the hairpin dimer would be favored over the extended dimer on DOPS, which would contradict the expected heterogeneity of Aβ dimers. Nevertheless, it is important to remember that our calculations are only for thermodynamic properties of the system, not kinetic properties. In considering the system, it is not a stretch to imagine that it would be much quicker to arrange 14 residues at the two C-terminals of two monomers so that they have some sort of unstructured interaction, similar to the extended dimer, instead of fully arranging all 42 amino acids of two monomers into a hairpin structure. Thus, the most important result of this $\Delta G_{Dimerization}$ calculation is that the dimerization free energies calculated for all dimer structures are favorable considering the full membrane binding and membrane-assisted dimerization process.

The limitations of this work are very similar to previous computational studies. Simple one-dimensional reaction coordinates are not perfect for describing most biological systems and sampling will continue to be an issue for all-atom molecular

dynamics calculations with the current computing environment. Because of these limitations, we were not able to directly calculate $\Delta G_{Dimerization}$. However, it is our belief that use of this thermodynamic cycle helps to avoid these issues while still providing us with a substantial amount of data that is helpful towards understanding this system. While the data may not be quantitatively perfect due to sampling issues, we believe the trends and conclusions we have drawn in this work are reasonable. In the future, use of coarse-grain, replica exchange or other techniques that expand the sampling capabilities of molecular dynamics would be ideal for studying this system and testing our results. The ideal test would be direct experimental validation of the patterns we observed in our data. Hopefully, experimental techniques will progress enough in the near future and resolution can be improved to the extent that direct Aβ protein-protein interactions on the cell surface can be studied. Our work demonstrates that the interaction between Aβ proteins and lipid membranes during the aggregation process is a delicate balance that encompasses a variety of interactions, from hydrophobic to hydrogen-bonding to electrostatic interactions, which dictate the structure and feasibility of Aβ aggregation on a cell membrane.

**Conclusion**

From the results presented in this work, it appears that the interactions between Aβ dimers and cell membranes plays a significant role in aggregation. The $\Delta G_{Dimerization} + 2*\Delta G_{Binding}$ values we have calculated do not seem to support experimental evidence that shows anionic lipids strongly promote aggregation while zwitterionic lipids do not.

However, the reported values are deceiving. It does appear that the free energy of dimerization is much more favorable on DPPC. Yet, it is necessary to consider the results of the dimer release calculations. With these calculations, we demonstrated that the dimer on DPPC does not act much like a dimer, but as two monomers with weak interpeptide interactions and strong peptide-lipid interactions. Only through dimer release, which is highly unfavorable, does the dimer strength become significant. On DOPS, the situation changes substantially. DOPS favors a very strong protein-protein interaction and weak protein-lipid interactions. Even though the free energy values tend to make one believe that DPPC strongly favors dimer formation, it is actually DOPS that is more likely to create viable dimers for aggregation. With the small $\Delta G_{Release}$, DOPS actually acts much like a factory for creating Aβ dimers. An Aβ peptide binds to DOPS, where concentration effects increase local Aβ concentration, increasing the probability of two Aβ peptides coming into contact. Due to the anionic nature of the lipid headgroup, the local pH drops and Aβ can take a neutral charge. The lipids promote strong protein-protein interactions between monomers while weakening protein-lipid interactions during dimerization. The dimer is free to be released from the bilayer surface while maintaining very strong peptide-peptide interactions. Previously, experimental results have implicated the dimer as a key building block in Aβ aggregation (53). Further, a dimer could act as a seed for more extensive aggregation. Also, this favored dimerization on the bilayer interface would support subsequent peptide insertion, either in monomer or oligomer form, and pore formation. Finally, if these dimers are being released from the surface of the bilayer, the local concentration of dimers near the surface should be higher than in solution, promoting further aggregation. While DPPC promotes strong monomer

binding and weak dimerization interactions, DOPS forces dimerization and release of Aβ from the bilayer surface. Because of these complicated interactions between Aβ and membrane surface, the importance of lipid charge and properties of the Aβ peptide in aggregation becomes clearer.

**TABLE 4.1** Free energies calculated for steps of the thermodynamic cycle shown in Figure 4.2. All free energy values are in units of kcal/mol.

| Dimer Structure | $\Delta G_{Binding}$ | $\Delta G_{Dimerization}$[1] | | $\Delta G_{Release}$ | $\Delta G_{Dissociation}$ |
|---|---|---|---|---|---|
| | Step 1 | Step 2 | 2*Step1+Step2 | Step 3 | Step 4 |
| **Extended** | | | | | |
| Charged Aβ + DPPC | -14.42 | -14.59 | -43.43 | 27.74 | 15.69 |
| Neutral Aβ + DOPS | -12.52 | 4.19 | -20.85 | 6.73 | 14.12 |
| **Hairpin** | | | | | |
| Charged Aβ + DPPC | -14.42 | -17.07 | -45.91 | 28.69 | 17.22 |
| Neutral Aβ + DOPS | -12.52 | -11.16 | -36.20 | 4.55 | 31.65 |

[1] $\Delta G_{Dimerization} = -1 * (2*\Delta G_{Binding} + \Delta G_{Release} + \Delta G_{Dissociation})$

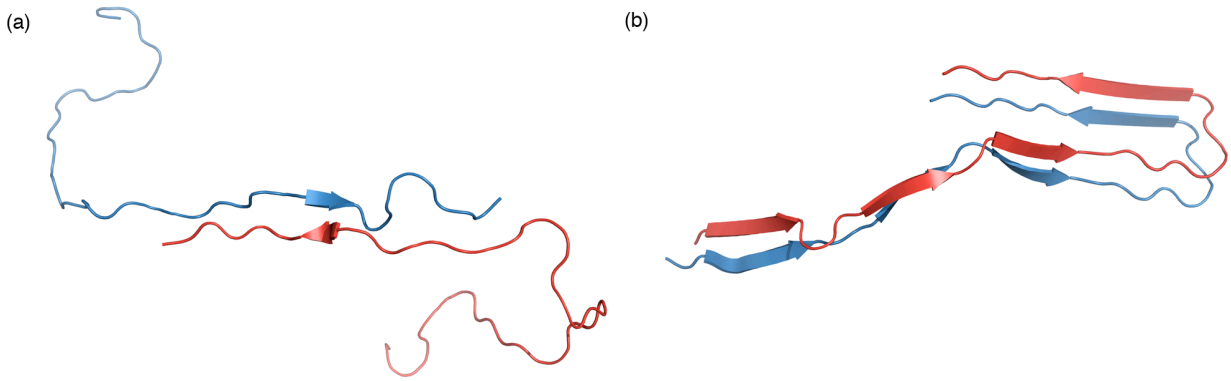


**Figure 4.1** Initial structures used for the (a) Extended and (b) Hairpin dimer simulations.

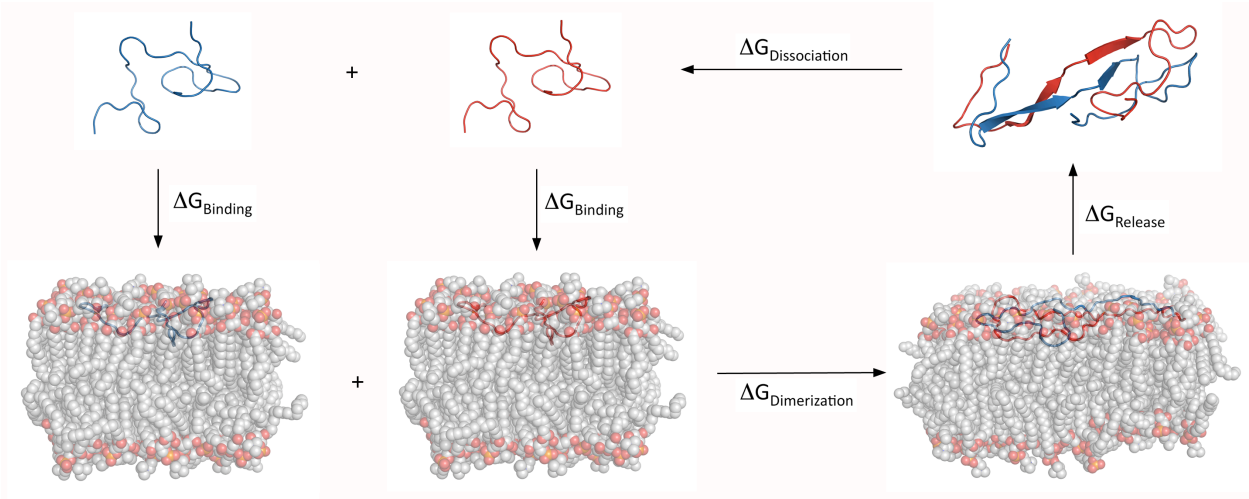


**Figure 4.2** Representation of the thermodynamic cycle used to approximate the free energy of dimerization for Aβ on a lipid bilayer.

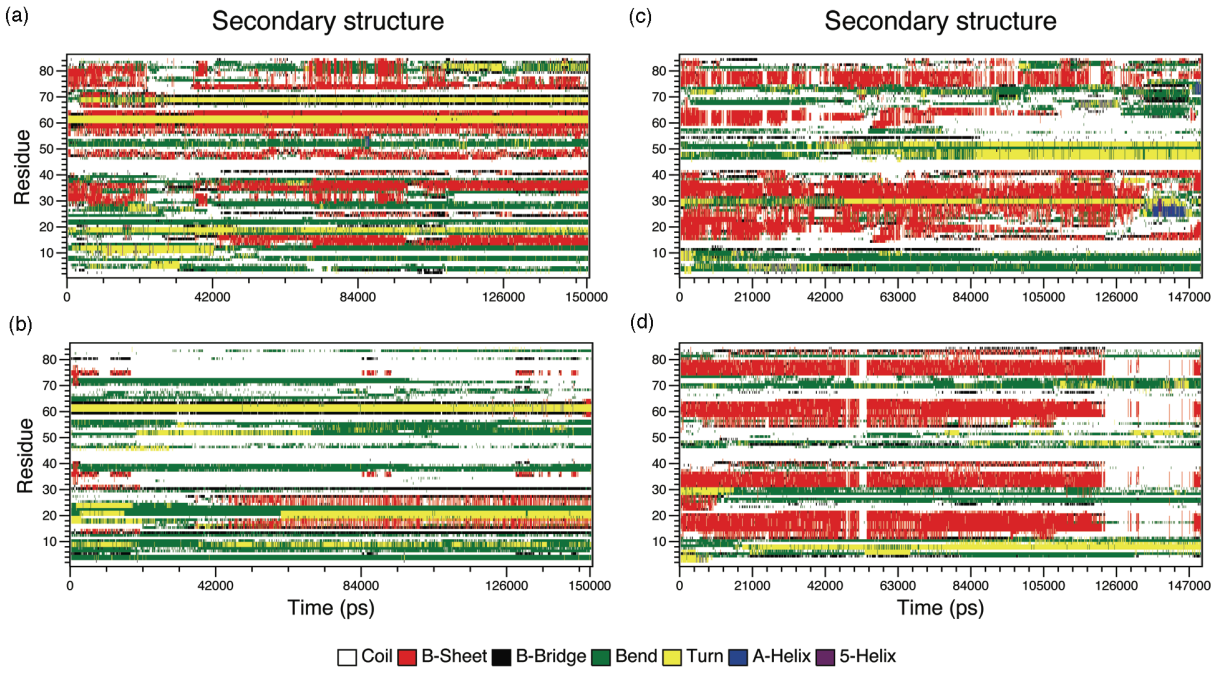


**Figure 4.3** Secondary structure output for DSSP for 150ns equilibration simulations of Aβ in the following conditions: (a) Extended charged dimer in solution (b) Extended charged dimer on DPPC bilayer (c) Hairpin uncharged dimer in solution (d) Hairpin uncharged dimer on DOPS bilayer.

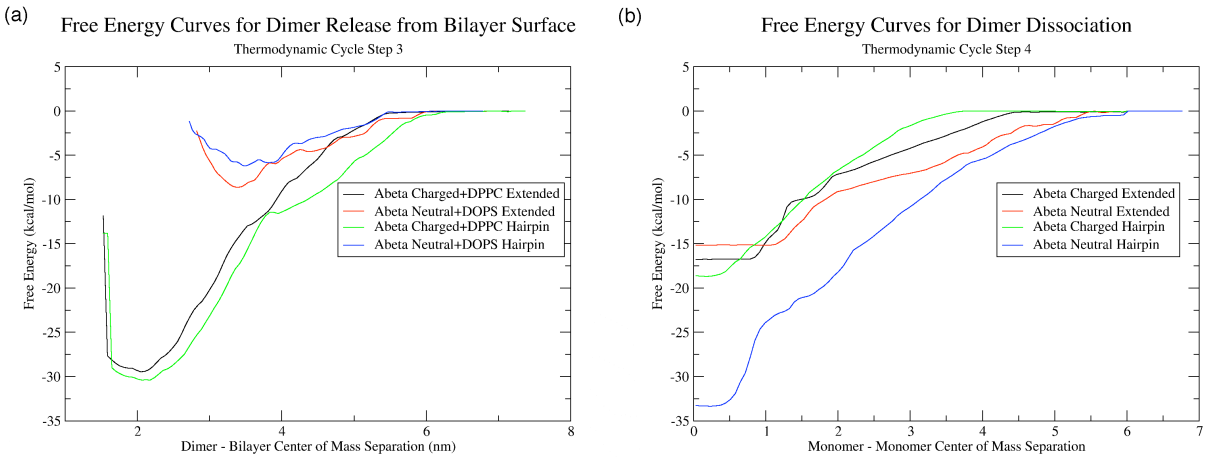


**Figure 4.4** Potentials of mean force for (a) Aβ dimer release from the lipid surface into solution (Step 3 of thermodynamic cycle) and (b) Aβ dimer dissolution in solution (Step 4 of thermodynamic cycle)

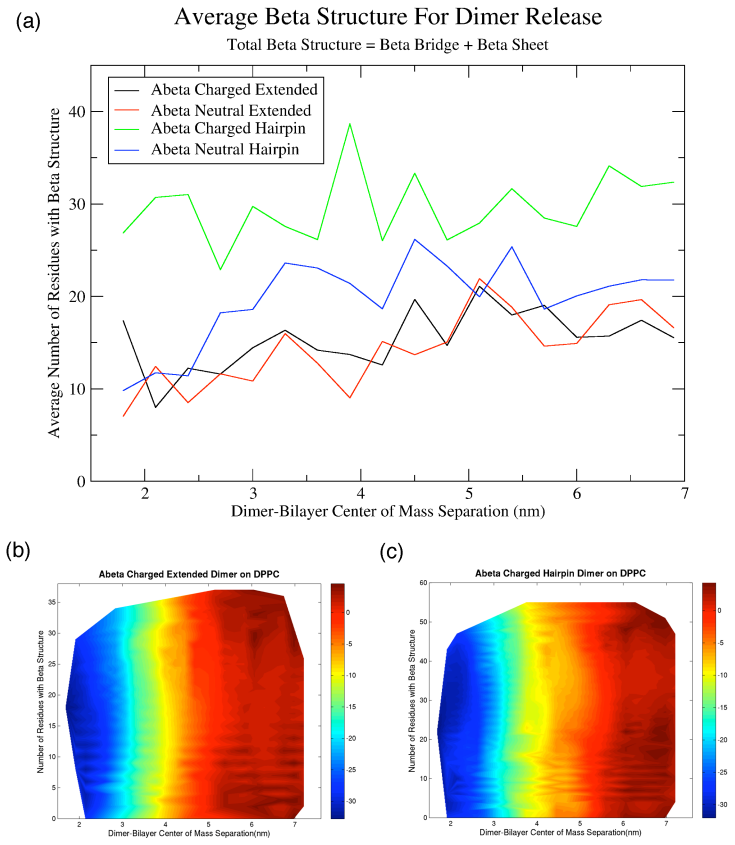


**Figure 4.5** (a) Plot of average number of residues with β-structure, where β-structure contains β-Bridge and β-Sheet residues, as a function of dimer-bilayer center of mass separation for the dimer release step of the thermodynamic cycle. (b) 2D free energy surface of number of residues with β-structure and center of mass separation with free energy in units of kcal/mol for the Extended charged dimer on DPPC. (c) Same plot as (b) except for the Hairpin charged dimer on DPPC.

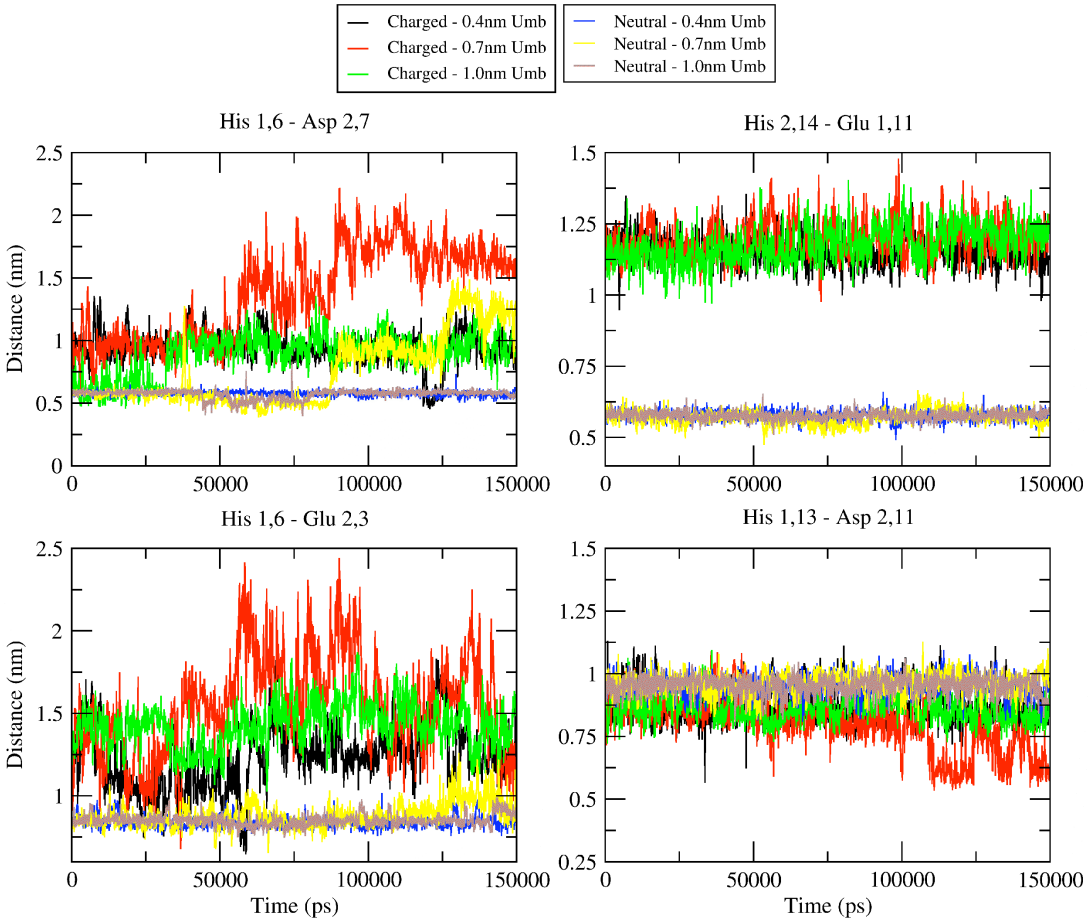


**Figure 4.6** Distance measurements between the centers of mass of indicated residues for either charged or neutral Hairpin dimer in solution. Distances were calculated within the 0.4nm, 0.7nm and 1.0nm umbrellas to show that the explained phenomenona were not due to a specific structure or initial condition. Amino acids are listed with the monomer number followed by the residue number on that monomer. For example, Asp2,7 is actually Asp7 on the second monomer.

## References


1. Xu, J., K.D. Kochanek, and B. Tejada-Vera. 2009. Deaths: Preliminary Data for 2007. *National Vital Statistics Reports* 58(1):1-52.

2. Berchtold, N.C., and C.W. Cotman. 1998. Evolution in the conceptualization of dementia and Alzheimer's disease: Greco-Roman period to the 1960s. *Neurobiol Aging* 19(3):173-189.

3. Selkoe, D.J. 2001. Alzheimer's disease: Genes, proteins, and therapy. *Physiological Reviews* 81(2):741-766.

4. Matsuzaki, K. 2007. Physicochemical interactions of amyloid β-peptide with lipid bilayers. *Biochimica Et Biophysica Acta-Biomembranes* 1768(8):1935-1942.

5. Aisenbrey, C., T. Borowik, R. Bystrom, M. Bokvist, F. Lindstrom, H. Misiak, M.A. Sani, and G. Grobner. 2008. How is protein aggregation in amyloidogenic diseases modulated by biological membranes? *European Biophysics Journal with Biophysics Letters* 37(3):247-255.

6. Masters, C.L., G. Simms, N.A. Weinman, G. Multhaup, B.L. McDonald, and K. Beyreuther. 1985. Amyloid plaque core protein in Alzheimer disease and Down syndrome. *Proc Natl Acad Sci U S A* 82(12):4245-4249.

7. Lansbury, P.T., Jr. 1999. Evolution of amyloid: what normal protein folding may tell us about fibrillogenesis and disease. *Proc Natl Acad Sci U S A* 96(7):3342-3344.

8. Rochet, J.C., and P.T. Lansbury, Jr. 2000. Amyloid fibrillogenesis: themes and variations. *Curr Opin Struct Biol* 10(1):60-68.

9. Haass, C., and D.J. Selkoe. 2007. Soluble protein oligomers in neurodegeneration: lessons from the Alzheimer's amyloid beta-peptide. *Nat Rev Mol Cell Biol* 8(2):101-112.

10. Cappai, R., and K.J. Barnham. 2008. Delineating the mechanism of Alzheimer's disease Aβ peptide neurotoxicity. *Neurochemical Research* 33(3):526-532.

11. Kang, J., H.G. Lemaire, A. Unterbeck, J.M. Salbaum, C.L. Masters, K.H. Grzeschik, G. Multhaup, K. Beyreuther, and B. Mullerhill. 1987. The precursor of Alzheimer's-disease Amyloid-A4 protein resembles a cell-surface receptor. *Nature* 325(6106):733-736.

12. Miller, D.L., I.A. Papayannopoulos, J. Styles, S.A. Bobin, Y.Y. Lin, K. Biemann, and K. Iqbal. 1993. Peptide compositions of the cerebrovascular and senile plaque

core amyloid deposits of Alzheimer's-Disease. *Archives of Biochemistry and Biophysics* 301(1):41-52.

13. Turner, P.R., K. O'Connor, W.P. Tate, and W.C. Abraham. 2003. Roles of amyloid precursor protein and its fragments in regulating neural activity, plasticity and memory. *Prog Neurobiol* 70(1):1-32.

14. Priller, C., T. Bauer, G. Mitteregger, B. Krebs, H.A. Kretzschmar, and J. Herms. 2006. Synapse formation and function is modulated by the amyloid precursor protein. *J Neurosci* 26(27):7212-7221.

15. Miyashita, N., J.E. Straub, and D. Thirumalai. 2009. Structures of β-Amyloid Peptide 1-40, 1-42, and 1-55-the 672-726 Fragment of APP-in a Membrane Environment with Implications for Interactions with γ-Secretase. *Journal of the American Chemical Society* 131(49):17843-17852.

16. Evin, G., and A. Weidemann. 2002. Biogenesis and metabolism of Alzheimer's disease Aβ amyloid peptides. *Peptides* 23(7):1285-1297.

17. Vassar, R., and M. Citron. 2000. Aβ-generating enzymes: recent advances in β- and γ-secretase research. *Neuron* 27(3):419-422.

18. Haass, C., M.G. Schlossmacher, A.Y. Hung, C. Vigo-Pelfrey, A. Mellon, B.L. Ostaszewski, I. Lieberburg, E.H. Koo, D. Schenk, D.B. Teplow, and et al. 1992. Amyloid β-peptide is produced by cultured cells during normal metabolism. *Nature* 359(6393):322-325.

19. Seubert, P., C. Vigo-Pelfrey, F. Esch, M. Lee, H. Dovey, D. Davis, S. Sinha, M. Schlossmacher, J. Whaley, C. Swindlehurst, and et al. 1992. Isolation and quantification of soluble Alzheimer's β-peptide from biological fluids. *Nature* 359(6393):325-327.

20. Iwatsubo, T., A. Odaka, N. Suzuki, H. Mizusawa, N. Nukina, and Y. Ihara. 1994. Visualization of Aβ 42(43) and Aβ 40 in senile plaques with end-specific Aβ monoclonals: evidence that an initially deposited species is Aβ 42(43). *Neuron* 13(1):45-53.

21. Hartmann, T., S.C. Bieger, B. Bruhl, P.J. Tienari, N. Ida, D. Allsop, G.W. Roberts, C.L. Masters, C.G. Dotti, K. Unsicker, and K. Beyreuther. 1997. Distinct sites of intracellular production for Alzheimer's disease Aβ40/42 amyloid peptides. *Nat Med* 3(9):1016-1020.

22. Citron, M. 2004. Strategies for disease modification in Alzheimer's disease. *Nat Rev Neurosci* 5(9):677-685.

23. Marchesi, V.T. 2005. An alternative interpretation of the amyloid Aβ hypothesis with regard to the pathogenesis of Alzheimer's disease. *Proc Natl Acad Sci U S A* 102(26):9093-9098.

24. Vetrivel, K.S., H. Cheng, W. Lin, T. Sakurai, T. Li, N. Nukina, P.C. Wong, H. Xu, and G. Thinakaran. 2004. Association of γ-secretase with lipid rafts in post-Golgi and endosome membranes. *J Biol Chem* 279(43):44945-44954.

25. Simons, M., P. Keller, B. De Strooper, K. Beyreuther, C.G. Dotti, and K. Simons. 1998. Cholesterol depletion inhibits the generation of β-amyloid in hippocampal neurons. *Proc Natl Acad Sci U S A* 95(11):6460-6464.

26. Hou, L.M., H.Y. Shao, Y.B. Zhang, H. Li, N.K. Menon, E.B. Neuhaus, J.M. Brewer, I.J.L. Byeon, D.G. Ray, M.P. Vitek, T. Iwashita, R.A. Makula, A.B. Przybyla, and M.G. Zagorski. 2004. Solution NMR studies of the Aβ (1-40) and Aβ (1-42) peptides establish that the Met35 oxidation state affects the mechanism of amyloid formation. *Journal of the American Chemical Society* 126(7):1992-2005.

27. Tomaselli, S., V. Esposito, P. Vangone, N.A.J. van Nuland, A.M.J.J. Bonvin, R. Guerrini, T. Tancredi, P.A. Temussi, and D. Picone. 2006. The α-to-β conformational transition of Alzheimer's Aβ-(1-42) peptide in aqueous media is reversible: A step by step conformational analysis suggests the location of beta conformation seeding. *Chembiochem* 7(2):257-267.

28. Yang, M.F., and D.B. Teplow. 2008. Amyloid β-protein monomer folding: Free-energy surfaces reveal alloform-specific differences. *Journal of Molecular Biology* 384(2):450-464.

29. Sgourakis, N.G., Y.L. Yan, S.A. McCallum, C.Y. Wang, and A.E. Garcia. 2007. The Alzheimer's peptides Aβ40 and 42 adopt distinct conformations in water: A combined MD/NMR study. *Journal of Molecular Biology* 368(5):1448-1457.

30. Roychaudhuri, R., M. Yang, M.M. Hoshi, and D.B. Teplow. 2009. Amyloid β-Protein Assembly and Alzheimer Disease. *Journal of Biological Chemistry* 284(8):4749-4753.

31. Jarrett, J.T., E.P. Berger, and P.T. Lansbury, Jr. 1993. The carboxy terminus of the β amyloid protein is critical for the seeding of amyloid formation: implications for the pathogenesis of Alzheimer's disease. *Biochemistry* 32(18):4693-4697.

32. Liao, M.Q., Y.J. Tzeng, L.Y. Chang, H.B. Huang, T.H. Lin, C.L. Chyan, and Y.C. Chen. 2007. The correlation between neurotoxicity, aggregative ability and secondary structure studied by sequence truncated Abeta peptides. *FEBS Lett* 581(6):1161-1165.

33. Yin, Y.I., B. Bassit, L. Zhu, X. Yang, C. Wang, and Y.M. Li. 2007. γ-Secretase Substrate Concentration Modulates the Abeta42/Abeta40 Ratio: IMPLICATIONS FOR ALZHEIMER DISEASE. *J Biol Chem* 282(32):23639-23644.

34. Sawaya, M.R., S. Sambashivan, R. Nelson, M.I. Ivanova, S.A. Sievers, M.I. Apostol, M.J. Thompson, M. Balbirnie, J.J. Wiltzius, H.T. McFarlane, A.O. Madsen, C. Riekel, and D. Eisenberg. 2007. Atomic structures of amyloid cross-β spines reveal varied steric zippers. *Nature* 447(7143):453-457.

35. Martins, I.C., I. Kuperstein, H. Wilkinson, E. Maes, M. Vanbrabant, W. Jonckheere, P. Van Gelder, D. Hartmann, R. D'Hooge, B. De Strooper, J. Schymkowitz, and F. Rousseau. 2008. Lipids revert inert Aβ amyloid fibrils to neurotoxic protofibrils that affect learning in mice. *Embo Journal* 27(1):224-233.

36. Xue, W.F., A.L. Hellewell, W.S. Gosal, S.W. Homans, E.W. Hewitt, and S.E. Radford. 2009. Fibril Fragmentation Enhances Amyloid Cytotoxicity. *Journal of Biological Chemistry* 284(49):34272-34282.

37. Klein, W.L., W.B. Stine, and D.B. Teplow. 2004. Small assemblies of unmodified amyloid β-protein are the proximate neurotoxin in Alzheimer's disease. *Neurobiology of Aging* 25(5):569-580.

38. Walsh, D.M., I. Klyubin, J.V. Fadeeva, W.K. Cullen, R. Anwyl, M.S. Wolfe, M.J. Rowan, and D.J. Selkoe. 2002. Naturally secreted oligomers of amyloid beta protein potently inhibit hippocampal long-term potentiation in vivo. *Nature* 416(6880):535-539.

39. Lambert, M.P., A.K. Barlow, B.A. Chromy, C. Edwards, R. Freed, M. Liosatos, T.E. Morgan, I. Rozovsky, B. Trommer, K.L. Viola, P. Wals, C. Zhang, C.E. Finch, G.A. Krafft, and W.L. Klein. 1998. Diffusible, nonfibrillar ligands derived from Aβ1-42 are potent central nervous system neurotoxins. *Proc Natl Acad Sci U S A* 95(11):6448-6453.

40. Shankar, G.M., S.M. Li, T.H. Mehta, A. Garcia-Munoz, N.E. Shepardson, I. Smith, F.M. Brett, M.A. Farrell, M.J. Rowan, C.A. Lemere, C.M. Regan, D.M. Walsh, B.L. Sabatini, and D.J. Selkoe. 2008. Amyloid-β protein dimers isolated directly from Alzheimer's brains impair synaptic plasticity and memory. *Nature Medicine* 14(8):837-842.

41. Rapoport, M., H.N. Dawson, L.I. Binder, M.P. Vitek, and A. Ferreira. 2002. Tau is essential to β-amyloid-induced neurotoxicity. *Proc Natl Acad Sci U S A* 99(9):6364-6369.

42. Sengupta, A., M. Novak, I. Grundke-Iqbal, and K. Iqbal. 2006. Regulation of phosphorylation of tau by cyclin-dependent kinase 5 and glycogen synthase kinase-3 at substrate level. *FEBS Lett* 580(25):5925-5933.

43. Wray, S., and W. Noble. 2009. Linking Amyloid and Tau Pathology in Alzheimer's Disease: The Role of Membrane Cholesterol in Aβ-Mediated Tau Toxicity. *Journal of Neuroscience* 29(31):9665-9667.

44. Nicholson, A.M., and A. Ferreira. 2009. Increased membrane cholesterol might render mature hippocampal neurons more susceptible to β-amyloid-induced calpain activation and tau toxicity. *J Neurosci* 29(14):4640-4651.

45. Stefani, M. 2004. Protein misfolding and aggregation: new examples in medicine and biology of the dark side of the protein world. *Biochimica Et Biophysica Acta-Molecular Basis of Disease* 1739(1):5-25.

46. Sachse, C., M. Fandrich, and N. Grigorieff. 2008. Paired β-sheet structure of an Aβ(1-40) amyloid fibril revealed by electron microscopy. *Proceedings of the National Academy of Sciences of the United States of America* 105(21):7462-7466.

47. Petkova, A.T., Y. Ishii, J.J. Balbach, O.N. Antzutkin, R.D. Leapman, F. Delaglio, and R. Tycko. 2002. A structural model for Alzheimer's beta-amyloid fibrils based on experimental constraints from solid state NMR. *Proceedings of the National Academy of Sciences of the United States of America* 99(26):16742-16747.

48. Petkova, A.T., W.M. Yau, and R. Tycko. 2006. Experimental constraints on quaternary structure in Alzheimer's beta-amyloid fibrils. *Biochemistry* 45(2):498-512.

49. Luhrs, T., C. Ritter, M. Adrian, D. Riek-Loher, B. Bohrmann, H. Doeli, D. Schubert, and R. Riek. 2005. 3D structure of Alzheimer's amyloid-β(1-42) fibrils. *Proceedings of the National Academy of Sciences of the United States of America* 102(48):17342-17347.

50. Paravastu, A.K., R.D. Leapman, W.M. Yau, and R. Tycko. 2008. Molecular structural basis for polymorphism in Alzheimer's β-amyloid fibrils. *Proceedings of the National Academy of Sciences of the United States of America* 105(47):18349-18354.

51. Meinhardt, J., C. Sachse, P. Hortschansky, N. Grigorieff, and M. Fandrich. 2009. Aβ(1-40) Fibril Polymorphism Implies Diverse Interaction Patterns in Amyloid Fibrils. *Journal of Molecular Biology* 386(3):869-877.

52. Ono, K., M.M. Condron, and D.B. Teplow. 2009. Structure-neurotoxicity relationships of amyloid β-protein oligomers. *Proceedings of the National Academy of Sciences of the United States of America* 106(35):14745-14750.

53. Bernstein, S.L., N.F. Dupuis, N.D. Lazo, T. Wyttenbach, M.M. Condron, G. Bitan, D.B. Teplow, J.E. Shea, B.T. Ruotolo, C.V. Robinson, and M.T. Bowers. 2009.

Amyloid-β protein oligomerization and the importance of tetramers and dodecamers in the aetiology of Alzheimer's disease. *Nature Chemistry* 1(4):326-331.

54. Miller, Y., B.Y. Ma, and R. Nussinov. 2009. Polymorphism of Alzheimer's Aβ(17-42) (p3) Oligomers: The Importance of the Turn Location and Its Conformation. *Biophysical Journal* 97(4):1168-1177.

55. Picone, P., R. Carrotta, G. Montana, M.R. Nobile, P.L.S. Biagio, and M. Di Carlo. 2009. Aβ Oligomers and Fibrillar Aggregates Induce Different Apoptotic Pathways in LAN5 Neuroblastoma Cell Cultures. *Biophysical Journal* 96(10):4200-4211.

56. Necula, M., R. Kayed, S. Milton, and C.G. Glabe. 2007. Small molecule inhibitors of aggregation indicate that amyloid β oligomerization and fibrillization pathways are independent and distinct. *Journal of Biological Chemistry* 282(14):10311-10324.

57. Terzi, E., G. Holzemann, and J. Seelig. 1995. Self-association of β-Amyloid peptide(1-40) in solution and binding to lipid-membranes. *Journal of Molecular Biology* 252(5):633-642.

58. McLaurin, J., and A. Chakrabartty. 1997. Characterization of the interactions of Alzheimer β-amyloid peptides with phospholipid membranes. *European Journal of Biochemistry* 245(2):355-363.

59. Ege, C., J. Majewski, G.H. Wu, K. Kjaer, and K.Y.C. Lee. 2005. Templating effect of lipid membranes on Alzheimer's amyloid β peptide. *Chemphyschem* 6(2):226-229.

60. Sengupta, P., K. Garai, B. Sahoo, Y. Shi, D.J. Callaway, and S. Maiti. 2003. The amyloid β peptide (Aβ(1-40)) is thermodynamically soluble at physiological concentrations. *Biochemistry* 42(35):10506-10513.

61. Chen, Y.R., and C.G. Glabe. 2006. Distinct early folding and aggregation properties of Alzheimer amyloid-β peptides Aβ40 and Aβ42: stable trimer or tetramer formation by Aβ42. *J Biol Chem* 281(34):24414-24422.

62. Kirkitadze, M.D., M.M. Condron, and D.B. Teplow. 2001. Identification and characterization of key kinetic intermediates in amyloid β-protein fibrillogenesis. *Journal of Molecular Biology* 312(5):1103-1119.

63. Klement, K., K. Wieligmann, J. Meinhardt, P. Hortschansky, W. Richter, and M. Fandrich. 2007. Effect of different salt ions on the propensity of aggregation and on the structure of Alzheimer's Aβ(1-40) amyloid fibrils. *Journal of Molecular Biology* 373(5):1321-1333.

64. Smith, D.G., R. Cappai, and K.J. Barnham. 2007. The redox chemistry of the Alzheimer's disease amyloid β peptide. *Biochimica Et Biophysica Acta-Biomembranes* 1768(8):1976-1990.

65. Bystrom, R., C. Aisenbrey, T. Borowik, M. Bokvist, F. Lindstrom, M.A. Sani, A. Olofsson, and G. Grobner. 2008. Disordered Proteins: Biological Membranes as Two-Dimensional Aggregation Matrices. *Cell Biochemistry and Biophysics* 52(3):175-189.

66. Gorbenko, G.P., and P.K.J. Kinnunen. 2006. The role of lipid-protein interactions in amyloid-type protein fibril formation. *Chemistry and Physics of Lipids* 141(1-2):72-82.

67. Krishtalik, L.I., and W.A. Cramer. 1995. On the physical basis for the cis-positive rule describing protein orientation in biological-membranes. *Febs Letters* 369(2-3):140-143.

68. van Klompenburg, W., and B. de Kruijff. 1998. The role of anionic lipids in protein insertion and translocation in bacterial membranes. *J Membr Biol* 162(1):1-7.

69. Xu, Y.C., J.J. Shen, X.M. Luo, W.L. Zhu, K.X. Chen, J.P. Ma, and H.L. Jiang. 2005. Conformational transition of amyloid β-peptide. *Proceedings of the National Academy of Sciences of the United States of America* 102(15):5403-5407.

70. Murray, I.V., M.E. Sindoni, and P.H. Axelsen. 2005. Promotion of oxidative lipid membrane damage by amyloid β proteins. *Biochemistry* 44(37):12606-12613.

71. Cuajungco, M.P., L.E. Goldstein, A. Nunomura, M.A. Smith, J.T. Lim, C.S. Atwood, X. Huang, Y.W. Farrag, G. Perry, and A.I. Bush. 2000. Evidence that the beta-amyloid plaques of Alzheimer's disease represent the redox-silencing and entombment of abeta by zinc. *J Biol Chem* 275(26):19439-19442.

72. Usui, K., J.D. Hulleman, J.F. Paulsson, S.J. Siegel, E.T. Powers, and J.W. Kelly. 2009. Site-specific modification of Alzheimer's peptides by cholesterol oxidation products enhances aggregation energetics and neurotoxicity. *Proceedings of the National Academy of Sciences of the United States of America* 106(44):18563-18568.

73. Peters, I., U. Igbavboa, T. Schutt, S. Haidari, U. Hartig, X. Rosello, S. Bottner, E. Copanaki, T. Deller, D. Kogel, W.G. Wood, W.E. Muller, and G.P. Eckert. 2009. The interaction of β-amyloid protein with cellular membranes stimulates its own production. *Biochimica Et Biophysica Acta-Biomembranes* 1788(5):964-972.

74. Jang, H.B., J. Zheng, R. Lal, and R. Nussinov. 2008. New structures help the modeling of toxic amyloidβ ion channels. *Trends in Biochemical Sciences* 33(2):91-100.

75. Arispe, N., H.B. Pollard, and E. Rojas. 1994. β-Amyloid Ca(2+)-channel hypothesis for neuronal death in Alzheimer disease. *Mol Cell Biochem* 140(2):119-125.

76. Kayed, R., Y. Sokolov, B. Edmonds, T.M. McIntire, S.C. Milton, J.E. Hall, and C.G. Glabe. 2004. Permeabilization of lipid bilayers is a common conformation-dependent activity of soluble amyloid oligomers in protein misfolding diseases. *J Biol Chem* 279(45):46363-46366.

77. Sokolov, Y., J.A. Kozak, R. Kayed, A. Chanturiya, C. Glabe, and J.E. Hall. 2006. Soluble amyloid oligomers increase bilayer conductance by altering dielectric structure. *J Gen Physiol* 128(6):637-647.

78. Capone, R., F.G. Quiroz, P. Prangkio, I. Saluja, A.M. Sauer, M.R. Bautista, R.S. Turner, J. Yang, and M. Mayer. 2009. Amyloid-β-induced ion flux in artificial lipid bilayers and neuronal cells: resolving a controversy. *Neurotox Res* 16(1):1-13.

79. Quist, A., L. Doudevski, H. Lin, R. Azimova, D. Ng, B. Frangione, B. Kagan, J. Ghiso, and R. Lal. 2005. Amyloid ion channels: A common structural link for protein-misfolding disease. *Proceedings of the National Academy of Sciences of the United States of America* 102(30):10427-10432.

80. Jang, H., F.T. Arce, R. Capone, S. Ramachandran, R. Lal, and R. Nussinov. 2009. Misfolded Amyloid Ion Channels Present Mobile β-Sheet Subunits in Contrast to Conventional Ion Channels. *Biophysical Journal* 97(11):3029-3037.

81. Bokvist, M., F. Lindstrom, A. Watts, and G. Grobner. 2004. Two types of Alzheimer's β-amyloid (1-40) peptide membrane interactions: Aggregation preventing transmembrane anchoring Versus accelerated surface fibril formation. *Journal of Molecular Biology* 335(4):1039-1049.

82. Terzi, E., G. Holzemann, and J. Seelig. 1997. Interaction of Alzheimer β-amyloid peptide(1-40) with lipid membranes. *Biochemistry* 36(48):14845-14852.

83. Yip, C.M., A.A. Darabie, and J. McLaurin. 2002. Aβ42-peptide assembly on lipid Bilayers. *Journal of Molecular Biology* 318(1):97-107.

84. Devanathan, S., Z. Salamon, G. Lindblom, G. Grobner, and G. Tollin. 2006. Effects of sphingomyelin, cholesterol and zinc ions on the binding, insertion and aggregation of the amyloid Aβ(1-40) peptide in solid-supported lipid bilayers. *Febs J* 273(7):1389-1402.

85. Yip, C.M., and J. McLaurin. 2001. Amyloid-β peptide assembly: A critical step in fibrillogenesis and membrane disruption. *Biophysical Journal* 80(3):1359-1371.

86. Tashima, Y., R. Oe, S. Lee, G. Sugihara, E.J. Chambers, M. Takahashi, and T. Yamada. 2004. The effect of cholesterol and monosialoganglioside (GM1) on the release and aggregation of amyloid β-peptide from liposomes prepared from brain membrane-like lipids. *J Biol Chem* 279(17):17587-17595.

87. Wong, P.T., J.A. Schauerte, K.C. Wisser, H. Ding, E.L. Lee, D.G. Steel, and A. Gafni. 2009. Amyloid-β membrane binding and permeabilization are distinct processes influenced separately by membrane charge and fluidity. *Journal of Molecular Biology* 386(1):81-96.

88. Waschuk, S.A., E.A. Elton, A.A. Darabie, P.E. Fraser, and J.A. McLaurin. 2001. Cellular membrane composition defines Aβ-lipid interactions. *J Biol Chem* 276(36):33561-33568.

89. Walsh, D.M., B.P. Tseng, R.E. Rydel, M.B. Podlisny, and D.J. Selkoe. 2000. The oligomerization of amyloid β-protein begins intracellularly in cells derived from human brain. *Biochemistry* 39(35):10831-10839.

90. Seelig, J. 2004. Thermodynamics of lipid-peptide interactions. *Biochimica Et Biophysica Acta-Biomembranes* 1666(1-2):40-50.

91. Dante, S., T. Hauss, and N.A. Dencher. 2002. β-amyloid 25 to 35 is intercalated in anionic and zwitterionic lipid membranes to different extents. *Biophysical Journal* 83(5):2610-2616.

92. McLaurin, J., and A. Chakrabartty. 1996. Membrane disruption by Alzheimer β-amyloid peptides mediated through specific binding to either phospholipids or gangliosides. Implications for neurotoxicity. *J Biol Chem* 271(43):26482-26489.

93. Matsuzaki, K., and C. Horikiri. 1999. Interactions of amyloid β-peptide (1-40) with ganglioside-containing membranes. *Biochemistry* 38(13):4137-4142.

94. Choucair, A., M. Chakrapani, B. Chakravarthy, J. Katsaras, and L.J. Johnston. 2007. Preferential accumulation of Aβ(1-42) on gel phase domains of lipid bilayers: An AFM and fluorescence study. *Biochimica Et Biophysica Acta-Biomembranes* 1768(1):146-154.

95. Yoda, M., T. Miura, and H. Takeuchi. 2008. Non-electrostatic binding and self-association of amyloid β-peptide on the surface of tightly packed phosphatidylcholine membranes. *Biochemical and Biophysical Research Communications* 376(1):56-59.

96. Norton, W.T., T. Abe, S.E. Poduslo, and G.H. DeVries. 1975. The lipid composition of isolated brain cells and axons. *J Neurosci Res* 1(1):57-75.

97. Curtain, C.C., F.E. Ali, D.G. Smith, A.I. Bush, C.L. Masters, and K.J. Barnham. 2003. Metal ions, pH, and cholesterol regulate the interactions of Alzheimer's disease amyloid-beta peptide with membrane lipid. *J Biol Chem* 278(5):2977-2982.

98. Simakova, O., and N.J. Arispe. 2007. The cell-selective neurotoxicity of the Alzheimer's Aβ peptide is determined by surface phosphatidylserine and cytosolic ATP levels. Membrane binding is required for Aβ toxicity. *J Neurosci* 27(50):13719-13729.

99. Elliott, J.I., A. Surprenant, F.M. Marelli-Berg, J.C. Cooper, R.L. Cassady-Cain, C. Wooding, K. Linton, D.R. Alexander, and C.F. Higgins. 2005. Membrane phosphatidylserine distribution as a non-apoptotic signalling mechanism in lymphocytes. *Nat Cell Biol* 7(8):808-816.

100. Fadok, V.A., D.L. Bratton, D.M. Rose, A. Pearson, R.A. Ezekewitz, and P.M. Henson. 2000. A receptor for phosphatidylserine-specific clearance of apoptotic cells. *Nature* 405(6782):85-90.

101. Sims, P.J., and T. Wiedmer. 2001. Unraveling the mysteries of phospholipid scrambling. *Thromb Haemost* 86(1):266-275.

102. Cordy, J.M., N.M. Hooper, and A.J. Turner. 2006. The involvement of lipid rafts in Alzheimer's disease (Review). *Molecular Membrane Biology* 23(1):111-122.

103. Pike, L.J. 2006. Rafts defined: a report on the Keystone Symposium on Lipid Rafts and Cell Function. *J Lipid Res* 47(7):1597-1598.

104. Simons, K., and D. Toomre. 2000. Lipid rafts and signal transduction. *Nat Rev Mol Cell Biol* 1(1):31-39.

105. Brown, D.A., and E. London. 1998. Functions of lipid rafts in biological membranes. *Annu Rev Cell Dev Biol* 14:111-136.

106. Wolozin, B. 2001. A fluid connection: cholesterol and Aβ. *Proc Natl Acad Sci U S A* 98(10):5371-5373.

107. Ehehalt, R., P. Keller, C. Haass, C. Thiele, and K. Simons. 2003. Amyloidogenic processing of the Alzheimer β-amyloid precursor protein depends on lipid rafts. *J Cell Biol* 160(1):113-123.

108. Corder, E.H., A.M. Saunders, W.J. Strittmatter, D.E. Schmechel, P.C. Gaskell, G.W. Small, A.D. Roses, J.L. Haines, and M.A. Pericak-Vance. 1993. Gene dose of

apolipoprotein E type 4 allele and the risk of Alzheimer's disease in late onset families. *Science* 261(5123):921-923.

109. Cecchi, C., D. Nichino, M. Zampagni, C. Bernacchioni, E. Evangelisti, A. Pensalfini, G. Liguri, A. Gliozzi, M. Stefani, and A. Relini. 2009. A protective role for lipid raft cholesterol against amyloid-induced membrane damage in human neuroblastoma cells. *Biochimica Et Biophysica Acta-Biomembranes* 1788(10):2204-2216.

110. Lau, T.L., J.D. Gehman, J.D. Wade, C.L. Masters, K.J. Barnham, and F. Separovic. 2007. Cholesterol and Clioquinol modulation of Aβ(1-42) interaction with phospholipid bilayers and metals. *Biochimica Et Biophysica Acta-Biomembranes* 1768(12):3135-3144.

111. Qiu, L.M., A. Lewis, J. Como, M.W. Vaughn, J.Y. Huang, P. Somerharju, J. Virtanen, and K.H. Cheng. 2009. Cholesterol Modulates the Interaction of beta-Amyloid Peptide with Lipid Bilayers. *Biophysical Journal* 96(10):4299-4307.

112. Kim, S.I., J.S. Yi, and Y.G. Ko. 2006. Amyloid β oligomerization is induced by brain lipid rafts. *J Cell Biochem* 99(3):878-889.

113. Wood, W.G., F. Schroeder, U. Igbavboa, N.A. Avdulov, and S.V. Chochina. 2002. Brain membrane cholesterol domains, aging and amyloid beta-peptides. *Neurobiol Aging* 23(5):685-694.

114. Lee, S.J., U. Liyanage, P.E. Bickel, W. Xia, P.T. Lansbury, Jr., and K.S. Kosik. 1998. A detergent-insoluble membrane compartment contains Aβ in vivo. *Nat Med* 4(6):730-734.

115. Morishima-Kawashima, M., and Y. Ihara. 1998. The presence of amyloid β-protein in the detergent-insoluble membrane compartment of human neuroblastoma cells. *Biochemistry* 37(44):15247-15253.

116. Okada, T., K. Ikeda, M. Wakabayashi, M. Ogawa, and K. Matsuzaki. 2008. Formation of toxic Aβ(1-40) fibrils on GM1 ganglioside-containing membranes mimicking lipid rafts: Polymorphisms in Aβ(1-40) fibrils. *Journal of Molecular Biology* 382(4):1066-1074.

117. Nakazawa, Y., Y. Suzuki, M.P. Williamson, H. Saito, and T. Asakura. 2009. The interaction of amyloid Aβ(1-40) with lipid bilayers and ganglioside as studied by P-31 solid-state NMR. *Chemistry and Physics of Lipids* 158(1):54-60.

118. Ikeda, K., and K. Matsuzaki. 2008. Driving force of binding of amyloid β-protein to lipid bilayers. *Biochemical and Biophysical Research Communications* 370(3):525-529.

119. Choo-Smith, L.P., and W.K. Surewicz. 1997. The interaction between Alzheimer amyloid β(1-40) peptide and ganglioside GM1-containing membranes. *FEBS Lett* 402(2-3):95-98.

120. Kakio, A., S.I. Nishimoto, K. Yanagisawa, Y. Kozutsumi, and K. Matsuzaki. 2001. Cholesterol-dependent formation of GM1 ganglioside-bound amyloid β-protein, an endogenous seed for Alzheimer amyloid. *J Biol Chem* 276(27):24985-24990.

121. Anand, P., F.S. Nandel, and U.H.E. Hansmann. 2008. The Alzheimer's β amyloid (Aβ(1-39)) monomer in an implicit solvent. *Journal of Chemical Physics* 128(16):165102.

122. Anand, P., F.S. Nandel, and U.H.E. Hansmann. 2008. The Alzheimer β amyloid (Aβ(1-39)) dimer in an implicit solvent. *Journal of Chemical Physics* 129(19):195102.

123. Wu, C., M.M. Murray, S.L. Bernstein, M.M. Condron, G. Bitan, J.E. Shea, and M.T. Bowers. 2009. The structure of Aβ42 C-terminal fragments probed by a combined experimental and theoretical study. *Journal of Molecular Biology* 387(2):492-501.

124. Baumketner, A., and J.E. Shea. 2007. The structure of the Alzheimer amyloid β 10-35 peptide probed through replica-exchange molecular dynamics simulations in explicit solvent. *Journal of Molecular Biology* 366(1):275-285.

125. Jang, S., and S. Shin. 2008. Computational study on the structural diversity of amyloid beta peptide (Aβ(10-35)) oligomers. *Journal of Physical Chemistry B* 112(11):3479-3484.

126. Dong, X., W. Chen, N. Mousseau, and P. Derreumaux. 2008. Energy landscapes of the monomer and dimer of the Alzheimer's peptide Aβ(1-28). *Journal of Chemical Physics* 128(12):125108.

127. Reddy, G., J.E. Straub, and D. Thirumalai. 2009. Influence of preformed Asp23-Lys28 salt bridge on the conformational fluctuations of monomers and dimers of Aβ peptides with implications for rates of fibril formation. *Journal of Physical Chemistry B* 113(4):1162-1172.

128. Tarus, B., J.E. Straub, and D. Thirumalai. 2006. Dynamics of Asp23-Lys28 salt-bridge formation in Aβ(10-35) monomers. *Journal of the American Chemical Society* 128(50):16159-16168.

129. Buchete, N.V., R. Tycko, and G. Hummer. 2005. Molecular dynamics simulations of Alzheimer's β-amyloid protofilaments. *Journal of Molecular Biology* 353(4):804-821.

130. Cruz, L., B. Urbanc, J.M. Borreguero, N.D. Lazo, D.B. Teplow, and H.E. Stanley. 2005. Solvent and mutation effects on the nucleation of amyloid β-protein folding. *Proceedings of the National Academy of Sciences of the United States of America* 102(51):18258-18263.

131. Urbanc, B., L. Cruz, F. Ding, D. Sammond, S. Khare, S.V. Buldyrev, H.E. Stanley, and N.V. Dokholyan. 2004. Molecular dynamics simulation of amyloid β dimer formation. *Biophysical Journal* 87(4):2310-2321.

132. Chebaro, Y., N. Mousseau, and P. Derreumaux. 2009. Structures and Thermodynamics of Alzheimer's Amyloid-β Aβ(16-35) Monomer and Dimer by Replica Exchange Molecular Dynamics Simulations: Implication for Full-Length Aβ Fibrillation. *Journal of Physical Chemistry B* 113(21):7668-7675.

133. Masman, M.F., U.L.M. Eisel, I.G. Csizmadia, B. Penke, R.D. Enriz, S.J. Marrink, and P.G.M. Luiten. 2009. In Silico Study of Full-Length Amyloid β 1-42 Tri- and Penta-Oligomers in Solution. *Journal of Physical Chemistry B* 113(34):11710-11719.

134. O'Brien, E.P., Y. Okamoto, J.E. Straub, B.R. Brooks, and D. Thirumalai. 2009. Thermodynamic Perspective on the Dock-Lock Growth Mechanism of Amyloid Fibrils. *Journal of Physical Chemistry B* 113(43):14421-14430.

135. Takeda, T., and D.K. Klimov. 2009. Interpeptide interactions induce helix to strand structural transition in Aβ peptides. *Proteins-Structure Function and Bioinformatics* 77(1):1-13.

136. Lemkul, J.A., and D.R. Bevan. 2008. A comparative molecular dynamics analysis of the amyloid β-peptide in a lipid bilayer. *Archives of Biochemistry and Biophysics* 470(1):54-63.

137. Lemkul, J.A., and D.R. Bevan. 2009. Perturbation of membranes by the amyloid beta-peptide - a molecular dynamics study. *Febs Journal* 276(11):3060-3075.

138. Davis, C.H., and M.L. Berkowitz. 2009. Interaction between amyloid-β (1-42) peptide and phospholipid bilayers: A molecular dynamics study. *Biophysical Journal* 96(3):785-797.

139. Davis, C.H., and M.L. Berkowitz. 2009. Structure of the Amyloid-β (1-42) Monomer Absorbed To Model Phospholipid Bilayers: A Molecular Dynamics Study. *Journal of Physical Chemistry B* 113(43):14480-14486.

140. Chen, Y., F. Ding, H. Nie, A.W. Serohijos, S. Sharma, K.C. Wilcox, S. Yin, and N.V. Dokholyan. 2008. Protein folding: then and now. *Arch Biochem Biophys* 469(1):4-19.

141. Mobley, D.L., D.L. Cox, R.R. Singh, M.W. Maddox, and M.L. Longo. 2004. Modeling amyloid β-peptide insertion into lipid bilayers. *Biophys J* 86(6):3585-3597.

142. Friedman, R., R. Pellarin, and A. Caflisch. 2009. Amyloid Aggregation on Lipid Bilayers and Its Impact on Membrane Permeability. *Journal of Molecular Biology* 387(2):407-415.

143. Berendsen, H.J.C., D. van der Spoel, and R. van Drunen. 1995. GROMACS: A message-passing parallel molecular dynamics implementation. *Computer Physics Communications* 91(1-3):43-56.

144. Lindahl, E., B. Hess, and D. Van Der Spoel. 2001. GROMACS 3.0: a package for molecular simulation and trajectory analysis. *Journal of Molecular Modeling* 7(8):306-317.

145. Van der Spoel, D., E. Lindahl, B. Hess, G. Groenhof, A.E. Mark, and H.J.C. Berendsen. 2005. Gromacs: Fast, Flexible, and Free. *Journal of Computational Chemistry* 26(16):1701-1718.

146. Essmann, U., L. Perera, M.L. Berkowitz, T. Darden, H. Lee, and L.G. Pedersen. 1995. A smooth particle mesh ewald method. *Journal of Chemical Physics* 103(19):8577-8593.

147. Patey, G.N., and J.P. Valleau. 1973. Free-energy of spheres with dipoles - Monte-Carlo with multistage sampling. *Chemical Physics Letters* 21(2):297-300.

148. Torrie, G.M., and J.P. Valleau. 1977. Non-physical sampling distributions in Monte-Carlo free-energy estimation - umbrella sampling. *Journal of Computational Physics* 23(2):187-199.

149. Hukushima, K., and K. Nemoto. 1996. Exchange Monte Carlo method and application to spin glass simulations. *Journal of the Physical Society of Japan* 65(6):1604-1608.

150. Kumar, S., D. Bouzida, R.H. Swendsen, P.A. Kollman, and J.M. Rosenberg. 1992. The weighted histogram analysis method for free-energy calculations on biomolecules .1. The method. *Journal of Computational Chemistry* 13(8):1011-1021.

151. Nymeyer, H., T.B. Woolf, and A.E. Garcia. 2005. Folding is not required for bilayer insertion: Replica exchange simulations of an α-helical peptide with an explicit lipid bilayer. *Proteins-Structure Function and Bioinformatics* 59(4):783-790.

152. Sugita, Y., and Y. Okamoto. 1999. Replica-exchange molecular dynamics method for protein folding. *Chemical Physics Letters* 314(1-2):141-151.

153. Abraham, M.J., and J.E. Gready. 2008. Ensuring mixing efficiency of replica-exchange molecular dynamics simulations. *Journal of Chemical Theory and Computation* 4(7):1119-1128.

154. Thirumalai, D., D.K. Klimov, and R.I. Dima. 2003. Emerging ideas on the molecular basis of protein and peptide aggregation. *Current Opinion in Structural Biology* 13(2):146-159.

155. Kinnunen, P.K.J., A. Koiv, J.Y.A. Lehtonen, M. Rytomaa, and P. Mustonen. 1994. Lipid dynamics and peripheral interactions of proteins with membrane surfaces. *Chemistry and Physics of Lipids* 73(1-2):181-207.

156. Lee, A.G. 2004. How lipids affect the activities of integral membrane proteins. *Biochimica Et Biophysica Acta-Biomembranes* 1666(1-2):62-87.

157. Ambroggio, E.E., D.H. Kim, F. Separovic, C.J. Barrow, C.J. Barrow, K.J. Barnham, L.A. Bagatolli, and G.D. Fidelio. 2005. Surface behavior and lipid interaction of Alzheimer β-amyloid peptide 1-42: A membrane-disrupting peptide. *Biophysical Journal* 88(4):2706-2713.

158. Appelt, C., F. Eisenmenger, R. Kuhne, P. Schmieder, and J.A. Soderhall. 2005. Interaction of the antimicrobial peptide cyclo(RRWWRF) with membranes by molecular dynamics simulations. *Biophysical Journal* 89(4):2296-2306.

159. Gumbart, J., Y. Wang, A. Aksimentiev, E. Tajkhorshid, and K. Schulten. 2005. Molecular dynamics simulations of proteins in lipid bilayers. *Current Opinion in Structural Biology* 15(4):423-431.

160. Henin, J., A. Pohorille, and C. Chipot. 2005. Insights into the recognition and association of transmembrane α-helices. The free energy of α-helix dimerization in glycophorin A. *Journal of the American Chemical Society* 127(23):8478-8484.

161. Freitas, M.S., L.P. Gaspar, M. Lorenzoni, F.C.L. Almeida, L.W. Tinoco, M.S. Almeida, L.F. Maia, L. Degreve, A.P. Valente, and J.L. Silva. 2007. Structure of the Ebola fusion peptide in a membrane-mimetic environment and the interaction with lipid rafts. *Journal of Biological Chemistry* 282(37):27306-27314.

162. Kessel, A., D. Shental-Bechor, T. Haliloglu, and N. Ben-Tal. 2003. Interactions of hydrophobic peptides with lipid bilayers: Monte Carlo simulations with M2δ. *Biophysical Journal* 85(6):3431-3444.

163. Lazaridis, T. 2005. Implicit solvent simulations of peptide interactions with anionic lipid membranes. *Proteins-Structure Function and Bioinformatics* 58(3):518-527.

164. Zhang, J.M., and T. Lazaridis. 2006. Calculating the free energy of association of transmembrane helices. *Biophysical Journal* 91(5):1710-1723.

165. Mager, P.P. 1998. Molecular simulation of the primary and secondary structures of the Aβ(1-42)-peptide of Alzheimer's disease. *Medicinal Research Reviews* 18(6):403-430.

166. Simona, F., G. Tiana, R.A. Broglia, and G. Colombo. 2004. Modeling the α-helix to β-hairpin transition mechanism and the formation of oligomeric aggregates of the fibrillogenic peptide Aβ(12-28): insights from all-atom molecular dynamics simulations. *Journal of Molecular Graphics & Modelling* 23(3):263-273.

167. Han, W., and Y.D. Wu. 2005. A strand-loop-strand structure is a possible intermediate in fibril elongation: Long time simulations of amylold-β peptide (10-35). *Journal of the American Chemical Society* 127(44):15408-15416.

168. Jang, S., and S. Shin. 2006. Amyloid β-peptide oligomerization in silico: Dimer and trimer. *Journal of Physical Chemistry B* 110(5):1955-1958.

169. Wei, G.H., and J.E. Shea. 2006. Effects of solvent on the structure of the Alzheimer amyloid-β(25-35) peptide. *Biophysical Journal* 91(5):1638-1647.

170. Meinke, J.H., and U.H.E. Hansmann. 2007. Aggregation of β-amyloid fragments. *Journal of Chemical Physics* 126(1):014706.

171. Nose, S. 1984. A unified formulation of the constant temperature molecular-dynamics methods. *Journal of Chemical Physics* 81(1):511-519.

172. Hess, B., H. Bekker, H.J.C. Berendsen, and J.G.E.M. Fraaije. 1997. LINCS: A linear constraint solver for molecular simulations. *Journal of Computational Chemistry* 18(12):1463-1472.

173. Berendsen, H.J.C., J.R. Grigera, and T.P. Straatsma. 1987. The missing term in effective pair potentials. *Journal of Physical Chemistry* 91(24):6269-6271.

174. Kabsch, W., and C. Sander. 1983. Dictionary of protein secondary structure - pattern-recognition of hydrogen-bonded and geometrical features. *Biopolymers* 22(12):2577-2637.

175. Parrinello, M., and A. Rahman. 1981. Polymorphic transitions in single-crystals - a new molecular-dynamics method. *Journal of Applied Physics* 52(12):7182-7190.

176. Berger, O., O. Edholm, and F. Jahnig. 1997. Molecular dynamics simulations of a fluid bilayer of dipalmitoylphosphatidylcholine at full hydration, constant pressure, and constant temperature. *Biophysical Journal* 72(5):2002-2013.

177. Nagle, J.F., R.T. Zhang, S. TristramNagle, W.J. Sun, H.I. Petrache, and R.M. Suter. 1996. X-ray structure determination of fully hydrated L(α) phase dipalmitoylphosphatidylcholine bilayers. *Biophysical Journal* 70(3):1419-1431.

178. Smondyrev, A.M., and M.L. Berkowitz. 1999. United atom force field for phospholipid membranes: Constant pressure molecular dynamics simulation of dipalmitoylphosphatidicholine/water system. *Journal of Computational Chemistry* 20(5):531-545.

179. Petrache, H.I., S. Tristram-Nagle, K. Gawrisch, D. Harries, V.A. Parsegian, and J.F. Nagle. 2004. Structure and fluctuations of charged phosphatidylserine bilayers in the absence of salt. *Biophysical Journal* 86(3):1574-1586.

180. Bhide, S.Y., and M.L. Berkowitz. 2005. Structure and dynamics of water at the interface with phospholipid bilayers. *J Chem Phys* 123(22):224702.

181. Vivcharuk, V., B. Tomberli, I.S. Tolokh, and C.G. Gray. 2008. Prediction of binding free energy for adsorption of antimicrobial peptide lactoferricin B on a POPC membrane. *Physical Review E* 77(3):031913.

182. Chou, P.Y., and G.D. Fasman. 1977. β-Turns in Proteins. *Journal of Molecular Biology* 115(2):135-175.

183. Meier, M., and J. Seelig. 2007. Thermodynamics of the coil ↔ β-sheet transition in a membrane environment. *Journal of Molecular Biology* 369(1):277-289.

184. Chauhan, A., I. Ray, and V.P.S. Chauhan. 2000. Interaction of amyloid β-protein with anionic phospholipids: Possible involvement of Lys(28) and C-terminus aliphatic amino acids. *Neurochemical Research* 25(3):423-429.

185. Arispe, N., J.C. Diaz, and O. Simakova. 2007. Aβ ion channels. Prospects for treating Alzheimer's disease with Aβ channel blockers. *Biochimica Et Biophysica Acta-Biomembranes* 1768(8):1952-1965.

186. Hess, B., C. Kutzner, D. van der Spoel, and E. Lindahl. 2008. GROMACS 4: Algorithms for highly efficient, load-balanced, and scalable molecular simulation. *Journal of Chemical Theory and Computation* 4(3):435-447.

187. Hess, B. 2008. P-LINCS: A parallel linear constraint solver for molecular simulation. *Journal of Chemical Theory and Computation* 4(1):116-122.

188. Patriksson, A., and D. van der Spoel. 2008. A temperature predictor for parallel tempering simulations. *Physical Chemistry Chemical Physics* 10(15):2073-2077.

189. Sciarretta, K.L., D.J. Gordon, A.T. Petkova, R. Tycko, and S.C. Meredith. 2005. Aβ40-Lactam(D23/K28) models a conformation highly favorable for nucleation of amyloid. *Biochemistry* 44(16):6003-6014.

190. Valincius, G., F. Heinrich, R. Budvytyte, D.J. Vanderah, D.J. McGillivray, Y. Sokolov, J.E. Hall, and M. Losche. 2008. Soluble Amyloid β-Oligomers Affect Dielectric Membrane Properties by Bilayer Insertion and Domain Formation: Implications for Cell Toxicity. *Biophysical Journal* 95(10):4845-4861.

191. Wahlstrom, A., L. Hugonin, A. Peralvarez-Marin, J. Jarvet, and A. Graslund. 2008. Secondary structure conversions of Alzheimer's Aβ(1-40) peptide induced by membrane-mimicking detergents. *Febs Journal* 275(20):5117-5128.

192. Jamadagni, S.N., R. Godawat, and S. Garde. 2009. How Surface Wettabitity Affects the Binding, Folding, and Dynamics of Hydrophobic Polymers at Interfaces. *Langmuir* 25(22):13092-13099.